

TeV Scale Quark-Lepton Unification

K.S. Babu,^a Sumit Biswas,^a Shaikh Saad^b

^aDepartment of Physics, Oklahoma State University, Stillwater, OK 74078, USA

^bJožef Stefan Institute, Jamova 39, P. O. Box 3000, SI-1001 Ljubljana, Slovenia

E-mail: babu@okstate.edu, sumit.biswas@okstate.edu, shaikh.saad@ijs.si

Abstract. We propose a quark-lepton symmetric Pati-Salam (PS) model based on the gauge group $SU(2)_L \times SU(2)_R \times SU(4)_C$ with an E_6 -inspired particle spectrum which naturally accommodates a multi-TeV leptoquark gauge boson $X_\mu(3, 1, \frac{2}{3})$. A softly broken Z_2 symmetry plays a crucial role in realizing this scenario, under which the Standard Model (SM) fermions are even, while new vector-like fermions present in the model are odd. A notable feature of this model is that the PS gauge boson X_μ itself is Z_2 -odd, causing it to couple exclusively between SM fermions and the vector-like fermions, except in the right-handed down-quark sector, where mixing is induced by the soft breaking of Z_2 . This structure leads to helicity suppression of tree-level meson decays mediated by X_μ , with helicity-unsuppressed contributions arising only via one-loop diagrams. We show that X_μ can be as light as 1.1 TeV while being compatible with all flavor-violating constraints. However, mass relations among the $(W_\mu'^\pm, Z'_\mu, X_\mu)$ gauge bosons push the X_μ mass limit up to 4.3 TeV from the stringent LHC bounds on the Z' mass. This comparatively low PS-breaking scale opens up promising collider opportunities for probing the leptoquark gauge boson, as well as the distinctive signature of vector-like down-type quarks carrying an unusual baryon number of $2/3$. The model can be further tested via lepton flavor-violating processes induced by the leptoquark gauge boson, such as $\mu \rightarrow e\gamma$, $\mu \rightarrow eee$, and $\mu\text{-}e$ conversion in nuclei. Neutrino masses arise in the model through dimension-seven operators at tree-level, as well as from dimension-five operators via one-loop diagrams.

Contents

1	Introduction	2
2	E_6-inspired Pati-Salam Model	4
2.1	Fermionic content	4
2.2	Scalar content	5
2.3	Yukawa interactions and charged fermion masses	6
2.4	Softly broken Z_2 symmetry	9
2.5	Neutrino mass generation	10
2.6	Gauge Sector	13
2.6.1	Charged Gauge Boson Masses	13
2.6.2	Neutral Gauge Boson Masses	14
2.7	Higgs Sector	16
2.8	Interactions of the gauge bosons with light and heavy fermions	21
3	Collider Implications	25
4	Flavor violating processes	28
4.1	Meson decay at tree level	28
4.2	$K_L \rightarrow \mu e$ at one loop level	33
4.3	Limit on M_X from mass difference of neutral mesons	35
4.3.1	$K^0 - \bar{K}^0$ oscillation	37
4.3.2	$D^0 - \bar{D}^0$ oscillation	40
4.3.3	$B_q^0 - \bar{B}_q^0$ oscillation	42
4.3.4	Tree-level meson mixing processes	43
4.4	Limit on M_X from cLFV through leptoquark gauge boson X_μ	45
4.4.1	$\mu \rightarrow e\gamma$ decay	45
4.4.2	$\mu \rightarrow eee$	48
4.4.3	μ - e conversion in nuclei	53
4.4.4	Global fit with the three cLFV processes	56
5	Conclusions	57
A	Coefficients in renormalization group equations	59
B	Input parameters for meson mixing	59
B.1	$K^0 - \bar{K}^0$ oscillation	59
B.2	$D^0 - \bar{D}^0$ oscillation	60
B.3	$B_q^0 - \bar{B}_q^0$ oscillation	60
C	Input parameters for $\mu \rightarrow e$ conversion in nuclei	61

1 Introduction

The first successful attempt to unify quarks and leptons is the Pati–Salam [1, 2] (PS) model, where they transform as common multiplets of the gauge symmetry $SU(2)_L \times SU(2)_R \times SU(4)_C$. Lepton number is treated as the fourth color of the enhanced color group $SU(4)_C$. Beyond quark–lepton unification, the PS model has several attractive features: its non-Abelian nature implies that electric charge is quantized; the presence of right-handed neutrinos dictated by the gauge structure paves the way for light neutrino mass generation via the seesaw mechanism; and the matter–antimatter asymmetry of the universe can be explained via leptogenesis arising from the decays of the right-handed neutrinos. Furthermore, unlike Grand Unified Theories (GUTs) based on simple gauge groups, the new leptoquark gauge boson in the PS model, $X_\mu(3, 1, \frac{2}{3})$, where the quantum numbers refer to the Standard Model symmetry $SU(3)_C \times SU(2)_L \times U(1)_Y$, does not mediate proton decay, allowing the PS-breaking scale to be much lower than the traditional GUT scale of order 10^{16} GeV. There is, however, a strong lower limit on the PS-breaking scale from meson decay to leptons. In particular $K_L^0 \rightarrow \mu^\pm e^\mp$ constraint requires $M_X \gtrsim \mathcal{O}(2500)$ TeV [3–5]. This scale is still well beyond the reach of any foreseeable collider experiments.

The goal of this paper is to realize Pati–Salam symmetry at the multi-TeV scale, which can be probed directly at the Large Hadron Collider (LHC) and other near-future collider experiments. Our proposal makes use of an E_6 -inspired particle spectrum, which enables us to evade the stringent lower limits on X_μ mass from meson decay constraints. In E_6 GUTs [6], all fermions of a generation are unified in a 27_F -dimensional representation. Apart from the Standard Model (SM) fermions, this contains new vector-like fermions – an iso-singlet down-type quark, a vector-like lepton doublet, and two singlet neutrinos ν^c and N . An additional vector-like fermion belonging to $(1, 1, 6)$ of the Pati–Salam gauge symmetry is also introduced for realizing quark–lepton symmetry in the multi-TeV range. We are agnostic about the origin of this multiplet, but we note that it has no gauge anomaly and it can arise in specific compactification schemes that break E_6 down to the PS gauge group.

Our proposed model incorporates a softly broken Z_2 symmetry, under which all SM fermions are even, while the new vector-like fermions are odd. An exception to this assignment is that a vectorlike quark with baryon number of $+2/3$, D'^c , is odd under Z_2 . An important feature of the model is that the PS gauge boson X_μ is also Z_2 -odd, causing its coupling to involve one SM fermion and one vector-like fermion. The Z_2 symmetry is softly broken, which leads to mixing of the d_R quarks of the SM with D_R vector-like quarks. Meson decays arising at tree-level through the $d_R - D_R$ mixings and mediated by the X_μ gauge boson are helicity suppressed, with helicity-unsuppressed contributions arising only via loop diagrams. Consequently, the X_μ gauge boson can be remarkably as light as a TeV, while being consistent with all flavor-violating constraints. Although the model introduced in this work is new, the idea of suppressing meson decays through the inclusion of vector-like fermions has been explored previously in the context of the PS framework in Refs. [3–5, 7–11]. What is genuinely novel in our construction, however, is that the specific set of exotic fermionic multiplets we introduce allows the softly broken Z_2 symmetry to play a significant role in the suppression mechanism and admits a consistent baryon-number assignment for all fields, thereby ensuring absolute proton

stability. This combination of features—PS structure, vector-like fermions with a softly broken Z_2 symmetry, and exact baryon-number conservation—has not been realized in any of the prior models.

Our detailed analysis shows that the mass of the leptoquark gauge boson X_μ can be as low as 1.1 TeV while being fully consistent with all flavor-violating constraints. Such a low bound on M_X is obtained by eliminating the kaon decay at tree level by a suitable choice of flavor structure. The most stringent flavor bound then arises from $B_s \rightarrow \mu e$ and $B_s \rightarrow \mu\mu$ decays in this scenario. However, current LHC experiments set a lower limit of 5.6 TeV on the Z' mass, from the production and decay $Z' \rightarrow \ell\bar{\ell}$ process. Taking account of the theoretical relations among the masses of Z' and X_μ , this translates into an indirect collider limit of $M_X \gtrsim 4.3$ TeV. Such a low PS-breaking scale opens up promising opportunities for collider probes. While direct searches for W' and X gauge bosons are less sensitive, we find that the high-luminosity LHC (HL-LHC) can probe the Z' mass up to 6.6 TeV, whereas the FCC-hh has the potential to reach a sensitivity of order $\mathcal{O}(40)$ TeV [12]. Owing to the mass relations among the gauge bosons, this reach would also probe indirectly X_μ mass of the same order. The model predicts the existence of vector-like down-type quarks D' with an unusual baryon number of 2/3. Pair production of D' would lead to multi-jet final states, which already place a lower bound of $\mathcal{O}(1.5)$ TeV on D' mass, which can be further tested in upcoming LHC upgrades and at future colliders. The leptoquark gauge boson also mediates lepton flavor violation (LFV), with the most stringent constraints arising from $\mu \rightarrow e\gamma$, $\mu \rightarrow eee$, and $\mu - e$ conversion in nuclei. If we assume a CKM-like mixing structure for the mixing matrix involving X_μ , these processes would yield a lower bound of roughly $M_X \gtrsim 1.64$ TeV. The model proposed, therefore, can be tested indirectly by the observation of these LFV processes.

Within this setup, we find that there are two comparable sources of neutrino masses. The first one arises through mixing of ν with the other neutral leptons ν^c and N present in the model, leading to an effective dimension-7 operator $LLHHH^\dagger H$ (with L and H denoting the lepton and SM Higgs doublet) [13, 14]. The second contribution arises from one-loop diagrams analogous to neutrino mass generation in the scotogenic model [15, 16]. Neutrino masses arising from either of these sources are sufficiently small and allow for the PS breaking scale to be in the multi-TeV range. Depending on the choice of parameters of the model, one or the other can dominate, or both can be comparable. We also point out that, due to low-scale PS breaking, monopoles produced at a temperature of TeV are cosmologically harmless [8, 17, 18]. In sum, TeV-scale PS-breaking is not only theoretically motivated and consistent, but also ensures that the model remains fully accessible to experimental probes.

Extended versions of low scale Pati-Salam models have been studied in the context of explaining certain B -meson decay anomalies [19–22]. In contrast to these extended models, the model proposed here is more traditional. There have been several studies on realizing Pati-Salam theory in four dimensions from string compactification, see for example, Ref. [23–27]. For discussions on various other aspects of the Pati-Salam model, such as its origin from $SO(10)$ unified theory, baryon number violation, solution to the gauge hierarchy problem, and symmetry breaking sector, see Ref. [28–33].

The layout of the paper is as follows. In Sec. 2, we introduce the model and provide all necessary details. These include the fermion, gauge boson and Higgs boson spectra, interconnec-

tions among the gauge boson masses, and gauge interactions in the physical basis of fermions. Collider implications are discussed in Sec. 3. A detailed analysis of flavor-violating processes, including meson decays, meson–antimeson oscillations, and lepton flavor violation (LFV), is presented in Sec. 4. This analysis includes tree-level induced processes as well as loop-induced processes. Finally, we conclude in Sec. 5. Some computational details are relegated to Appendices A, B, and C.

2 E_6 -inspired Pati-Salam Model

In this section, we introduce the proposed Pati-Salam model with an E_6 -inspired fermion spectrum and provide the relevant details necessary to develop strategies to test the model.

2.1 Fermionic content

The proposed model is based on the Pati-Salam gauge symmetry $\mathcal{G}_{\text{PS}} \equiv SU(2)_L \times SU(2)_R \times SU(4)_C$. The fermionic content of the theory is inspired by E_6 GUT. To see this, first consider the decomposition of the fundamental representation 27 of E_6 under its maximal subgroup $SO(10) \times U(1)$ as well as its subgroup $\mathcal{G}_{\text{PS}} \times U(1)$:

$$\begin{aligned} 27 &= 16_1 \oplus 10_{-2} \oplus 1_4 \quad [E_6 \supset SO(10) \times U(1)] \\ &= (2, 1, 4)_1 \oplus (1, 2, \bar{4})_1 \oplus (2, 2, 1)_{-2} \oplus (1, 1, 6)_{-2} \oplus (1, 1, 1)_4 \quad [E_6 \supset \mathcal{G}_{\text{PS}} \times U(1)]. \end{aligned} \quad (2.1)$$

Our model contains three families of these fermion fields arising from 27. In addition, we introduce the multiplet $\Omega \equiv (1, 1, 6)_F$ of fermions, one per family, which may have its origin from a pair of vector-like fermions $27_F + \bar{27}_F$, or from compactification of a higher dimensional theory. The Ω field is crucial for defining baryon number consistently. The full fermionic content of the theory is given below, where all fields are taken to be left-handed.

$$\psi = (2, 1, 4) = \begin{pmatrix} u_1 & u_2 & u_3 & \nu_E \\ d_1 & d_2 & d_3 & E \end{pmatrix}, \quad (2.2)$$

$$\psi^c = (1, 2, \bar{4}) = \begin{pmatrix} D_1^c & D_2^c & D_3^c & e^c \\ u_1^c & u_2^c & u_3^c & \nu^c \end{pmatrix}, \quad (2.3)$$

$$\chi = (2, 2, 1) = \begin{pmatrix} E^c & \nu \\ \nu_E^c & e \end{pmatrix}, \quad (2.4)$$

$$\omega = (1, 1, 6) = \frac{1}{\sqrt{2}} \begin{pmatrix} 0 & d_3^c & -d_2^c & \textcolor{red}{D}'_1 \\ -d_3^c & 0 & d_1^c & \textcolor{red}{D}'_2 \\ d_2^c & -d_1^c & 0 & \textcolor{red}{D}'_3 \\ -\textcolor{red}{D}'_1 & -\textcolor{red}{D}'_2 & -\textcolor{red}{D}'_3 & 0 \end{pmatrix}, \quad (2.5)$$

$$N = (1, 1, 1), \quad (2.6)$$

$$\Omega = (1, 1, 6) = \frac{1}{\sqrt{2}} \begin{pmatrix} 0 & \textcolor{red}{D}'_3^c & -\textcolor{red}{D}'_2^c & D_1 \\ -\textcolor{red}{D}'_3^c & 0 & \textcolor{red}{D}'_1^c & D_2 \\ \textcolor{red}{D}'_2^c & -\textcolor{red}{D}'_1^c & 0 & D_3 \\ -D_1 & -D_2 & -D_3 & 0 \end{pmatrix}. \quad (2.7)$$

A feature worth noting about this assignment is the flipping of $d^c \leftrightarrow D^c$ and $(\nu, e) \leftrightarrow (\nu_E, E)$, compared to the standard PS assignment, which does not include the χ, ω, N , and Ω fields. This flipping plays an important role in realizing the PS symmetry at the multi-TeV scale, as we shall see later. The new fermions $\textcolor{red}{D}', \textcolor{red}{D}^c$ are denoted in red color throughout, to easily distinguish them from the usual quarks and the D vector-like quarks, as they carry an unusual baryon number of $\pm 2/3$.

2.2 Scalar content

The scalar sector of our theory is rather minimal and consists of the following Higgs fields:

$$\tilde{\psi} = (2, 1, 4) = \begin{pmatrix} \tilde{u}_1 & \tilde{u}_2 & \tilde{u}_3 & \tilde{\nu}_E \\ \tilde{d}_1 & \tilde{d}_2 & \tilde{d}_3 & \tilde{E} \end{pmatrix}, \quad (2.8)$$

$$\tilde{\psi}^c = (1, 2, \bar{4}) = \begin{pmatrix} \tilde{D}_1^c & \tilde{D}_2^c & \tilde{D}_3^c & \tilde{e}^c \\ \tilde{u}_1^c & \tilde{u}_2^c & \tilde{u}_3^c & \tilde{\nu}^c \end{pmatrix}, \quad (2.9)$$

$$\tilde{\chi} = (2, 2, 1) = \begin{pmatrix} \tilde{E}^c & \tilde{\nu} \\ \tilde{\nu}_E^c & \tilde{e} \end{pmatrix}. \quad (2.10)$$

Here we have used common symbols for the scalars and the fermions with the same quantum numbers, but with a tilde added for the scalars. Note again that these states can arise from $27_H \supset (2, 1, 4) \oplus (1, 2, \bar{4}) \oplus (2, 2, 1)$, with the remaining submultiplets of 27_H assumed to be decoupled and residing at the high scale.

The full particle content of the theory, as given in Eqs. (2.2)–(2.7) and Eqs. (2.8)–(2.10), allows the imposition of a discrete Z_2 symmetry. Table 1 shows the relevant transformations of the particle content under this Z_2 . It is apparent that all SM are even and exotic fermions (except $\textcolor{red}{D}'^c$), including the right-handed neutrino ν^c , are odd under this symmetry. Note that the Z_2 symmetry does not commute with the gauge symmetry. Such a discrete Z_2 has been known to be present in E_6 -inspired left-right symmetric models [34, 35] where the symmetry may remain unbroken. In the context of low scale Pati-Salam model, the Z_2 has to be softly broken, otherwise baryon number violation would occur through the exchange of scalar leptoquarks, or some of the vector-like quarks would be massless. As will be discussed in Sec. 2.4, the soft breaking of Z_2 arises through a $\omega - \Omega$ mass mixing, which is necessary to give $\textcolor{red}{D}'$ a mass.

The neutral components of the Higgs fields $\tilde{\psi}, \tilde{\psi}^c$, and $\tilde{\chi}$ all acquire vacuum expectation values (VEV) which are denoted as:

$$\langle \tilde{\nu}_E \rangle = \kappa_L, \quad \langle \tilde{\nu}^c \rangle = \kappa_R, \quad \langle \tilde{\nu}_E^c \rangle = v, \quad \langle \tilde{\nu} \rangle = \textcolor{magenta}{w}. \quad (2.11)$$

While the VEVs of $\tilde{\nu}_E$, $\tilde{\nu}^c$ and $\tilde{\nu}_E^c$ do not break the Z_2 symmetry, the VEV of $\tilde{\nu}$ breaks the Z_2 and is thus shown in magenta color. The soft breaking of Z_2 through the fermionic $\omega - \Omega$ mixing implies that there is a linear term in $\tilde{\nu}$ in the Higgs potential that needs to be shifted away, leading to a nonzero $\textcolor{magenta}{w}$ with a hierarchy $\textcolor{magenta}{w} \ll \kappa_L, v$. The spontaneous symmetry breaking proceeds in two stages as follows:

$$SU(2)_L \times SU(2)_R \times SU(4)_C \xrightarrow{\langle \tilde{\psi}^c \rangle} SU(3)_C \times SU(2)_L \times U(1)_Y \xrightarrow{\langle \tilde{\psi}, \tilde{\chi} \rangle} SU(3)_C \times U(1)_{\text{em}}. \quad (2.12)$$

We are interested in a scenario with $\kappa_R \sim \mathcal{O}(\text{few TeV}) > \kappa_L, v \sim \mathcal{O}(100 \text{ GeV}) > \textcolor{magenta}{w} \sim \mathcal{O}(100 \text{ MeV})$.

Z_2 Even			Z_2 Odd		
Field	Type	B	Field	Type	B
u, d	F	$\frac{1}{3}$	D, D^c	F	$(\frac{1}{3}, -\frac{1}{3})$
u^c, d^c	F	$-\frac{1}{3}$	$\textcolor{red}{D'}$	F	$-\frac{2}{3}$
e, ν	F	0	ν^c	F	0
e^c	F	0	ν_E, E	F	0
$\textcolor{red}{D'^c}$	F	$\frac{2}{3}$	E^c, ν_E^c	F	0
$\tilde{\nu}^c$	S	0	N	F	0
$\tilde{\nu}_E$	S	0	\tilde{u}, \tilde{d}	S	$\frac{1}{3}$
$\tilde{\nu}_E^c$	S	0	\tilde{u}^c	S	$-\frac{1}{3}$
\tilde{D}^c	S	$-\frac{1}{3}$	$\tilde{\nu}, \tilde{e}$	S	0
\tilde{E}	S	0	\tilde{e}^c	S	0
\tilde{E}^c	S	0	$X_\mu^{+2/3}$	GB	$\frac{1}{3}$
Z'_μ	GB	0	W'_μ^\pm	GB	0

Table 1: Z_2 -parity and baryon number B for all fermions (F), scalars (S), and gauge bosons (GB) of the theory.

2.3 Yukawa interactions and charged fermion masses

With the particle spectrum specified, we can write down the most general Yukawa interactions involving the fermions and the scalars of the model. In doing so, we impose baryon number as well as the Z_2 symmetry given in Table 1, but we allow for a soft breaking of the Z_2 symmetry. The gauge-invariant Yukawa Lagrangian for the charged fermions can be written as

$$\begin{aligned} \mathcal{L}_{\text{Yuk}} = & Y_u \psi_{\alpha i} (\psi^c)_{\dot{\alpha}}^i \tilde{\chi}_{\beta \dot{\beta}} \epsilon^{\alpha \beta} \epsilon^{\dot{\alpha} \dot{\beta}} + Y_E \psi_{\alpha i} (\tilde{\psi}^c)_{\dot{\alpha}}^i \chi_{\beta \dot{\beta}} \epsilon^{\alpha \beta} \epsilon^{\dot{\alpha} \dot{\beta}} + Y_e \tilde{\psi}_{\alpha i} (\psi^c)_{\dot{\alpha}}^i \chi_{\beta \dot{\beta}} \epsilon^{\alpha \beta} \epsilon^{\dot{\alpha} \dot{\beta}} \\ & + \frac{Y_d}{\sqrt{2}} \psi_{\alpha i} \omega_{kl} \psi_{\beta j} \epsilon^{\alpha \beta} \epsilon^{ijkl} + \sqrt{2} Y_D (\psi^c)_{\dot{\alpha}}^i \Omega_{ij} (\tilde{\psi}^c)_{\dot{\beta}}^j \epsilon^{\dot{\alpha} \dot{\beta}} + \frac{M_\omega}{2} \omega_{ij} \Omega_{kl} \epsilon^{ijkl} + \text{h.c.} \end{aligned} \quad (2.13)$$

where α, β denotes $SU(2)_L$ indices, $\dot{\alpha}, \dot{\beta}$ denotes $SU(2)_R$ indices, and i, j, k, l presents $SU(4)_C$ indices. The last term in Eq. (2.13) breaks Z_2 softly. In component form \mathcal{L}_{Yuk} reads as

$$\begin{aligned} \mathcal{L}_{\text{Yuk}} = & Y_u \left((uD^c + \nu_E e^c) \tilde{e} - (uu^c + \nu_E \nu^c) \tilde{\nu}_E^c - (dD^c + Ee^c) \tilde{\nu} + (du^c + E\nu^c) \tilde{E}^c \right) \\ & + Y_E \left((u\tilde{D}^c + \nu_E \tilde{e}^c) e - (u\tilde{u}^c + \nu_E \tilde{\nu}^c) \nu_E^c - (d\tilde{D}^c + E\tilde{e}^c) \nu + (d\tilde{u}^c + E\tilde{\nu}^c) E^c \right) \\ & + Y_e \left((\tilde{u}D^c + \tilde{\nu}_E e^c) e - (\tilde{u}u^c + \tilde{\nu}_E \nu^c) \nu_E^c - (\tilde{d}D^c + \tilde{E}e^c) \nu + (\tilde{d}u^c + \tilde{E}\nu^c) E^c \right) \\ & + Y_d \left(d^c (u\tilde{E} - d\tilde{\nu}_E) + d^c (E\tilde{u} - \nu_E \tilde{d}) + \textcolor{red}{D'}_i u_j \tilde{d}_k \epsilon^{ijk} + \textcolor{red}{D'}_i d_j \tilde{u}_k \epsilon^{ijk} \right) \\ & + Y_D \left((\textcolor{red}{D'^c})_i (D^c)_j (\tilde{u}^c)_k \epsilon^{ijk} - (\textcolor{red}{D'^c})_i (u^c)_j (\tilde{D}^c)_k \epsilon^{ijk} + DD^c \tilde{\nu}^c - De^c \tilde{u}^c \right. \\ & \left. + D\nu^c \tilde{D}^c - Du^c \tilde{e}^c \right) + M_\omega (d^c D + \textcolor{red}{D'} \textcolor{red}{D'^c}) + \text{h.c.} \end{aligned} \quad (2.14)$$

The soft breaking of Z_2 symmetry by the M_ω term allows us to generate a mass term for $\textcolor{red}{D}'\textcolor{red}{D}'^c$ which forms a Dirac fermion. The Yukawa interactions of the singlet fermion N field will be discussed in Sec. 2.5, where we also discuss the neutrino mass spectrum.

The charged fermion mass matrices obtained from Eq. (2.14), with the VEVs defined in Eq. (2.11), have the following form in a basis $f_i^T M_{ij} f_j^c$ (for $f = u, d, e, E, D, \textcolor{red}{D}'$):

$$M_u^{3 \times 3} = Y_u v, \quad M_{\textcolor{red}{D}'}^{3 \times 3} = M_\omega, \quad \mathcal{M}_E^{6 \times 6} = \begin{pmatrix} Y_e^T \kappa_L & 0 \\ -Y_u \textcolor{violet}{w} & Y_E \kappa_R \end{pmatrix}, \quad \mathcal{M}_D^{6 \times 6} = \begin{pmatrix} -Y_d^T \kappa_L & -Y_u \textcolor{violet}{w} \\ M_\omega^T & Y_D \kappa_R \end{pmatrix}. \quad (2.15)$$

Here, the basis chosen for the 2×2 block matrices is $e - E$ and $d - D$. We define, for these matrices,

$$\hat{M}_D = Y_D \kappa_R, \quad \hat{M}_E = Y_E^T \kappa_R \quad (2.16)$$

and proceed to diagonalize them perturbatively. The elements of the blocks in the first row of \mathcal{M}_D are much smaller than those in the second row, due to the hierarchy $w \ll \kappa_L \ll \kappa_R$ realized in the model. Similarly, the first column of \mathcal{M}_E is much smaller than the nonzero second column. A general block matrix of the form

$$\mathcal{M} = \begin{pmatrix} m_0 & m \\ M' & M \end{pmatrix} \quad (2.17)$$

with $m_0, m \ll M', M$ can be block-diagonalized to second order in m, m_0 by the following transformation:

$$U_L^T \mathcal{M} U_R = M^{\text{Block}}, \quad (2.18)$$

where U_R and U_L are unitary matrices given, to linear order linear in m_0, m , as

$$U_R = \begin{pmatrix} (\mathbb{I} + x^\dagger x)^{-1/2} & x^\dagger M^\dagger (M(\mathbb{I} + x x^\dagger) M^\dagger)^{-1/2} \\ -x(\mathbb{I} + x^\dagger x)^{-1/2} & M^\dagger (M(\mathbb{I} + x x^\dagger) M^\dagger)^{-1/2} \end{pmatrix}, \quad U_L = \begin{pmatrix} \mathbb{I} & \rho^* \\ -\rho^T & \mathbb{I} \end{pmatrix}. \quad (2.19)$$

Here we have defined the 3×3 matrices x and ρ as

$$x \equiv M^{-1} M', \quad \rho = (m_0 x^\dagger + m)(\mathbb{I} + x x^\dagger)^{-1} M^{-1}. \quad (2.20)$$

The block diagonal mass matrix has the form

$$M^{\text{Block}} = \begin{pmatrix} (m_0 - m x)(1 + x^\dagger x)^{-1/2} & \mathbb{O} & \mathbb{O} \\ \mathbb{O} & (M M^\dagger + M' M'^\dagger)^{1/2} & \mathbb{O} \end{pmatrix}. \quad (2.21)$$

Here we use the symbols \mathbb{I} to denote the 3×3 identity matrix and \mathbb{O} for the 3×3 zero matrix with all elements equal to zero.

Each of the block diagonal matrix, written as $f'^T M^{\text{Block}} f'^c$, where

$$f = U_L f', \quad f^c = U_R f'^c, \quad (2.22)$$

is further diagonalized by the transformation

$$f' = V_f f_0, \quad f'^c = V_{f^c} f_0^c \quad (2.23)$$

with the f_0 and f_0^c denoting the mass eigenstates (for $f = u, d, e, E, D, \textcolor{red}{D}'$). These unitary matrices V_f, V_{f^c} diagonalize the block mass matrix:

$$V_f^T M^{\text{Block}} V_{f^c} = M^{\text{diagonal}}. \quad (2.24)$$

The transformation from the gauge eigenstates to the mass eigenstates can then be obtained from the combined effects of Eq. (2.18), Eq. (2.22) and Eq. (2.24).

These general results can be applied to block diagonalize \mathcal{M}_D of Eq. (2.15). We identify

$$M = \hat{M}_D, \quad x = \hat{M}_D^{-1} M_\omega^T, \quad \rho = -(Y_d^T \kappa_L x^\dagger + Y_u \textcolor{pink}{w})(\mathbb{I} + x x^\dagger)^{-1} \hat{M}_D^{-1}. \quad (2.25)$$

We can now write down the transformations that take (d, D) and (d^c, D^c) into their respective mass eigenstates as

$$\begin{pmatrix} d \\ D \end{pmatrix} = U_L \begin{pmatrix} V_d & \mathbb{O} \\ \mathbb{O} & V_D \end{pmatrix} \begin{pmatrix} d_0 \\ D_0 \end{pmatrix}, \quad \begin{pmatrix} d^c \\ D^c \end{pmatrix} = U_R \begin{pmatrix} V_{d^c} & \mathbb{O} \\ \mathbb{O} & V_{D^c} \end{pmatrix} \begin{pmatrix} d_0^c \\ D_0^c \end{pmatrix}. \quad (2.26)$$

More explicitly, we have

$$\begin{aligned} d &= V_d d_0 + \rho^* V_D D_0 \\ D &= V_D D_0 - \rho^T V_d d_0 \\ d^c &= (\mathbb{I} + x^\dagger x)^{-1/2} V_{d^c} d_0^c + x^\dagger M^\dagger \left(M(\mathbb{I} + x x^\dagger) M^\dagger \right)^{-1/2} V_{D^c} D_0^c \\ D^c &= -x (\mathbb{I} + x^\dagger x)^{-1/2} V_{d^c} d_0^c + M^\dagger \left(M(\mathbb{I} + x x^\dagger) M^\dagger \right)^{-1/2} V_{D^c} D_0^c \end{aligned} \quad (2.27)$$

with M , x and ρ defined in Eq. (2.25).

Similarly, the 6×6 matrix \mathcal{M}_E^T arising from Eq. (2.15) can be block diagonalized with the identification

$$x = 0, \quad \rho_\ell = -(Y_u^T \textcolor{pink}{w}) \hat{M}_E^{-1}. \quad (2.28)$$

The block-diagonal matrices are then diagonalized following the definitions of Eq. (2.24). We find explicitly the following transformation equations (with U_R being an identity matrix):

$$\begin{aligned} e &= V_e e_0 \\ E &= V_E E_0 \\ e^c &= V_{e^c} e_0^c + \rho_\ell^* V_{E^c} E_0^c \\ E^c &= -\rho_\ell^T V_{e^c} e_0^c + V_{E^c} E_0^c. \end{aligned} \quad (2.29)$$

As an application, the gauge interactions of X_μ in the original basis given as $\overline{D^c} \gamma_\mu e^c X^\mu$ will contain light fermion fields as

$$\overline{D^c} \gamma_\mu e^c X^\mu \supset \overline{d_0^c} \left[-V_{d^c}^\dagger (\mathbb{I} + x^\dagger x)^{-1/2} x^\dagger V_{e^c} \right] \gamma_\mu e_0^c X^\mu. \quad (2.30)$$

We shall present the complete interactions of the gauge bosons with the mass eigenstate fermions later in Sec. 2.6 using these results.

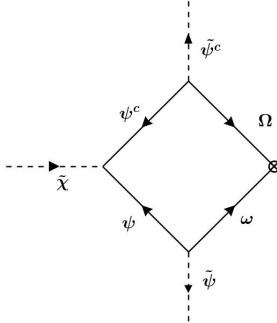


Figure 1: Induced cubic scalar coupling $\tilde{\psi}\tilde{\psi}^c\tilde{\chi}^*$ through the softly broken Z_2 mass term $M_\omega\Omega\omega$.

2.4 Softly broken Z_2 symmetry

Within the model, baryon number B of each particle can be uniquely determined from its gauge interactions, which are listed in Table 1. We shall assume that B is an exact symmetry of the Lagrangian. All quarks carry $B = 1/3$, except for $\textcolor{red}{D}'$ which has $B = -2/3$. Note also that scalars with identical quantum numbers carry the same B -charge as the corresponding fermions.

The couplings $\psi^c\omega\tilde{\psi}^c$, $\omega\omega$, and $\Omega\Omega$ are absent in \mathcal{L}_{Yuk} (see Eq. (2.13)), since they do not conserve baryon number. But the last term in Eq. (2.13), $\frac{M_\omega}{2}\omega_{ij}\Omega_{kl}\epsilon^{ijkl}$, does conserve baryon number and is necessary to generate a Dirac mass for the down-type state $\textcolor{red}{D}'$ with B charge of $-2/3$. This term breaks the Z_2 symmetry softly, and will induce mixing between d^c and D^c anti-quark fields. Such mixings are proportional to the matrix x defined in Eq. (2.25), viz.,

$$x_{ij} = (\hat{M}_D^{-1}M_\omega^T)_{ij} \approx 0.2 \quad \forall i, j. \quad (2.31)$$

Here $\hat{M}_D = Y_D\kappa_R$. This numerical choice is motivated by the desire to realize the lowest mass leptoquark gauge boson X_μ in the model. The logic behind this is as follows. The x_{ij} parameters control the $d^c - D^c$ mixing angles, which lead to tree-level meson decays mediated by X_μ . Only right-handed quarks take part in these decays. To suppress these tree-level decays, we wish to have x_{ij} as small as possible. Reducing M_ω would help, but collider bounds on the vector-like quark $\textcolor{red}{D}'$ require $M_\omega \gtrsim 1.3$ TeV (see Sec. 3). Increasing κ_R would also suppress x_{ij} , but at the price of raising the leptoquark gauge boson mass M_X (see Eq. (2.62)). We therefore go with the smallest κ_R allowed by the $M_{Z'}$ mass limit, and require that all elements of x_{ij} are of the same order.¹ We assume $Y_D \sim \mathcal{O}(1)$ (consistent with perturbative unitarity [36]), $M_\omega \simeq 1.3$ TeV, and $\kappa_R \geq 6.3$ TeV, the lowest value allowed by the limit $M_{Z'} \geq 5.6$ TeV, and arrive at $x_{ij} \sim 0.2$. A benchmark point for the matrix elements x_{ij} is given in Eq. (4.5). In principle, all soft Z_2 breaking terms that conserve baryon number should be allowed in the Lagrangian. These include the terms

$$\mathcal{L}_{\text{soft}} \supset M_\chi \chi\chi + M_{\tilde{\chi}}^2 \tilde{\chi}\tilde{\chi} + \mu\tilde{\psi}\tilde{\psi}^c\tilde{\chi}^* + \text{h.c.} \quad (2.32)$$

¹Flavor effects may further lower the $d^c - D^c$ mixing parameters. If we consider the presence of $\Phi(1, 1, 15)$ Higgs with $\langle\Phi\rangle = v_\Phi/(2\sqrt{6}) \text{ diag}(1, 1, 1, -3)$, the coupling $\Omega^{ab}\Phi_b^c\epsilon_{acdf}\omega^{df}$ is allowed, as well as a bare mass term, and the $\textcolor{red}{D}'\textcolor{red}{D}'^c$ mass becomes $(M_\omega + v_\Phi/\sqrt{6})$, and $d^c - D$ entry will be now $(M_\omega - v_\Phi/\sqrt{6})$. In this case, $d^c - D^c$ mixing may even vanish.

Among these three, only the third term $\tilde{\psi}\tilde{\psi}^c\tilde{\chi}^*$ will get induced in the presence of the term soft Z_2 breaking $M_\omega\Omega\omega$. This can be seen by the induced trilinear term shown in Fig. 1 which is log-divergent. Therefore, we must allow this term in the Lagrangian. On the other hand, the terms $M_\chi\chi\chi$ and $M_\chi^2\tilde{\chi}\tilde{\chi}$ will not be induced through $M_\omega\Omega\omega$ coupling. We can think of M_ω as arising from the VEV of a spurion field $(1,1,15)_H$ through the coupling $\Omega\omega(1,1,15)_H$. But this putative Higgs cannot couple to $\chi\chi$ or $\tilde{\chi}\tilde{\chi}$. Thus, it is consistent to consider only the soft breaking term $\mu\tilde{\psi}\tilde{\psi}^c\tilde{\chi}^*$ in the Lagrangian, along with the $M_\omega\Omega\omega$ mass term. To summarize, the soft Z_2 breaking Lagrangian is taken to be

$$\mathcal{L}_{\text{soft}} = M_\omega\Omega\omega + \mu\tilde{\psi}\tilde{\psi}^c\tilde{\chi}^* + \text{h.c.} \quad (2.33)$$

To get an estimate of the order of magnitude for the coefficient μ in Eq. (2.33) we evaluate the log-divergent correction from Fig. 1, which is found to be

$$\mu \approx \frac{3}{16\pi^2} \text{Tr} \left(Y_u Y_D^\dagger M_\omega Y_d^\dagger \right) \left(\ln \frac{\Lambda^2}{M_D^2} \right), \quad (2.34)$$

where 3 is the color factor. With the assumption that the cut-off scale for the theory is $\Lambda \sim 10^{11}$ GeV, $Y_{\text{top}} \sim Y_D \sim 1$, $Y_{\text{bottom}} \sim 1.6 \times 10^{-2}$, $M_D \sim 6.3$ TeV, $M_\omega \sim 1.3$ TeV, Eq. (2.34) yields

$$\mu \sim 13 \text{ GeV}. \quad (2.35)$$

We may translate this naturalness bound on μ into a constraint on the induced vacuum expectation value $\langle \tilde{\nu} \rangle = \textcolor{red}{w}$ using $\mu_{\tilde{\chi}} \sim 10$ TeV for the mass of the corresponding scalar:

$$\textcolor{red}{w} = \frac{\mu\kappa_L\kappa_R}{\mu_{\tilde{\chi}}^2} \sim 100 \text{ MeV}. \quad (2.36)$$

Here, we have used $\kappa_R \geq 6.3$ TeV using the limit $M_{Z'} \geq 5.6$ TeV, see Fig. 5.

2.5 Neutrino mass generation

With the choice of N being Z_2 odd (see Table 1), we can write down the Yukawa couplings involving N :

$$\mathcal{L}_{\text{Yuk}}^N = Y_{\nu_E} \psi_{\alpha i} \tilde{\psi}^{*\alpha i} N + Y_{\nu^c} (\psi^c)_{\dot{\alpha}}^i (\tilde{\psi}^c)_i^{*\dot{\alpha}} N + Y_\nu \chi_{\alpha\dot{\alpha}} (\tau_2 \tilde{\chi}^* \tau_2)_{\beta\dot{\beta}} N \epsilon^{\alpha\beta} \epsilon^{\dot{\alpha}\dot{\beta}} + \frac{1}{2} M_N N^2 + \text{h.c.} \quad (2.37)$$

Expanding in component form, this becomes

$$\begin{aligned} \mathcal{L}_{\text{Yuk}}^N = & Y_{\nu_E} (u\tilde{u}^* + \nu_E\tilde{\nu}_E^* + d\tilde{d}^* + E\tilde{E}^*) N + Y_{\nu^c} (u^c\tilde{u}^{c*} + \nu^c\tilde{\nu}_E^{c*} + D^c\tilde{D}^{c*} + e^c\tilde{e}^{c*}) N \\ & + Y_\nu (E^c\tilde{E}^{c*} + \nu_E^c\tilde{\nu}_E^{c*} + \nu\tilde{\nu}^* + e\tilde{e}^*) N + \frac{1}{2} M_N N^2 + \text{h.c.} \end{aligned} \quad (2.38)$$

The term $\chi_{\alpha\dot{\alpha}} \tilde{\chi}_{\beta\dot{\beta}} N \epsilon^{\alpha\beta} \epsilon^{\dot{\alpha}\dot{\beta}}$ is absent here because it would be a hard breaking of Z_2 by a dimension four operator. Collecting terms from Eq. (2.14) and Eq. (2.38), we can write down the neutral lepton mass matrix in the basis $(\nu, \nu_E, \nu_E^c, \nu^c, N)$ as:

$$M_\nu = \begin{pmatrix} 0 & \mathcal{B} \\ \mathcal{B}^T & \mathcal{H} \end{pmatrix} \quad (2.39)$$

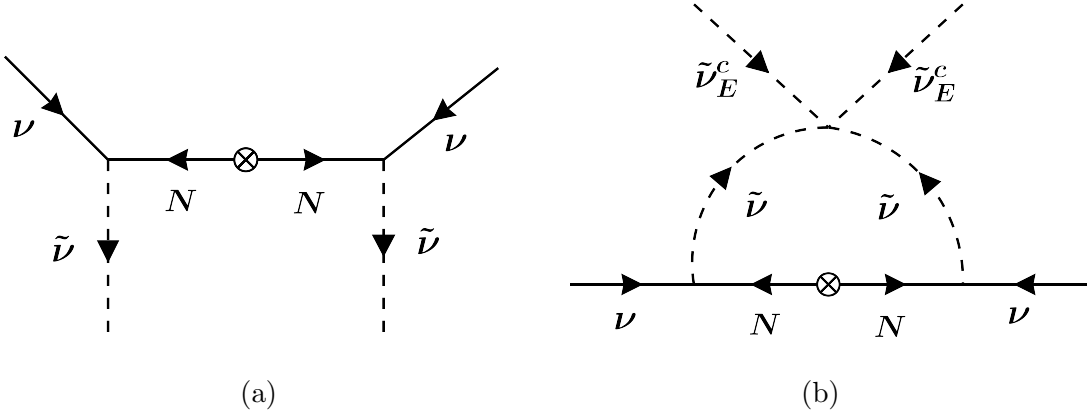


Figure 2: (a) Tree-level neutrino mass through seesaw diagram, (b) One-loop neutrino mass through Scotogenic-type diagram.

with

$$\mathcal{B} = (0 \ 0 \ 0 \ Y_\nu \mathbf{w}^*), \quad \mathcal{H} = \begin{pmatrix} 0 & -Y_E \kappa_R & -Y_u v & Y_{\nu_E} \kappa_L \\ -Y_E^T \kappa_R & 0 & -Y_e^T \kappa_L & Y_\nu v^* \\ -Y_u^T v & -Y_e^T \kappa_L & 0 & Y_{\nu^c} \kappa_R \\ Y_{\nu_E}^T \kappa_L & Y_\nu^T v^* & Y_{\nu^c}^T \kappa_R & M_N \end{pmatrix}. \quad (2.40)$$

Integrating out the heavy block \mathcal{H} [37, 38] one would get the tree-level light neutrino mass matrix as

$$m_\nu^{\text{tree}} = -\mathcal{B} \mathcal{H}^{-1} \mathcal{B}^T = -(Y_\nu \mathbf{w}^*) [\mathcal{H}^{-1}]_{NN} (Y_\nu \mathbf{w}^*)^T. \quad (2.41)$$

To calculate the closed form expression for $[\mathcal{H}^{-1}]_{NN}$, let's partition \mathcal{H} into 2×2 blocks by grouping (ν_E, ν_E^c) and (ν^c, N) :

$$\mathcal{H} = \begin{pmatrix} \underline{A} & \underline{C} \\ \underline{C}^T & \underline{D} \end{pmatrix}. \quad (2.42)$$

With the assumption that $Y_E \kappa_R$ is invertible, the Schur complement can be written as²

$$\underline{S} \equiv \underline{D} - \underline{C}^T \underline{A}^{-1} \underline{C} = \begin{pmatrix} s_{11} & s_{12} \\ s_{21} & s_{22} \end{pmatrix} \quad (2.43)$$

which gives

$$[\mathcal{H}^{-1}]_{NN} = (\underline{S}^{-1})_{22} = (s_{22} - s_{21} s_{11}^{-1} s_{12})^{-1}. \quad (2.44)$$

²For the inverse of a 2×2 block matrix, assuming that the (1,1) block is non-singular, we can implement the following recipe [39]:

$$\begin{pmatrix} A & B \\ C & D \end{pmatrix}^{-1} = \begin{pmatrix} A^{-1} + A^{-1} B S^{-1} C A^{-1} & -A^{-1} B S^{-1} \\ -S^{-1} C A^{-1} & S^{-1} \end{pmatrix}$$

where the Schur complement $S = D - C A^{-1} B$ of A is invertible.

With the definition $E \equiv Y_E \kappa_R$, the block multiplication leads to the relations

$$s_{11} = v \kappa_L \left(Y_u^T (\underline{E}^{-1})^T Y_e^T + Y_e \underline{E}^{-1} Y_u \right), \quad (2.45)$$

$$s_{12} = Y_{\nu^c} \kappa_R + |v|^2 Y_u^T (\underline{E}^{-1})^T Y_\nu + \kappa_L^2 Y_e \underline{E}^{-1} Y_{\nu_E}, \quad (2.46)$$

$$s_{21} = s_{12}^T, \quad (2.47)$$

$$s_{22} = M_N + \kappa_L v^* \left(Y_{\nu_E}^T (\underline{E}^{-1})^T Y_\nu + Y_\nu^T \underline{E}^{-1} Y_{\nu_E} \right). \quad (2.48)$$

In the hierarchical limit $\kappa_R \gg \kappa_L, v$, the (ν_E, ν_E^c) block dominates the heavy sector. Let's define,

$$\underline{X} \equiv Y_e Y_E^{-1} Y_u, \quad \underline{S}_0 \equiv \underline{X} + \underline{X}^T. \quad (2.49)$$

Then from Eq. (2.45), we see that $s_{11} = \frac{v \kappa_L}{\kappa_R} \underline{S}_0$, while $s_{12} \approx Y_{\nu^c} \kappa_R$ and $s_{22} = M_N + \mathcal{O}(\kappa_L v^* / \kappa_R)$. Keeping the leading term in $v/\kappa_R, \kappa_L/\kappa_R$ we find from Eq. (2.44)

$$[\mathcal{H}^{-1}]_{NN} \simeq \frac{v \kappa_L}{\kappa_R^3} \left(Y_{\nu^c}^T \underline{S}_0^{-1} Y_{\nu^c} \right)^{-1} \quad (2.50)$$

Here, the explicit M_N dependence is sub-leading provided that $M_N \ll \kappa_R^3 / (v \kappa_L)$ after the Yukawa factors have been accounted for. In this controlled limit, we see a “triple seesaw” structure for neutrino mass:

$$m_\nu^{\text{tree}} \simeq \frac{v \kappa_L}{\kappa_R^3} (Y_\nu \textcolor{magenta}{w}^*) \left(Y_{\nu^c}^T \underline{S}_0^{-1} Y_{\nu^c} \right)^{-1} (Y_\nu \textcolor{magenta}{w}^*)^T. \quad (2.51)$$

The effective operator that generates this mass is of dimension-seven, given as $(LLHH)(H^\dagger H)$ [40]. Thus, we can write down the light neutrino mass matrix in terms of the original matrices explicitly as

$$m_\nu^{\text{tree}} \simeq \frac{v \kappa_L}{\kappa_R^3} (Y_\nu \textcolor{magenta}{w}^*) Y_{\nu^c}^{-1} \left[Y_e Y_E^{-1} Y_u + Y_u^T (Y_E^{-1})^T Y_e^T \right] (Y_{\nu^c}^T)^{-1} (Y_\nu \textcolor{magenta}{w}^*)^T. \quad (2.52)$$

We note in passing that in the opposite limit where $M_N \gg \kappa_R^3 / (v \kappa_L)$, the neutrino mass matrix takes the form $m_\nu^{\text{tree}} \approx -(Y_\nu \textcolor{magenta}{w}^*) M_N^{-1} (Y_\nu \textcolor{magenta}{w}^*)^T$. This is a dimension-five operator shown in Fig. 2 (a). However, in this limit, the mass of the right-handed neutrino states ν^c will be well below the electroweak scale, which we wish to avoid in our setup.

We now present a benchmark point that gives the right order of magnitude of the neutrino masses from m_ν^{tree} given in Eq. (2.52):

$$\text{Input : } \kappa_R = 7 \text{ TeV}, \quad \kappa_L = v = 123 \text{ GeV}, \quad \textcolor{magenta}{w} = 0.1 \text{ GeV},$$

$$Y_\nu = 0.24, \quad Y_e = 10^{-2}, \quad Y_E^{-1} = 1, \quad Y_u = 1, \quad Y_{\nu^c} = 0.10,$$

$$\text{Output : } m_\nu^{\text{tree}} \approx 5 \times 10^{-2} \text{ eV}.$$

Radiative (scotogenic-type) neutrino mass: The tree-level contribution to neutrino mass shown in Eq. (2.52) is proportional to $\textcolor{magenta}{w}^2$, where $\textcolor{magenta}{w} \sim 100$ MeV. There are also one-loop corrections to the neutrino mass from the diagram shown in Fig. 2(b). These loop corrections are independent of the small VEV $\textcolor{magenta}{w}$ and can be comparable to or exceed the tree-level mass. Here we evaluate these loop-induced neutrino masses in the limit of neglecting $\textcolor{magenta}{w}$. In this limit,

the discrete Z_2 symmetry is unbroken, and the diagram shown in Fig. 2 (b) is analogous to the radiative neutrino mass generation in the Scotogenic model [15, 16].

The scalar field that couples with the external ν line in Fig. 2(b) is $\tilde{\nu}$ which is Z_2 -odd (see Table 1), which does not mix with the other neutral scalars in the limit of setting w to zero. The real and imaginary components of the $\tilde{\nu}$ will acquire slightly different masses from the quartic couplings in the Higgs potential. We define their mass splitting as

$$m_{R,a}^2 = m_a^2 + \frac{1}{2}\Delta m_a^2, \quad m_{I,a}^2 = m_a^2 - \frac{1}{2}\Delta m_a^2. \quad (2.53)$$

Δm_a^2 is small since the splitting is proportional to v^2 , while the $\tilde{\nu}$ is in the multi-TeV range. To evaluate the loop diagrams we choose a basis where the mass matrix for the N fields, M_N , is real and diagonal. The radiatively induced neutrino mass is found to be

$$(m_\nu^{\text{loop}})_{\alpha\beta} \simeq \frac{1}{16\pi^2} \sum_k (Y_\nu)_{\alpha k} (Y_\nu)_{\beta k} M_{N_k} \frac{\Delta m^2}{m^2 - M_{N_k}^2} \left[1 - \frac{M_{N_k}^2}{m^2 - M_{N_k}^2} \ln \frac{m^2}{M_{N_k}^2} \right]. \quad (2.54)$$

with $m = m_{\tilde{\nu}}$, and $\Delta m^2 = \Delta m_{\tilde{\nu}}^2$ is defined in Eq. (2.53).

We present a benchmark point where the right order of magnitude for the neutrino mass arises from the loop corrections.

$$\text{Input : } \kappa_R = 7 \text{ TeV}, \quad \kappa_L = 123 \text{ GeV}, \quad v = 123 \text{ GeV}, \quad w = 0 \text{ GeV},$$

$$m = 1.5 \text{ TeV}, \quad M_N = 1.0 \text{ TeV}, \quad Y_\nu = 0.1, \quad (Y_\nu V_N)_{\alpha k} (Y_\nu V_N)_{\beta k} \sim 0.01.$$

$$\text{Output : } m_\nu^{\text{loop}} \approx 5 \times 10^{-2} \text{ eV}, \quad (2.55)$$

with a modest CP-even/odd splitting of $\Delta m = 0.05$ GeV.

This analysis shows that naturally small neutrino masses can be generated in the model even with the PS breaking scale being in the multi-TeV range. The mass generation mechanism may be either tree-level $d = 7$ operator, or loop-induced $d = 5$ operator, or a combination of the two.

2.6 Gauge Sector

Now we turn to the masses of the various gauge bosons in the model.

2.6.1 Charged Gauge Boson Masses

The kinetic terms for each scalar field are given by:

$$\mathcal{L}_{\text{kin}}^S = \text{Tr} \left[(D_\mu \tilde{\psi})^\dagger (D^\mu \tilde{\psi}) + (D_\mu \tilde{\psi}^c)^\dagger (D^\mu \tilde{\psi}^c) + (D_\mu \tilde{\chi})^\dagger (D^\mu \tilde{\chi}) \right]. \quad (2.56)$$

The covariant derivatives are defined as:

$$\begin{aligned} D_\mu \tilde{\psi}^{\alpha i} &= \partial_\mu \tilde{\psi}^{\alpha i} - ig_L (W_{L\mu}^b \frac{\sigma^b}{2})_\beta^\alpha \tilde{\psi}^{\beta i} - ig_4 (G_\mu^d \frac{T_4^d}{2})_i^\alpha \tilde{\psi}^{\alpha\gamma} \\ D_\mu (\tilde{\psi}^c)_i^{\dot{\alpha}} &= \partial_\mu (\tilde{\psi}^c)_i^{\dot{\alpha}} - ig_R (W_{R\mu}^b \frac{\sigma^b}{2})_{\dot{\beta}}^{\dot{\alpha}} (\tilde{\psi}^c)_i^{\dot{\beta}} + ig_4 (G_\mu^d \frac{T_4^d}{2})_i^{\dot{\gamma}} (\tilde{\psi}^c)_\gamma^{\dot{\alpha}} \\ D_\mu \tilde{\chi}^{\alpha\dot{\alpha}} &= \partial_\mu \tilde{\chi}^{\alpha\dot{\alpha}} - ig_L (W_{L\mu}^b \frac{\sigma^b}{2})_\beta^\alpha \tilde{\chi}^{\beta\dot{\alpha}} - ig_R (W_{R\mu}^b \frac{\sigma^b}{2})_{\dot{\beta}}^{\dot{\alpha}} \tilde{\chi}^{\alpha\dot{\beta}}. \end{aligned} \quad (2.57)$$

Here, $b = 1 - 3$ runs over $SU(2)_{L/R}$ generators, while $d = 1 - 15$ runs over $SU(4)_C$ generators. The indices α , $\dot{\alpha}$, and i , respectively, denote the indices for $SU(2)_L$, $SU(2)_R$, and $SU(4)_C$. The charged gauge bosons $W_{L\mu}^\pm$ and $W_{R\mu}^\pm$ mix, with the mixing angle being proportional to the soft Z_2 breaking term, and their mass matrix is given by:

$$M_{W-W'}^2 = \begin{pmatrix} \frac{1}{2}g_L^2(\kappa_L^2 + v^2 + \textcolor{red}{w}^2) & g_L g_R v \textcolor{red}{w} \\ \bullet & \frac{1}{2}g_R^2(\kappa_R^2 + v^2 + \textcolor{red}{w}^2) \end{pmatrix}. \quad (2.58)$$

We can define the physical states as,

$$W_1^{\mu\pm} = \cos \zeta W^{\mu\pm} - \sin \zeta W'^{\mu\pm}, \quad W_2 = \sin \zeta W^{\mu\pm} + \cos \zeta W'^{\mu\pm},$$

with the mixing angle ζ given by

$$\tan 2\zeta = \frac{4g_L g_R v \textcolor{red}{w}}{g_R^2(k_R^2 + v^2 + \textcolor{red}{w}^2) - g_L^2(k_L^2 + v^2 + \textcolor{red}{w}^2)}. \quad (2.59)$$

Their mass eigenvalues are given by

$$M_{W_1^{\mu\pm}}^2 \simeq \frac{1}{2}g_L^2(\kappa_L^2 + v^2 + \textcolor{red}{w}^2), \quad (2.60)$$

$$M_{W_2^{\mu\pm}}^2 \simeq \frac{1}{2}g_R^2(\kappa_R^2 + v^2 + \textcolor{red}{w}^2). \quad (2.61)$$

With $\textcolor{red}{w} = 0$, $W_1^{\mu\pm}$ is identified as the W boson.

The mass of the leptoquark gauge boson $X_\mu(3, 1, \frac{2}{3})$ is given by

$$M_{X_\mu}^2 = \frac{1}{2}g_4^2(\kappa_L^2 + \kappa_R^2). \quad (2.62)$$

2.6.2 Neutral Gauge Boson Masses

The neutral gauge bosons associated with the diagonal generators of $SU(2)_L$, $SU(2)_R$, and $SU(4)_C$ are denoted as $W_{\mu L}^0$, $W_{\mu R}^0$, and G_μ^{15} , respectively. These gauge fields will mix and produce the massless photon field A_μ , while the other two orthogonal states $Z_{\mu L}$ and $Z_{\mu R}$ will further mix. The corresponding mass-squared matrix in the basis $(W_{\mu L}^0, W_{\mu R}^0, G_\mu^{15})$ reads as

$$M_0^2 = \begin{pmatrix} \frac{1}{2}g_L^2(\kappa_L^2 + v^2 + \textcolor{red}{w}^2) & -\frac{1}{2}g_L g_R(v^2 + \textcolor{red}{w}^2) & -\sqrt{\frac{3}{8}}g_4 g_L \kappa_L^2 \\ \bullet & \frac{1}{2}g_R^2(\kappa_R^2 + v^2 + \textcolor{red}{w}^2) & -\sqrt{\frac{3}{8}}g_4 g_R \kappa_R^2 \\ \bullet & \bullet & \frac{3}{4}g_4^2(\kappa_L^2 + \kappa_R^2) \end{pmatrix}. \quad (2.63)$$

where ‘•’ represents the symmetric elements. The compositions of these fields, expressed in a suitable basis, take the form:

$$A_\mu = \frac{\sqrt{3}g_4 g_R W_{\mu L}^0 + \sqrt{3}g_4 g_L W_{\mu R}^0 + \sqrt{2}g_L g_R G_\mu^{15}}{\sqrt{2g_L^2 g_R^2 + 3g_4^2(g_L^2 + g_R^2)}}, \quad (2.64)$$

$$Z_\mu = \frac{g_L(3g_4^2 + 2g_R^2)W_{\mu L}^0 - 3g_4^2 g_R W_{\mu R}^0 - \sqrt{6}g_R^2 g_4 G_\mu^{15}}{\sqrt{(3g_4^2 + 2g_R^2)(2g_L^2 g_R^2 + 3g_4^2(g_L^2 + g_R^2))}}, \quad (2.65)$$

$$Z'_\mu = \frac{-\sqrt{2}g_R W_{\mu R}^0 + \sqrt{3}g_4 G_\mu^{15}}{\sqrt{3g_4^2 + 2g_R^2}}. \quad (2.66)$$

In this basis, the photon field decouples from other gauge fields, leading to a 2×2 mass-mixing matrix B^2 for $Z - Z'$ which reads as:

$$M_{Z-Z'}^2 = \frac{1}{2} \begin{pmatrix} (g_L^2 + g_Y^2) (\kappa_L^2 + v^2 + \textcolor{red}{w}^2) & \sqrt{\frac{g_L^2 + g_Y^2}{g_R^2 - g_Y^2}} ((v^2 + \textcolor{red}{w}^2) (g_R^2 - g_Y^2) - g_Y^2 \kappa_L^2) \\ \bullet & \frac{(v^2 + \textcolor{red}{w}^2) (g_R^2 - g_Y^2)^2 + g_Y^4 \kappa_L^2 + g_R^4 \kappa_R^2}{g_R^2 - g_Y^2} \end{pmatrix}. \quad (2.67)$$

Here we have traded g_4 in favor of g_Y using the following coupling matching condition

$$\frac{1}{g_Y^2} = \frac{1}{g_R^2} + \frac{2}{3} \frac{1}{g_4^2}. \quad (2.68)$$

The physical states can be written as

$$Z = \cos \xi Z_L - \sin \xi Z_R, \quad Z' = \sin \xi Z_L + \cos \xi Z_R. \quad (2.69)$$

with the small mixing angle ξ given approximately by

$$\xi \simeq \frac{((g_R^2 - g_Y^2) (v^2 + \textcolor{red}{w}^2) - g_Y^2 \kappa_L^2)}{g_R^4 \kappa_R^2} \sqrt{(g_L^2 + g_Y^2) (g_R^2 - g_Y^2)}. \quad (2.70)$$

The mass eigenvalues of Z and Z' are given by

$$M_Z^2 \simeq \frac{1}{2} (g_L^2 + g_Y^2) (\kappa_L^2 + v^2 + \textcolor{red}{w}^2), \quad (2.71)$$

$$M_{Z'}^2 \simeq \frac{1}{2} \frac{(v^2 + \textcolor{red}{w}^2) (g_R^2 - g_Y^2)^2 + g_Y^4 \kappa_L^2 + g_R^4 \kappa_R^2}{g_R^2 - g_Y^2}. \quad (2.72)$$

With small ξ , Z is identified as the SM Z boson.

To get the relations among the gauge boson masses, we solve the two-loop renormalization group equations for the gauge couplings within the SM:

$$\mu \frac{dg_i}{d\mu} = \frac{1}{(4\pi)^2} \beta_{g_i}^{(1)} + \frac{1}{(4\pi)^4} \beta_{g_i}^{(2)}. \quad (2.73)$$

Since the new particles present in the model lie around or above the PS breaking scale, they do not contribute to the running of the gauge couplings below the scale of PS symmetry breaking. Thus, we include the two-loop beta functions in the SM given as

$$\beta_{g_i}^{(1)} = b_i [g_i(\mu)]^3, \quad (2.74)$$

$$\beta_{g_i}^{(2)} = g_i^3(\mu) \left[\sum_j b_{ij} g_j^2(\mu) - C_{iu} \text{Tr}(Y_u Y_u^\dagger) - C_{id} \text{Tr}(Y_d Y_d^\dagger) - C_{ie} \text{Tr}(Y_e Y_e^\dagger) \right]. \quad (2.75)$$

with b_i , b_{ij} , $C_{i(u,d,e)}$ are the SM two-loop coefficients (summarized in appendix A) and Y_u , Y_d , Y_e are the SM Yukawa matrices. g_1 has the usual $SU(5)$ normalization $g_1^2 = (5/3)g_Y^2$. The PS gauge couplings are related to the SM gauge couplings at the PS breaking scale (μ_{PS}) by the following matching conditions:

$$g_L^2(\mu_{\text{PS}}) = g_2^2(\mu_{\text{PS}}), \quad g_R^2(\mu_{\text{PS}}) = \frac{3g_Y^2(\mu_{\text{PS}})g_3^2(\mu_{\text{PS}})}{3g_3^2(\mu_{\text{PS}}) - 2g_Y^2(\mu_{\text{PS}})}, \quad g_4^2(\mu_{\text{PS}}) = g_3^2(\mu_{\text{PS}}). \quad (2.76)$$

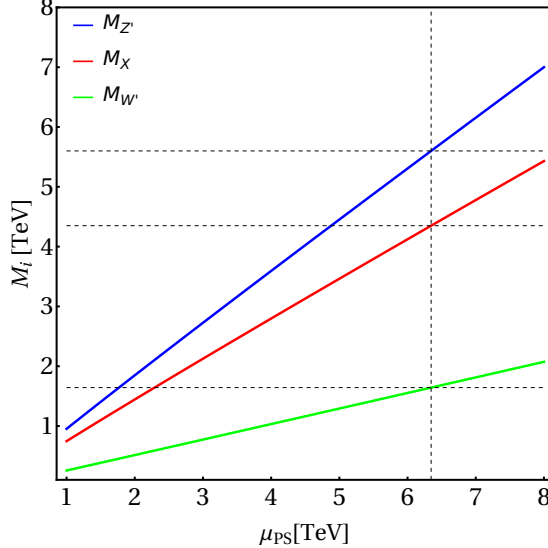


Figure 3: Masses of the heavy gauge bosons for different choices of the Pati–Salam breaking scale μ_{PS} . The curves for $M_{W'}$, M_X , and $M_{Z'}$ are obtained numerically from Eqs. (2.61), (2.62), and (2.72) respectively, using gauge couplings fixed by the matching conditions in Eq. (2.76) and by running the Standard Model gauge couplings up to μ_{PS} with their renormalization group equations as discussed in Sec. 2.6.2. The horizontal dashed line at 5.6 TeV corresponds to the lower limit on the Z' mass from LHC constraints on the $Z' \rightarrow \ell\bar{\ell}$ process (see Sec. 3). This collider constraint on $M_{Z'}$ indirectly sets the lower bounds on the masses of X_μ and W'_μ .

With these considerations, we show in Fig. 3 the interplay of the heavy gauge boson masses due to the presence of a single $(1, 2, \bar{4})$ Higgs VEV, κ_R . The neutral gauge boson, Z' , is heavier ($M_{Z'} > M_X > M_{W'}$) than the charged ones due to the additional mixing effects occurring in the neutral sector. If we take the limit on the mass of Z' from LHC for our setup (see Fig. 5), which is $M_{Z'} \approx 5.6$ TeV, that immediately puts a lower limit on M_X and $M_{W'}$ given by $M_X \geq 4.3$ TeV and $M_{W'} \geq 1.8$ TeV. Later, we will see that this LHC limit on $M_{Z'}$ is the most stringent bound on the mass of the leptoquark gauge boson X_μ in the model.

2.7 Higgs Sector

Now we turn to the symmetry-breaking sector of the theory. One of the goals here is to establish the consistency of the two-step symmetry breaking. The most general renormalizable potential involving the $(\tilde{\psi}, \tilde{\psi}^c, \tilde{\chi})$ fields can be written as:

$$\begin{aligned}
V = & -\mu_L^2 \tilde{\psi}_{\alpha i} \tilde{\psi}^{\alpha i} - \mu_R^2 (\tilde{\psi}^c)_i^{\dot{\alpha}} (\tilde{\psi}^c)_i^{\dot{\alpha}} - \mu_{\tilde{\chi}}^2 \tilde{\chi}_{\alpha \dot{\alpha}} \tilde{\chi}^{\alpha \dot{\alpha}} + \lambda_{L1} (\tilde{\psi}_{\alpha i} \tilde{\psi}^{\alpha i})^2 + \lambda_{R1} ((\tilde{\psi}^c)_i^{\dot{\alpha}} (\tilde{\psi}^c)_i^{\dot{\alpha}})^2 \\
& + \lambda_{\chi_1} (\tilde{\chi}_{\alpha \dot{\alpha}} \tilde{\chi}^{\alpha \dot{\alpha}})^2 + \lambda_{L2} \tilde{\psi}_{\alpha i} \tilde{\psi}^{\alpha j} \tilde{\psi}_{\beta j} \tilde{\psi}^{\beta i} + \lambda_{R2} (\tilde{\psi}^c)_i^{\dot{\alpha}} (\tilde{\psi}^c)_j^{\dot{\beta}} (\tilde{\psi}^c)_j^{\dot{\beta}} (\tilde{\psi}^c)_i^{\dot{\alpha}} \\
& + \lambda_{LR1} \tilde{\psi}_{\alpha i} \tilde{\psi}^{\alpha j} (\tilde{\psi}^c)_j^{\dot{\alpha}} (\tilde{\psi}^c)_i^{\dot{\alpha}} + \lambda_{LR2} \tilde{\psi}_{\alpha i} \tilde{\psi}^{\alpha i} (\tilde{\psi}^c)_i^{\dot{\alpha}} (\tilde{\psi}^c)_j^{\dot{\alpha}} + \lambda_{L\chi_1} \tilde{\chi}_{\alpha \dot{\alpha}} \tilde{\chi}^{\alpha \dot{\alpha}} \tilde{\psi}_{\beta i} \tilde{\psi}^{\beta i} \\
& + \lambda_{R\chi_1} \tilde{\chi}_{\alpha \dot{\alpha}} \tilde{\chi}^{\alpha \dot{\alpha}} (\tilde{\psi}^c)_i^{\dot{\beta}} (\tilde{\psi}^c)_i^{\dot{\beta}} + \lambda_{L\chi_2} \tilde{\psi}_{\alpha i} \tilde{\psi}^{\beta \dot{\alpha}} \tilde{\chi}^{\beta \dot{\alpha}} \tilde{\chi}_{\alpha \dot{\alpha}} + \lambda_{R\chi_2} (\tilde{\psi}^c)_i^{\dot{\alpha}} (\tilde{\psi}^c)_i^{\dot{\beta}} \tilde{\chi}^{\alpha \dot{\beta}} \tilde{\chi}_{\alpha \dot{\alpha}} \\
& + \lambda_{\chi_2} ((\tilde{\chi}_{\alpha \dot{\alpha}} \epsilon^{\alpha \beta} \tilde{\chi}_{\beta \dot{\alpha}} \epsilon^{\dot{\beta} \dot{\alpha}})^2 + \text{h.c.}) + \lambda_{\chi_3} \tilde{\chi}_{\alpha \dot{\alpha}} \epsilon^{\alpha \beta} \tilde{\chi}_{\beta \dot{\beta}} \epsilon^{\dot{\beta} \dot{\alpha}} \epsilon_{\gamma \delta} \tilde{\chi}^{\delta \dot{\delta}} \epsilon_{\dot{\delta} \dot{\gamma}} \tilde{\chi}^{\gamma \dot{\gamma}} \\
& + (\rho \tilde{\psi}^{\alpha i} \epsilon_{\alpha \beta} \tilde{\chi}^{\beta \dot{\beta}} \epsilon_{\dot{\beta} \dot{\alpha}} (\tilde{\psi}^c)_i^{\dot{\alpha}} + \text{h.c.}) + (\mu \tilde{\psi}^{\alpha i} \tilde{\chi}_{\alpha \dot{\alpha}} (\tilde{\psi}^c)_i^{\dot{\alpha}} + \text{h.c.}) \tag{2.77}
\end{aligned}$$

Here, we have used the notation $\tilde{\psi}^{\alpha i} = (\tilde{\psi}^*)_{\alpha i}$; $(\tilde{\psi}^c)_i^{\dot{\alpha}} = ((\tilde{\psi}^c)^*)_{\dot{\alpha}}^i$ and $\tilde{\chi}^{\alpha \dot{\alpha}} = (\tilde{\chi}^*)_{\alpha \dot{\alpha}}$. The parameters ρ and μ are complex in general. One of these, which we take to be ρ , can be made real by field redefinitions, in which case the other (μ) will remain complex. Since this is a small parameter that breaks Z_2 symmetry softly with its value estimated in Eq. (2.35), its complexity will have little effect on the Higgs boson spectrum. Therefore, for simplicity, we take μ and ρ to be real.

Among the 40 real degrees of freedom – 16 come from the $SU(2)_L$ doublet $\tilde{\psi}$, 16 from the $SU(2)_R$ doublet $\tilde{\psi}^c$, and 8 from the bi-doublet $\tilde{\chi}$ – 28 fields get mass, while the remaining 12 fields are Nambu-Goldstone modes absorbed by the 12 massive gauge bosons. To determine the Higgs mass spectrum, it is necessary to consider small oscillations around the true vacuum. We choose to eliminate $\mu_L^2, \mu_R^2, \mu_{\tilde{\chi}}^2$ and ρ in favor of the VEVs given in Eq. (2.11) through the extrema conditions:

$$\begin{aligned} \mu_L^2 = & 2(\lambda_{L1} + \lambda_{L2})\kappa_L^2 + \frac{v^2}{\kappa_L^2} (\lambda_{R\chi_2}\kappa_R^2 - 4(2\lambda_{\chi_2} - \lambda_{\chi_3})(v^2 - \textcolor{red}{w}^2)) + \frac{\mu}{\textcolor{red}{w}} \frac{\kappa_R}{\kappa_L} (v^2 + \textcolor{red}{w}^2) \\ & + (\lambda_{LR1} + \lambda_{LR2})\kappa_R^2 + (\lambda_{L\chi_1} + \lambda_{L\chi_2})(v^2 + \textcolor{red}{w}^2), \end{aligned} \quad (2.78)$$

$$\begin{aligned} \mu_R^2 = & 2(\lambda_{R1} + \lambda_{R2})\kappa_R^2 + \frac{v^2}{\kappa_R^2} (\lambda_{L\chi_2}\kappa_L^2 - 4(2\lambda_{\chi_2} - \lambda_{\chi_3})(v^2 - \textcolor{red}{w}^2)) + \frac{\mu}{\textcolor{red}{w}} \frac{\kappa_L}{\kappa_R} (v^2 + \textcolor{red}{w}^2) \\ & + (\lambda_{LR1} + \lambda_{LR2})\kappa_L^2 + (\lambda_{R\chi_1} + \lambda_{R\chi_2})(v^2 + \textcolor{red}{w}^2), \end{aligned} \quad (2.79)$$

$$\begin{aligned} \mu_{\tilde{\chi}}^2 = & (\lambda_{L\chi_1} + \lambda_{L\chi_2})\kappa_L^2 + (\lambda_{R\chi_1} + \lambda_{R\chi_2})\kappa_R^2 + 2\lambda_{\chi_1}(v^2 + \textcolor{red}{w}^2) - 4(2\lambda_{\chi_2} - \lambda_{\chi_3})v^2 + \frac{\mu}{\textcolor{red}{w}} \kappa_L \kappa_R, \end{aligned} \quad (2.80)$$

$$\rho = \left(\lambda_{L\chi_2} \frac{\kappa_L}{\kappa_R} + \lambda_{R\chi_2} \frac{\kappa_R}{\kappa_L} + \frac{\mu}{\textcolor{red}{w}} \right) v - 4(2\lambda_{\chi_2} - \lambda_{\chi_3}) \frac{v}{\kappa_L \kappa_R} (v^2 - \textcolor{red}{w}^2). \quad (2.81)$$

With these conditions, we derive the mass spectrum of all scalars by taking the second derivatives of the potential with respect to the fields. Our results are summarized below, sector by sector.

Leptoquark scalars with $\pm 2/3$ charge: The $SU(3)$ fundamental and Z_2 odd up-type charged leptoquark fields, $\tilde{u}(\tilde{u}^c)$, coming from $\tilde{\psi}(\tilde{\psi}^c)$, have the following mixing matrix in the $(\tilde{u}, (\tilde{u}^c)^*)$ basis:

$$M_{\tilde{u}}^2 = A_{\tilde{u}} \begin{pmatrix} 1 & -\frac{\kappa_L}{\kappa_R} \\ -\frac{\kappa_L}{\kappa_R} & \frac{\kappa_L^2}{\kappa_R^2} \end{pmatrix}. \quad (2.82)$$

Here we have defined

$$A_{\tilde{u}} = \frac{v^2}{\kappa_L^2} (4(2\lambda_{\chi_2} - \lambda_{\chi_3})(v^2 - \textcolor{red}{w}^2) - \lambda_{R\chi_2}\kappa_R^2) - \frac{\mu}{\textcolor{red}{w}} \frac{\kappa_R}{\kappa_L} (v^2 + \textcolor{red}{w}^2) - \lambda_{LR1}\kappa_R^2 - \lambda_{L\chi_2}v^2. \quad (2.83)$$

The physical state and its mass is given by

$$\phi_X = \frac{-\kappa_R \tilde{u} + \kappa_L (\tilde{u}^c)^*}{\sqrt{\kappa_L^2 + \kappa_R^2}}, \quad m_{\phi_X}^2 = A_{\tilde{u}} (1 + \kappa_L^2/\kappa_R^2) \quad (2.84)$$

while the orthogonal state, given by

$$G_X = \frac{\kappa_L \tilde{u} + \kappa_R (\tilde{u}^c)^*}{\sqrt{\kappa_L^2 + \kappa_R^2}} \quad (2.85)$$

corresponds to the Goldstone mode, which gets absorbed and becomes the longitudinal component of leptoquark gauge bosons X^μ .

Leptoquark scalars with $\pm 1/3$ charge: The colored $\pm 1/3$ charged Higgs field $\tilde{d}(\tilde{D}^c)$, coming from $\tilde{\psi}(\tilde{\psi}^c)$, has the following mixing matrix on the basis $(\tilde{d}, (\tilde{D}^c)^*)$:

$$M_{\tilde{d}}^2 = \begin{pmatrix} A_{\tilde{d}} & B_{\tilde{d}} \\ B_{\tilde{d}} & C_{\tilde{d}} \end{pmatrix}. \quad (2.86)$$

where

$$A_{\tilde{d}} = \frac{v^2}{\kappa_L^2} (4(2\lambda_{\chi_2} - \lambda_{\chi_3})(v^2 - \textcolor{red}{w}^2) - \lambda_{R\chi_2}\kappa_R^2) - \frac{\mu}{\textcolor{red}{w}} \frac{\kappa_R}{\kappa_L} (v^2 + \textcolor{red}{w}^2) - 2\lambda_{L2}\kappa_L^2 - \lambda_{LR1}\kappa_R^2 - \lambda_{L\chi_2}\textcolor{red}{w}^2. \quad (2.87)$$

$$B_{\tilde{d}} = -\frac{\textcolor{red}{w}v}{\kappa_L\kappa_R} (4(2\lambda_{\chi_2} - \lambda_{\chi_3})(v^2 - \textcolor{red}{w}^2) - \lambda_{R\chi_2}\kappa_R^2) + 2\mu v + \frac{\kappa_L}{\kappa_R} \lambda_{L\chi_2} \textcolor{red}{w}v \quad (2.88)$$

$$C_{\tilde{d}} = \frac{v^2}{\kappa_R^2} (4(2\lambda_{\chi_2} - \lambda_{\chi_3})(v^2 - \textcolor{red}{w}^2) - \lambda_{R\chi_2} \left(\frac{\textcolor{red}{w}^2}{v^2}\right) \kappa_R^2) - \frac{\mu}{\textcolor{red}{w}} \frac{\kappa_L}{\kappa_R} (v^2 + \textcolor{red}{w}^2) - 2\lambda_{R2}\kappa_R^2 - \lambda_{LR1}\kappa_L^2 - \lambda_{L\chi_2} \left(\frac{\kappa_L^2}{\kappa_R^2}\right) v^2. \quad (2.89)$$

Here \tilde{d} is Z_2 odd and \tilde{D}^c is Z_2 even, and the elements of the off-diagonal block depend on $\langle v \rangle = \textcolor{red}{w}$ as well as the parameter μ of the Z_2 soft-breaking Lagrangian of Eq. (2.32). Note that there is no Goldstone mode appearing from this sector.

Color singlet scalars with ± 1 charge: The Z_2 odd electron-type charged Higgs fields $\tilde{e}(\tilde{e}^c)$ originating from $\tilde{\chi}(\tilde{\psi}^c)$ and the Z_2 even electron-type charged Higgs fields $\tilde{E}(\tilde{E}^c)$ originating from $\tilde{\psi}(\tilde{\chi})$ mix, with the mass matrix is given in the $(\tilde{e}, (\tilde{e}^c)^*, \tilde{E}, (\tilde{E}^c)^*)$ as:

$$M_{\tilde{e}\tilde{E}}^2 = \begin{pmatrix} (m_{\tilde{e}}^2)_{2 \times 2} & (m_{\tilde{e}\tilde{E}}^2)_{2 \times 2} \\ \hline (m_{\tilde{e}\tilde{E}}^2)_{2 \times 2} & (m_{\tilde{E}}^2)_{2 \times 2} \end{pmatrix}. \quad (2.90)$$

The off-diagonal $(m_{\tilde{e}\tilde{E}}^2)_{2 \times 2}$ block arises from the mixing of the Z_2 even and odd sectors due to its soft breaking, and the various blocks have the following structures:

- The upper-half block:

$$m_{\tilde{e}}^2 = \begin{pmatrix} A_{\tilde{e}} & B_{\tilde{e}} \\ B_{\tilde{e}} & C_{\tilde{e}} \end{pmatrix}. \quad (2.91)$$

where

$$A_{\tilde{e}} = 4v^2(2\lambda_{\chi_2} - \lambda_{\chi_3}) - \lambda_{L\chi_2}\kappa_L^2 - \frac{\mu}{\textcolor{red}{w}}\kappa_L\kappa_R, \quad (2.92)$$

$$B_{\tilde{e}} = \frac{v}{\kappa_R} (4(2\lambda_{\chi_2} - \lambda_{\chi_3})(v^2 - \textcolor{red}{w}^2) - \lambda_{L\chi_2}\kappa_L^2) - \frac{\mu}{\textcolor{red}{w}}\kappa_L v, \quad (2.93)$$

$$C_{\tilde{e}} = \frac{v^2}{\kappa_R^2} (4(2\lambda_{\chi_2} - \lambda_{\chi_3})(v^2 - \textcolor{red}{w}^2) - \lambda_{L\chi_2}\kappa_L^2) - \frac{\mu}{\textcolor{red}{w}} \frac{\kappa_L}{\kappa_R} (v^2 + \textcolor{red}{w}^2) - \lambda_{R\chi_2}\textcolor{red}{w}^2. \quad (2.94)$$

- The non-diagonal block:

$$m_{\tilde{e}\tilde{E}}^2 = \begin{pmatrix} A_{\tilde{e}\tilde{E}} & B_{\tilde{e}\tilde{E}} \\ C_{\tilde{e}\tilde{E}} & D_{\tilde{e}\tilde{E}} \end{pmatrix}. \quad (2.95)$$

where

$$A_{\tilde{e}\tilde{E}} = \lambda_{L\chi_2} \textcolor{red}{w} \kappa_L + \mu \kappa_R, \quad (2.96)$$

$$B_{\tilde{e}\tilde{E}} = 4v \textcolor{red}{w} (2\lambda_{\chi_2} - \lambda_{\chi_3}), \quad (2.97)$$

$$C_{\tilde{e}\tilde{E}} = -\frac{\textcolor{red}{w} v}{\kappa_L \kappa_R} (4(2\lambda_{\chi_2} - \lambda_{\chi_3})(v^2 - \textcolor{red}{w}^2) - \lambda_{L\chi_2} \kappa_L^2 - \lambda_{R\chi_2} \kappa_R^2) + 2\mu v, \quad (2.98)$$

$$D_{\tilde{e}\tilde{E}} = \lambda_{R\chi_2} \textcolor{red}{w} \kappa_R + \mu \kappa_L. \quad (2.99)$$

- The lower-half block:

$$m_{\tilde{E}}^2 = \begin{pmatrix} A_{\tilde{E}} & B_{\tilde{E}} \\ B_{\tilde{E}} & C_{\tilde{E}} \end{pmatrix}. \quad (2.100)$$

where

$$A_{\tilde{E}} = \frac{v^2}{\kappa_L^2} (4(2\lambda_{\chi_2} - \lambda_{\chi_3})(v^2 - \textcolor{red}{w}^2) - \lambda_{R\chi_2} \kappa_R^2) - \frac{\mu \kappa_R}{\textcolor{red}{w} \kappa_L} (v^2 + \textcolor{red}{w}^2) - \lambda_{L\chi_2} \textcolor{red}{w}^2, \quad (2.101)$$

$$B_{\tilde{E}} = \frac{v}{\kappa_L} (4(2\lambda_{\chi_2} - \lambda_{\chi_3})(v^2 - \textcolor{red}{w}^2) - \lambda_{R\chi_2} \kappa_R^2) - \frac{\mu}{\textcolor{red}{w}} \kappa_R v, \quad (2.102)$$

$$C_{\tilde{E}} = 4v^2 (2\lambda_{\chi_2} - \lambda_{\chi_3}) - \lambda_{R\chi_2} \kappa_R^2 - \frac{\mu}{\textcolor{red}{w}} \kappa_L \kappa_R. \quad (2.103)$$

The combinations of orthogonal massless states, denoted by G_W and $G_{W'}$ are given by:

$$G_W = \left(-\textcolor{red}{w}(v^2 - \textcolor{red}{w}^2 + \kappa_R^2) \tilde{e} - 2v \textcolor{red}{w} \kappa_R (\tilde{e}^c)^* - \kappa_L (v^2 + \textcolor{red}{w}^2 + \kappa_R^2) \tilde{E} + v(v^2 - \textcolor{red}{w}^2 + \kappa_R^2) (\tilde{E}^c)^* \right) / N_1, \quad (2.104)$$

where the normalization factor N_1 is given by

$$N_1 = \sqrt{(v^2 + \textcolor{red}{w}^2 + \kappa_R^2) ((v^2 - \textcolor{red}{w}^2)^2 + (v^2 + \textcolor{red}{w}^2) \kappa_R^2 + (v^2 + \textcolor{red}{w}^2 + \kappa_R^2) \kappa_L^2)}, \quad (2.105)$$

and

$$G_{W'} = \left(-v \tilde{e} + \kappa_R (\tilde{e}^c)^* + \textcolor{red}{w} (\tilde{E}^c)^* \right) / N_2, \quad \text{with} \quad N_2 = \sqrt{\kappa_R^2 + v^2 + \textcolor{red}{w}^2}. \quad (2.106)$$

These states are eaten by the charged gauge bosons W_μ^\pm , and $W_\mu'^\pm$ by the Higgs mechanism. Later, we will take the limit $\textcolor{red}{w} \approx 0$ in our calculations of flavor observables, and the definition of $G_W/G_{W'}$ becomes identical to G_{W_L}/G_{W_R} :

$$G_{W_L} = \frac{-\kappa_L \tilde{E} + v (\tilde{E}^c)^*}{\sqrt{\kappa_L^2 + v^2}}, \quad G_{W_R} = \frac{-v \tilde{e} + \kappa_R (\tilde{e}^c)^*}{\sqrt{\kappa_R^2 + v^2}}. \quad (2.107)$$

Neutral Higgs: Among the four complex neutral Higgs fields, $\tilde{\nu}_E$, $\tilde{\nu}^c$, $\tilde{\nu}_E^c$, and $\tilde{\nu}$ three are Z_2 -even, namely $\tilde{\nu}_E$, $\tilde{\nu}^c$, and $\tilde{\nu}_E^c$, and naturally acquire vacuum expectation values. On the other hand, although $\tilde{\nu}$ is Z_2 -odd, due to the soft Z_2 breaking, it will acquire a small VEV $\textcolor{red}{w}$. The absence of scalar-pseudo-scalar mixing allows us to express the field as, for example, $\tilde{\nu} = \frac{1}{\sqrt{2}} (\text{Re}[\tilde{\nu}] + i \text{Im}[\tilde{\nu}])$, and consider the real and imaginary components separately.

The mass matrix for the neutral Higgs fields in the basis $(\text{Im}[\tilde{\nu}_E], \text{Im}[\tilde{\nu}^c], \text{Im}[\tilde{\nu}], \text{Im}[\tilde{\nu}_E^c])$ is given by:

$$M_{\text{Im}[\tilde{N}]}^2 = \begin{pmatrix} A_{\text{Im}[\tilde{N}]} & -\frac{\kappa_L}{\kappa_R} A_{\text{Im}[\tilde{N}]} & \mu \kappa_R & B_{\text{Im}[\tilde{N}]} \\ \bullet & \frac{\kappa_L^2}{\kappa_R^2} A_{\text{Im}[\tilde{N}]} & -\mu \kappa_L & -\frac{\kappa_L}{\kappa_R} B_{\text{Im}[\tilde{N}]} \\ \bullet & \bullet & 16\lambda_{\chi_2}v^2 - \frac{\mu}{w}\kappa_L\kappa_R & -16\lambda_{\chi_2}v w \\ \bullet & \bullet & \bullet & C_{\text{Im}[\tilde{N}]} \end{pmatrix}. \quad (2.108)$$

where

$$A_{\text{Im}[\tilde{N}]} = \frac{v^2}{\kappa_L^2} (4(2\lambda_{\chi_2} - \lambda_{\chi_3})(v^2 - w^2) - \lambda_{R\chi_2}\kappa_R^2) - \frac{\mu}{w} \frac{\kappa_R}{\kappa_L} (v^2 + w^2) - \lambda_{L\chi_2}v^2, \quad (2.109)$$

$$B_{\text{Im}[\tilde{N}]} = -\frac{v}{\kappa_L} (4(2\lambda_{\chi_2} - \lambda_{\chi_3})(v^2 - w^2) - \lambda_{R\chi_2}\kappa_R^2) + \frac{\mu}{w} v\kappa_R + \lambda_{L\chi_2}\kappa_L v, \quad (2.110)$$

$$C_{\text{Im}[\tilde{N}]} = 4v^2(2\lambda_{\chi_2} - \lambda_{\chi_3}) + 4w^2(2\lambda_{\chi_2} + \lambda_{\chi_3}) - \frac{\mu}{w} \kappa_L\kappa_R - \lambda_{L\chi_2}\kappa_L^2 - \lambda_{R\chi_2}\kappa_R^2. \quad (2.111)$$

Among these four states, two orthogonal states,

$$G_Z = (\kappa_L \text{Im}[\tilde{\nu}_E] + w \text{Im}[\tilde{\nu}] + v \text{Im}[\tilde{\nu}_E^c]) / N_4, \quad \text{with} \quad N_4 = \sqrt{\kappa_L^2 + v^2 + w^2}, \quad (2.112)$$

and

$$G'_Z = (\kappa_L(v^2 + w^2) \text{Im}[\tilde{\nu}_E] + \kappa_R N_5 \text{Im}[\tilde{\nu}^c] - \kappa_L^2 w \text{Im}[\tilde{\nu}] - \kappa_L^2 v \text{Im}[\tilde{\nu}_E^c]) / N_5, \quad (2.113)$$

where the normalization factor N_5 is given by:

$$N_5 = \sqrt{(\kappa_L^2 + v^2 + w^2)(\kappa_R^2(v^2 + w^2) + \kappa_L^2(\kappa_R^2 + v^2 + w^2))}, \quad (2.114)$$

are massless and are absorbed by Z and Z' , respectively.

The mass matrix for the real components of the neutral Higgs fields in the basis $(\text{Re}[\tilde{\nu}_E], \text{Re}[\tilde{\nu}^c], \text{Re}[\tilde{\nu}], \text{Re}[\tilde{\nu}_E^c])$ can be expressed as:

$$M_{\text{Re}[\tilde{N}]}^2 = \begin{pmatrix} A_{\text{Re}[\tilde{N}]} & B_{\text{Re}[\tilde{N}]} & 2(\lambda_{L\chi_1} + \lambda_{L\chi_2})w\kappa_L + \mu\kappa_R & C_{\text{Re}[\tilde{N}]} \\ \bullet & D_{\text{Re}[\tilde{N}]} & 2(\lambda_{R\chi_1} + \lambda_{R\chi_2})w\kappa_R + \mu\kappa_L & E_{\text{Re}[\tilde{N}]} \\ \bullet & \bullet & 4\lambda_{\chi_1}w^2 - \frac{\mu}{w}\kappa_L\kappa_R & 4(\lambda_{\chi_1} - 4\lambda_{\chi_2} + 2\lambda_{\chi_3})v w \\ \bullet & \bullet & \bullet & F_{\text{Re}[\tilde{N}]} \end{pmatrix}. \quad (2.115)$$

where

$$A_{\text{Re}[\tilde{N}]} = \frac{v^2}{\kappa_L^2} (4(2\lambda_{\chi_2} - \lambda_{\chi_3})(v^2 - \textcolor{red}{w}^2) - \lambda_{L\chi_2}\kappa_L^2 - \lambda_{R\chi_2}\kappa_R^2) - \frac{\mu}{\textcolor{red}{w}} \frac{\kappa_R}{\kappa_L} (v^2 + \textcolor{red}{w}^2) + 4(\lambda_{L1} + \lambda_{L2})\kappa_L^2, \quad (2.116)$$

$$B_{\text{Re}[\tilde{N}]} = -\frac{\kappa_L}{\kappa_R} \left(\frac{v^2}{\kappa_L^2} (4(2\lambda_{\chi_2} - \lambda_{\chi_3})(v^2 - \textcolor{red}{w}^2) - \lambda_{L\chi_2}\kappa_L^2 - \lambda_{R\chi_2}\kappa_R^2) - \frac{\mu}{\textcolor{red}{w}} \frac{\kappa_R}{\kappa_L} (v^2 + \textcolor{red}{w}^2) - 2(\lambda_{L1} + \lambda_{L2})\kappa_R^2 \right) \quad (2.117)$$

$$C_{\text{Re}[\tilde{N}]} = -\frac{v}{\kappa_L} \left(4(2\lambda_{\chi_2} - \lambda_{\chi_3})(v^2 - \textcolor{red}{w}^2) - \lambda_{R\chi_2}\kappa_R^2 - \frac{\mu}{\textcolor{red}{w}} \kappa_L \kappa_R - (2\lambda_{L\chi_1} + \lambda_{L\chi_2})\kappa_L^2 \right), \quad (2.118)$$

$$D_{\text{Re}[\tilde{N}]} = \frac{v^2}{\kappa_R^2} (4(2\lambda_{\chi_2} - \lambda_{\chi_3})(v^2 - \textcolor{red}{w}^2) - \lambda_{L\chi_2}\kappa_L^2 - \lambda_{R\chi_2}\kappa_R^2) - \frac{\mu}{\textcolor{red}{w}} \frac{\kappa_L}{\kappa_R} (v^2 + \textcolor{red}{w}^2) + 4(\lambda_{R1} + \lambda_{R2})\kappa_R^2, \quad (2.119)$$

$$= A_{\text{Re}[\tilde{N}]}(L \leftrightarrow R), \quad (2.120)$$

$$E_{\text{Re}[\tilde{N}]} = -\frac{v}{\kappa_R} \left(4(2\lambda_{\chi_2} - \lambda_{\chi_3})(v^2 - \textcolor{red}{w}^2) - \lambda_{L\chi_2}\kappa_L^2 - \frac{\mu}{\textcolor{red}{w}} \kappa_L \kappa_R - (2\lambda_{R\chi_1} + \lambda_{R\chi_2})\kappa_R^2 \right), \quad (2.121)$$

$$= C_{\text{Re}[\tilde{N}]}(L \leftrightarrow R), \quad (2.122)$$

$$F_{\text{Re}[\tilde{N}]} = 4(2\lambda_{\chi_2} - \lambda_{\chi_3})(v^2 - \textcolor{red}{w}^2) - \lambda_{L\chi_2}\kappa_L^2 - \lambda_{R\chi_2}\kappa_R^2 - \frac{\mu}{\textcolor{red}{w}} \kappa_L \kappa_R + 4\lambda_{\chi_1} v^2. \quad (2.123)$$

All the mass eigenvalues of physical scalars of the model are positive for a wide range of parameter space of the model, which shows consistency with symmetry breaking.

In summary, this subsection establishes a consistent Higgs spectrum that is compatible with the spontaneous symmetry breaking pattern. We have identified the physical scalar states and the Goldstone modes eaten by the gauge bosons, and expressed the neutral and charged Higgs sectors in such a form that will be used. In particular, the neutral Higgs analysis has already entered our discussion of neutrino mass generation (see Sec. 2.5), and the identification of the Goldstone modes will be needed when we compute flavor-violating processes in the 't Hooft–Feynman gauge in subsequent sections.

2.8 Interactions of the gauge bosons with light and heavy fermions

The gauge bosons couple to fermions that are charged under the corresponding gauge groups through their kinetic terms:

$$\mathcal{L}_{\text{kin}} = i\bar{\psi} \not{D} \psi + i\bar{\psi^c} \not{D} \psi^c + i\bar{\chi} \not{D} \chi + i\bar{\omega} \not{D} \omega + i\bar{\Omega} \not{D} \Omega. \quad (2.124)$$

For fields in the $(1, 1, 6)$ representation, say ω (same for Ω as well), we can define the covariant derivative as follows:

$$D_\mu \omega_{ij} = \partial_\mu \omega_{ij} - ig_4 (G_\mu^d \frac{T_4^d}{2})_i^k \omega_{kj} - ig_4 (G_\mu^d \frac{T_4^d}{2})_j^k \omega_{ik}, \quad (2.125)$$

where d runs over the $SU(4)_C$ generators and i, j, k are $SU(4)_C$ indices. The definitions of the other fields charged under the gauge group are given in Eq. (2.57).

Couplings of leptoquark gauge boson, X_μ : We can expand the covariant derivative to get the explicit couplings of X_μ to fermions in the gauge eigenstates:

$$\mathcal{L}_{\text{kin}}^{X_\mu} = \frac{g_4}{\sqrt{2}} \left[(\bar{u}\gamma^\mu\nu_E + \bar{d}\gamma^\mu E)X_\mu + (\bar{D^c}\gamma^\mu e^c + \bar{u^c}\gamma^\mu\nu^c)X_\mu^* + \epsilon^{ijk}(\bar{d_j^c}\gamma^\mu \textcolor{red}{D}'_k + \bar{D_j^c}\gamma^\mu D_k)X_{i\mu} \right] + \text{h.c.} \quad (2.126)$$

Now we rotate the gauge eigenstates to the mass eigenstates following the definitions used in Sec. 2.3 for charged fermions and Sec. 2.5 for neutral lepton, and write down the light-light (L-L) fermion and light-heavy (L-H) fermion interactions with X_μ (the heavy-heavy interactions are irrelevant for our analysis):

$$\mathcal{L}_{\text{L-L}}^{X_\mu} = \frac{g_4}{\sqrt{2}} \bar{d}_0^c K_{d^c e^c} \gamma^\mu e_0^c X_\mu^* + \text{h.c.} \quad (2.127)$$

$$\begin{aligned} \mathcal{L}_{\text{L-H}}^{X_\mu} = & \frac{g_4}{\sqrt{2}} \left[\bar{u}_0 V_{uE} \gamma^\mu \nu_{E0} X_\mu + \bar{d}_0 V_{dE} \gamma^\mu E_0 X_\mu + \bar{d}_0^c K_{d^c E^c} \gamma^\mu E_0^c X_\mu^* + \bar{D}_0^c K_{D^c e^c} \gamma^\mu e_0^c X_\mu^* \right. \\ & \left. + \bar{u}_0^c V_{u^c \nu^c} \gamma^\mu \nu_0^c X_\mu^* + \epsilon^{ijk} (\bar{d}_j^c) K_{d^c \textcolor{red}{D}'} \gamma^\mu \textcolor{red}{D}'_k X_{i\mu} + \epsilon^{ijk} (\bar{D}_j^c) K_{\textcolor{red}{D}'^c d} \gamma^\mu d_{k0} X_{i\mu} \right] + \text{h.c.} \end{aligned} \quad (2.128)$$

where we have defined

$$K_{d^c e^c} = -V_{d^c}^\dagger (\mathbb{I} + x^\dagger x)^{-1/2} x^\dagger V_{e^c}, \quad (2.129)$$

$$V_{f_1 f_2} = V_{f_1}^\dagger V_{f_2}, \quad (2.130)$$

$$K_{d^c E^c} = -V_{d^c}^\dagger (\mathbb{I} + x^\dagger x)^{-1/2} x^\dagger \rho_\ell^* V_{E^c}, \quad (2.131)$$

$$K_{D^c e^c} = V_{D^c}^\dagger \left(\hat{M}_D (\mathbb{I} + x x^\dagger) \hat{M}_D^\dagger \right)^{-1/2} \hat{M}_D V_{e^c}, \quad (2.132)$$

$$K_{d^c \textcolor{red}{D}'} = V_{d^c}^\dagger (\mathbb{I} + x^\dagger x)^{-1/2} V_{\textcolor{red}{D}'}, \quad (2.133)$$

$$K_{\textcolor{red}{D}'^c d} = -V_{\textcolor{red}{D}'^c}^\dagger \rho^T V_d. \quad (2.134)$$

Here the definition for \hat{M}_D can be found in Eq. (2.16), x and ρ are given in Eq. (2.25) and ρ_ℓ in Eq. (2.28). Later, for the flavor-violating processes, we would follow 't Hooft-Feynman gauge, and we would require the couplings of the unphysical mode of X_μ (defined as G_X in Eq. (2.85)) with the fermions. One such example is given by

$$\mathcal{L}_{\text{L-L}}^{G_X} = \frac{g_4}{\sqrt{2}M_X} \left[(d_0^c)^\dagger K_{d^c e^c} M_e^{\text{diag}} e_0^c - d_0^T M_d^{\text{diag}} K_{d^c e^c} e_0^c \right] G_X^* + \text{h.c.} \quad (2.135)$$

$$\begin{aligned} \mathcal{L}_{\text{L-H}}^{G_X} \supset & \frac{g_4}{\sqrt{2}M_X} \left[-u_0^\dagger V_{uE} M_E^{\text{diag}} (\nu_{E0}^c)^* G_X + d_0^\dagger V_{dE} M_E^{\text{diag}} (E_0^c)^* G_X - D_0^T M_D^{\text{diag}} K_{D^c e^c} e^c G_X^* \right. \\ & \left. + (u_0^c)^\dagger V_{u^c \nu^c} m_{N0}^{\text{diag}} (\nu_0^c)^* G_X^* + \epsilon^{ijk} (d_j^c)^\dagger K_{d^c \textcolor{red}{D}'} M_\omega^{\text{diag}} (\textcolor{red}{D}'_{k0})^* (G_X)_i \right] + \text{h.c.} \end{aligned} \quad (2.136)$$

In the $\mathcal{L}_{\text{L-H}}^{G_X}$ equation, we have not shown the couplings proportional to the light quark mass and the couplings involving the terms ρ, ρ_ℓ proportional to soft breaking, but they can be arrived at similarly.

Couplings of $SU(2)_R$ gauge boson W'_μ : Ignoring the mixing between W - W' , we can expand the covariant derivative to get the couplings of W'_μ to fermions:

$$\mathcal{L}_{\text{kin}}^{W'_\mu} = \frac{g_R}{\sqrt{2}} \left[(\bar{D^c}\gamma^\mu u^c + \bar{e^c}\gamma^\mu \nu^c) W_\mu'^+ + (\bar{E^c}\gamma^\mu \nu + \bar{\nu_E^c}\gamma^\mu e) W_\mu'^+ \right] + \text{h.c.}, \quad (2.137)$$

Here, the generation indices and color indices are implicit. Rotating the gauge eigenstates to the mass eigenstates allows us to write down the interactions with light-light (L-L) fermion and

light-heavy (L-H) fermions as:

$$\mathcal{L}_{\text{L-L}}^{W'_\mu} = \frac{g_R}{\sqrt{2}} \left[\overline{d_0^c} K_{d^c u^c} \gamma^\mu u_0^c W_\mu'^+ + \overline{e_0^c} K_{e^c \nu} \gamma^\mu \nu_0 W_\mu'^+ \right] + \text{h.c.} \quad (2.138)$$

$$\mathcal{L}_{\text{L-H}}^{W'_\mu} = \frac{g_R}{\sqrt{2}} \left[\overline{D_0^c} K_{D^c u} \gamma^\mu u_0^c W_\mu'^+ + \overline{E_0^c} V_{E^c \nu} \gamma^\mu \nu_0 W_\mu'^+ + \overline{\nu_{E0}^c} V_{\nu_E^c e} \gamma^\mu e_0 W_\mu'^+ \right] + \text{h.c.} \quad (2.139)$$

where we have defined

$$K_{d^c u^c} = -V_{d^c}^\dagger (\mathbb{I} + x^\dagger x)^{-1/2} x^\dagger V_{u^c}, \quad (2.140)$$

$$K_{e^c \nu} = -V_{e^c}^\dagger \rho_\ell^*, \quad (2.141)$$

$$K_{D^c u} = V_{D^c}^\dagger \left(\hat{M}_D (\mathbb{I} + x x^\dagger) \hat{M}_D^\dagger \right)^{-1/2} \hat{M}_D V_{u^c}. \quad (2.142)$$

The couplings with the associated Goldstone, G'_W (see Eq. (2.107) for definition) can be understood similarly as discussed in Eq. (2.135)-(2.136).

Couplings of SM neutral gauge boson Z_μ : Ignoring the mixing between Z - Z' , we can expand the covariant derivative in Eq. (2.124) to get the couplings of Z_μ (see Eq. (2.65) for the definition of Z_μ basis) with fermions in their gauge eigenstates:

$$\mathcal{L}_{\text{kin}}^{Z_\mu} = \frac{g_L}{\cos\theta_W} \left[\bar{f} \left\{ T_{3L}^f - Q_f \sin^2\theta_W \right\} \gamma^\mu f + \bar{f^c} \left(-Q_f \sin^2\theta_W \right) \gamma^\mu f^c \right] Z_\mu. \quad (2.143)$$

Here, $\tan\theta_W = g_Y/g_L$ and T_{3L}^f is the $SU(2)_L$ generator (third component of weak isospin) acting on f . T_{3L}^f charge assignment for $\chi(2, 2, 1)$ is

$$T_{3L}^{E^c} = \frac{1}{2}, \quad T_{3L}^{\nu_E^c} = -\frac{1}{2}, \quad T_{3L}^\nu = \frac{1}{2}, \quad T_{3L}^e = -\frac{1}{2}. \quad (2.144)$$

The interactions of light fermions in their mass eigenbasis with Z_μ become:

$$\mathcal{L}_{\text{L-L}}^{Z_\mu} = \frac{g_L}{\cos\theta_W} \left[\overline{d_0} L^d \gamma^\mu d_0 + \overline{d_0^c} L^{d^c} \gamma^\mu d_0^c + \overline{u_0} L^u \gamma^\mu u_0 + \overline{u_0^c} L^{u^c} \gamma^\mu u_0^c + \overline{e_0} L^e \gamma^\mu e_0 + \overline{e_0^c} L^{e^c} \gamma^\mu e_0^c + \overline{\nu_0} L^\nu \gamma^\mu \nu_0 \right] Z_\mu. \quad (2.145)$$

where we have defined

$$L^d = -\frac{1}{2} \mathbb{I} + \frac{1}{3} \sin^2\theta_W \left(\mathbb{I} + V_d^\dagger \rho^* \rho^T V_d \right), \quad (2.146)$$

$$L^{d^c} = -\frac{1}{3} \sin^2\theta_W \mathbb{I}, \quad (2.147)$$

$$L^u = \frac{1}{2} \mathbb{I} - \frac{2}{3} \sin^2\theta_W \mathbb{I}, \quad (2.148)$$

$$L^{u^c} = \frac{2}{3} \sin^2\theta_W \mathbb{I}, \quad (2.149)$$

$$L^e = -\frac{1}{2} \mathbb{I} + \sin^2\theta_W \mathbb{I}, \quad (2.150)$$

$$L^{e^c} = -\sin^2\theta_W \left(\mathbb{I} + V_{e^c}^\dagger \rho_\ell^* \rho_\ell^T V_{e^c} \right), \quad (2.151)$$

$$L^\nu = \frac{1}{2} \mathbb{I}. \quad (2.152)$$

Couplings of heavy neutral gauge boson Z'_μ : Similarly, we can get the couplings of Z'_μ (see Eq. (2.66) for the definition of Z'_μ basis) with fermions in their gauge eigenstates:

$$\mathcal{L}_{\text{kin}}^{Z'_\mu} = -\frac{g_R^2}{\sqrt{g_R^2 - g_Y^2}} \left[\bar{f} \gamma^\mu \left(T_{3R}^f - \frac{Y_f}{2} \frac{g_Y^2}{g_R^2} \right) f + \bar{f}^c \gamma^\mu \left(T_{3R}^{f^c} - \frac{Y_{f^c}}{2} \frac{g_Y^2}{g_R^2} \right) f^c \right] Z'^\mu. \quad (2.153)$$

Here d, u, u^c have the usual hypercharge with the normalization $Y_{e^c} = 2$. Thus, $Y_d = -2/3, Y_u = 4/3, Y_{u^c} = -4/3$. For D^c coming from $(1, 2, 4)$ also has the usual assignment $Y_{D^c} = 2/3$ follows. For $(1, 1, 6)$, we identify d^c as SM right-handed down quark with the usual $Y_{d^c} = 2/3$, then the gauge interactions fix $Y_D, Y_{D^c} = -2/3, Y_{D'^c} = 2/3$ and $Y_{E^c} = 1$. T_{3R}^f is the $SU(2)_R$ generator (third component of weak isospin) acting on f , its charge assignments for the components of $\chi(2, 2, 1)$ are

$$T_{3R}^{E^c} = \frac{1}{2}, \quad T_{3R}^\nu = -\frac{1}{2}, \quad T_{3R}^{\nu^c} = \frac{1}{2}, \quad T_{3R}^e = -\frac{1}{2}. \quad (2.154)$$

We can now write down the interactions of light fermions in their mass eigenbasis with Z'_μ as:

$$\begin{aligned} \mathcal{L}_{\text{L-L}}^{Z'_\mu} = -\frac{g_R^2}{\sqrt{g_R^2 - g_Y^2}} & \left[\bar{d}_0 P^d \gamma^\mu d_0 + \bar{d}_0^c P^{d^c} \gamma^\mu d_0^c + \bar{u}_0 P^u \gamma^\mu u_0 + \bar{u}_0^c P^{u^c} \gamma^\mu u_0^c + \right. \\ & \left. \bar{e}_0 P^e \gamma^\mu e_0 + \bar{e}_0^c P^{e^c} \gamma^\mu e_0^c + \bar{\nu}_0 P^\nu \gamma^\mu \nu_0 \right] Z'_\mu. \end{aligned} \quad (2.155)$$

Here, we have defined

$$P^d = \frac{1}{3} \frac{g_Y^2}{g_R^2} \left(-\frac{1}{2} \mathbb{I} + V_d^\dagger \rho^* \rho^T V_d \right), \quad (2.156)$$

$$P^{d^c} = V_{d^c}^\dagger (\mathbb{I} + x^\dagger x)^{-1/2} \left(\frac{1}{2} x^\dagger x - \frac{1}{3} (\mathbb{I} + x^\dagger x) \frac{g_Y^2}{g_R^2} \right) (\mathbb{I} + x^\dagger x)^{-1/2} V_{d^c}, \quad (2.157)$$

$$P^u = -\frac{1}{6} \frac{g_Y^2}{g_R^2} \mathbb{I}, \quad (2.158)$$

$$P^{u^c} = -\frac{1}{2} \mathbb{I} + \frac{2}{3} \frac{g_Y^2}{g_R^2} \mathbb{I}, \quad (2.159)$$

$$P^e = -\frac{1}{2} \mathbb{I} + \frac{1}{2} \frac{g_Y^2}{g_R^2} \mathbb{I}, \quad (2.160)$$

$$P^{e^c} = \frac{1}{2} \left(\mathbb{I} + V_{e^c}^\dagger \rho_\ell^* \rho_\ell^T V_{e^c} \right) - \frac{g_Y^2}{g_R^2} \left(\mathbb{I} + \frac{1}{2} V_{e^c}^\dagger \rho_\ell^* \rho_\ell^T V_{e^c} \right), \quad (2.161)$$

$$P^\nu = -\frac{1}{2} \mathbb{I} + \frac{1}{2} \frac{g_Y^2}{g_R^2} \mathbb{I}. \quad (2.162)$$

From now on, for notational simplicity, we drop the subscript “0” on mass-eigenstate fields, thus d^c should be understood as d_0^c , e^c as e_0^c , and so on.

To summarize, in this subsection, we have collected the couplings of the light-light and light-heavy fermion combinations with the gauge bosons X_μ, W'_μ, Z_μ , and Z'_μ . These couplings form the basic ingredients for the rest of the paper. They will enter the collider analysis to get constraints on the new gauge boson masses and production channels, and all subsequent calculations of flavor-violating observables.

3 Collider Implications

Realizing TeV-scale Pati-Salam symmetry in our model, together with the presence of new vector-like fermions and a softly broken Z_2 symmetry, opens up unique opportunities for collider probes. The relatively light leptoquark gauge boson X_μ as well as Z' and W' gauge bosons, and the vector-like quarks carrying unusual baryon number $-2/3$, lead to distinct experimental signatures. In this section, we explore the current bounds from the LHC and discuss the prospects of discovery at the high-luminosity LHC. The limits derived from direct searches will then be used in the subsequent discussion of flavor violation mediated by these particles.

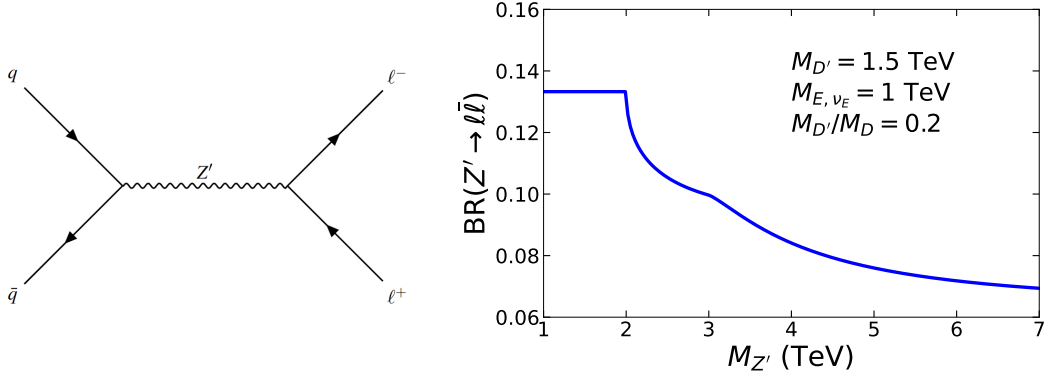


Figure 4: Left panel: Production and decay of Z' gauge boson at the LHC. Right panel: Branching ratio of $Z' \rightarrow \ell\bar{\ell}$ ($\ell = e, \mu$) in our theory. Here, we have assumed the masses of all three generations of D' (E, ν_E) to $M_{D'} = 1.5$ TeV ($M_{E, \nu_E} = 1$ TeV). Moreover, Z' decays to scalars is not considered, which can be arranged by taking their masses somewhat heavy, see text for details.

Phenomenology of Z' : First, we investigate the production and the leptonic decay of Z' at the LHC, which proceeds through the Drell-Yan (DY) processes, as shown in Fig. 4. The relevant interactions of Z' are provided in Eq. (2.153), which we implemented in **FeynRules** [41] (similarly, other processes, to be discussed below, are also implemented in **FeynRules** for the

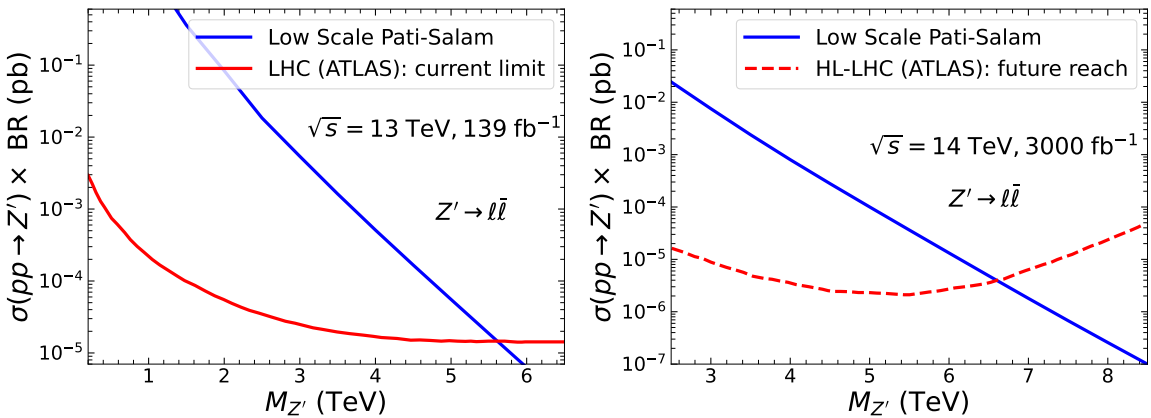


Figure 5: Left panel: branching ratio of $Z' \rightarrow \ell\bar{\ell}$ ($\ell = e, \mu$). Right left panel: current LHC limit on Z' mass from $pp \rightarrow Z' \rightarrow \ell\bar{\ell}$ searches. Lower right panel: future reach for the same process at the HL-LHC.

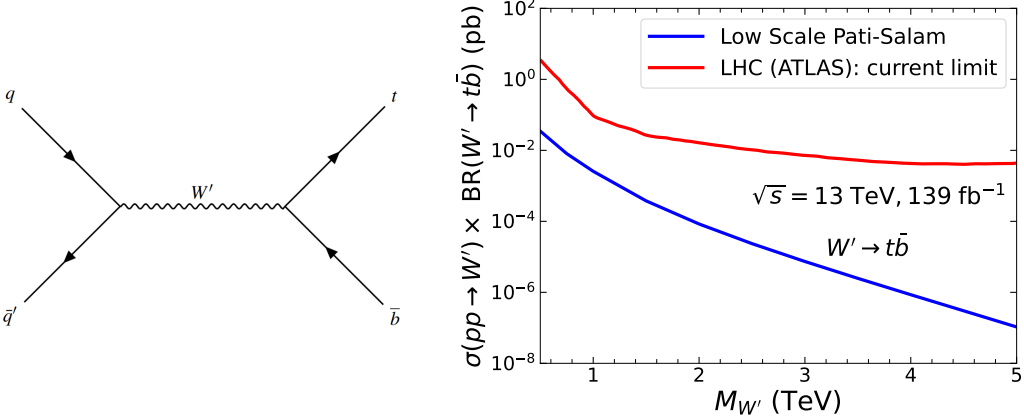


Figure 6: Current LHC limit on W' mass from $pp \rightarrow W' \rightarrow t\bar{b}$ searches. The W' production is $d^c - D^c$ mixing suppressed, and as before, we have assumed $M_{D'}/M_D \sim 0.2$ and $2M_{\nu^c} = M_{E,\nu_E} = 1$ TeV.

purpose of computing the production cross sections). The associated **Universal FeynRules Output** (UFO) [42] file is then fed to **MadGraph5 aMC@NLO** (MG5aMC) [43] to compute the production cross section. For this numerical analysis, we use gauge coupling values at 1 TeV, which are $(g_1, g_R, g_2, g_C) = (0.467, 0.377, 0.638, 1.060)$. The decay branching ratios of Z' , on the other hand, are dependent on the mass spectrum of the BSM states. Following the aforementioned discussion on flavor constraints, here we fix the mass ratio $M_{D'}/M_D \sim 0.2$ as a benchmark value and take $M_{D'} = 1.5$ TeV, $M_{E,\nu_E} = 1$ TeV. Furthermore, Z' decays to scalars are not considered, which can be arranged by taking their masses somewhat heavy. The corresponding relevant branching ratio, namely, $Z' \rightarrow \ell\bar{\ell}$ ($\ell = e, \mu$) is presented in Fig. 4 (left panel). With these, we obtain a very strong constraint of $M_{Z'} \gtrsim 5.6$ TeV from the current LHC searches [44], as shown in the left panel of Fig. 5. By appropriately assigning the couplings, the procedure adopted correctly reproduces the sequential SM Z' [45] mass limit from LHC, which is an independent check of our method. Moreover, the future sensitivity [46] of HL-LHC is also depicted in Fig. 5 (right panel). This figure shows that, if not discovered, the LHC operating at high luminosity can rule out a Z' -boson mass up to $M_{Z'} \gtrsim 6.6$ TeV. Intriguingly, if the FCC-hh is built, it could potentially reach a sensitivity of order $M_{Z'} \gtrsim \mathcal{O}(40)$ TeV [12].

Phenomenology of W' : Although, in most of the models, W' gauge boson mass is also strongly constrained from LHC searches, within our model, its production, see Fig. 6, is highly suppressed. It is because W' , in the flavor basis, couples to $u^c D^c$, see Eq. (2.137). Therefore, the production $pp \rightarrow W'$ as well as the decay $W' \rightarrow t\bar{b}$ are $d^c - D^c$ mixing suppressed. Consequently, current LHC searches cannot provide a meaningful bound to its mass. However, for completeness, in Fig. 6, we show the corresponding production cross section times the branching ratio along with the current LHC bounds [47] as a function of its mass. For producing this plot, as before, we take $M_{D'}/M_D \sim 0.2$ and to incorporate the rest of its decays, we assumed $2M_{\nu^c} = M_{E,\nu_E} = 1$ TeV.

Phenomenology of X_μ : Since the Pati-Salam gauge boson, X_μ , carries color charge, they can be pair produced at the LHC through gluon fusion, as shown in Fig. 7. Each gauge boson then decays to three quarks and a lepton, leading to, for example, $pp \rightarrow XX^* \rightarrow 6j + \ell\bar{\ell}$. To

estimate an approximate collider bound on the mass of this exotic gauge boson, we employ the LHC limit [48] on $6j$ final state. Ref. [48] considered R-parity violating (RPV) supersymmetric (SUSY) scenario, where gluinos are pair produced, and subsequently, each gluino decays to three quarks utilizing RVP coupling, already present within the minimal SUSY extension of the SM. As can be seen in Fig. 7, this, however, for our scenario, does not provide a meaningful bound on its mass.

Phenomenology of D' VLQ: To realize multi-TeV scale Pati-Salam theory, one of the main predictions of our model is that the vector-like quark D' , having a baryon number of $-2/3$, must be as light as possible. However, LHC searches restrict its mass to lie below the TeV scale. In our model, the pair-produced VLQs, through cascade decays, lead to multi-jet final states along with two leptons. In finding collider limit on its mass, relevant decay chains are shown in Fig. 8.

The process on the left panel in Fig. 8 somewhat mimics the RPV SUSY model where cascade decays from pair-produced gluinos eventually lead to high jet-multiplicity [49]. For this case of $pp \rightarrow D' \bar{D}' \rightarrow 8j + \ell\bar{\ell}$, an exact bound depends also on the mass of ν^c . For a dedicated study, see Ref. [49]. However, taking the model independent limit quoted in Ref. [49], which is applicable for $M_X > M_{\nu^c}$, our study (for simplicity, we set branching ratio to unity) shows that current LHC searches provide $m_{D'} \gtrsim 1.5$ TeV, as shown in Fig. 9. This estimated bound can be somewhat relaxed in our scenario once all branching ratios are incorporated, as well as by engaging the mass dependence of M_{ν^c} (which is, however, beyond the scope of this work).

Finally, we also obtain a similar bound (namely, $M_{D'} \gtrsim 1.3$ TeV) from the process on the right panel of Fig. 8, where we consider $D' \rightarrow q\bar{q} + \text{MET}$ (missing transverse energy). This scenario mimics the SUSY model where, after direct gluino pair production, each gluino undergoes a three-body decay to light-flavor quarks and a neutralino, where the latter gives rise to MET [50]. For the estimation of this limit, we again assumed the branching ratio to be unity. The right panel in Fig. 9 depicts the production cross section and the current LHC limit, which is taken from Ref. [50] for a vanishing neutralino mass.

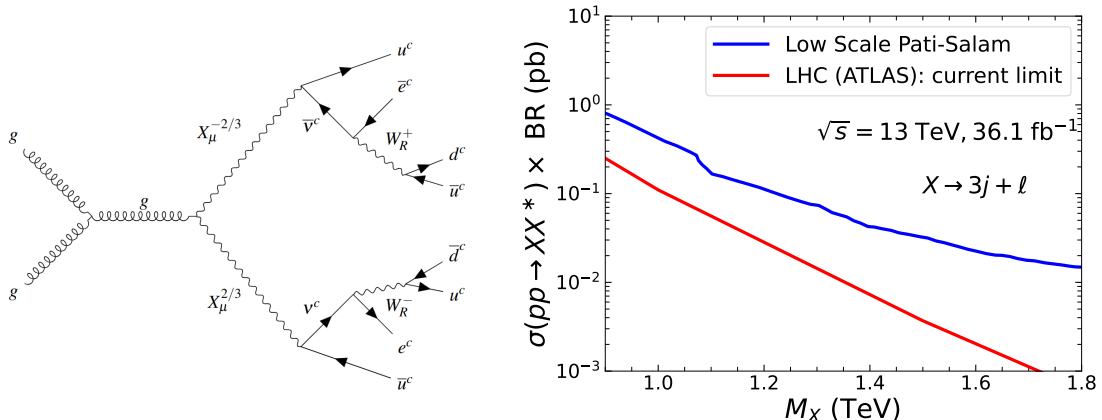


Figure 7: Pair-production of Pati-Salam gauge boson at the LHC $pp \rightarrow XX^*$. The left panel shows the production cross section $pp \rightarrow XX^*$ (for simplicity, here, the branching ratio is set to unity) along with the current LHC limit on $6j$ final state.

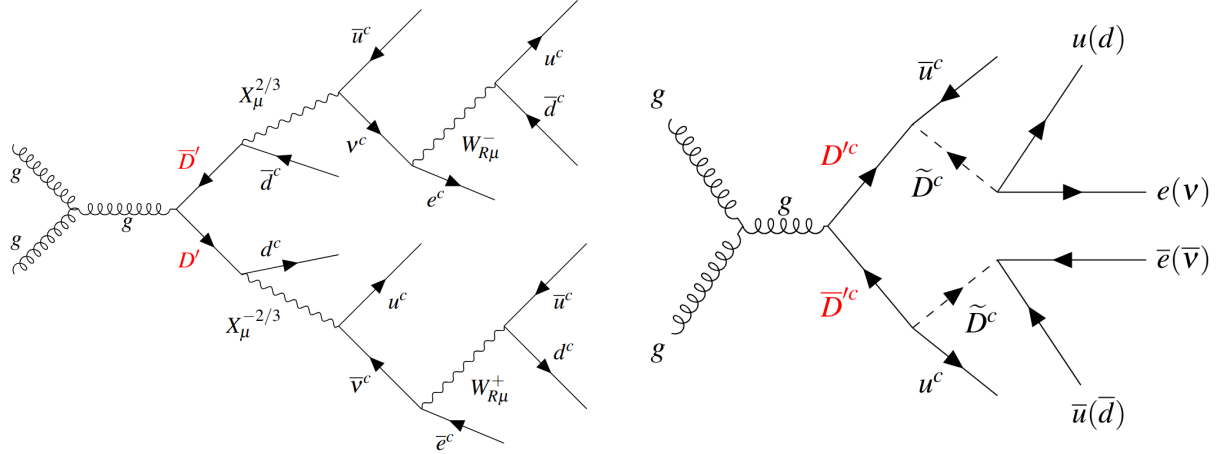


Figure 8: The VLQ can be pair produced at the LHC via gluon fusion $pp \rightarrow D'D'$. Through cascade decay, the process on the left leads to $pp \rightarrow D'D' \rightarrow 8j + \ell\bar{\ell}$ final states. Whereas, the process on the right can give rise to 4 jets+opposite sign leptons, or 4 jets+lepton and missing energy, 4 jets+missing energy.

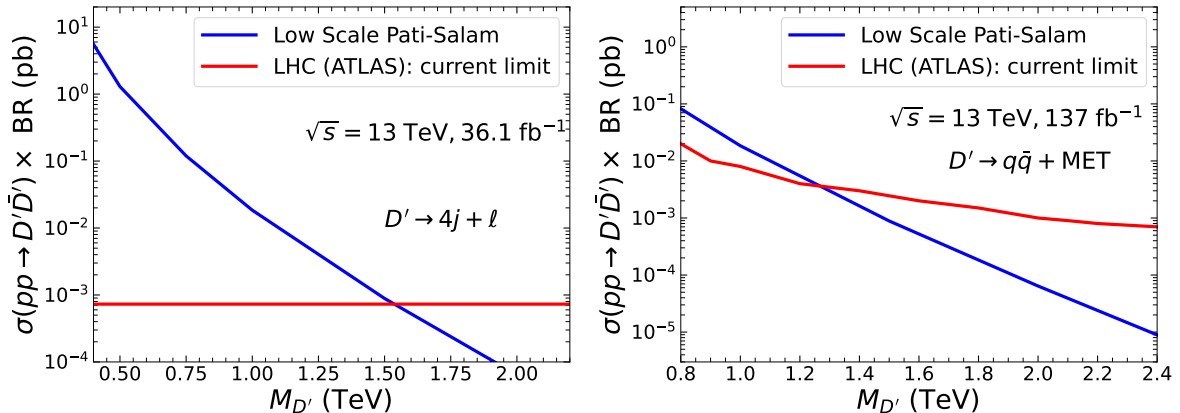


Figure 9: Left panel: LHC (model independent) limit on pair-produced VLQ, $pp \rightarrow D'D'$, decaying into 8 jets and leptons. Right panel: instead, decay of the type $D' \rightarrow q\bar{q} + \text{MET}$ (leading to 4j+MET in the final state) is assumed.

4 Flavor violating processes

In this section, we analyze various flavor-changing processes that are mediated by the new gauge bosons of the model. These include meson decays such as $K_L \rightarrow \mu e$ which arise by the tree-level exchanges of the leptoquark gauge boson X_μ , as well as loop-induced processes such as $K^0 - \bar{K}^0$ mixing, and leptonic decays of mesons. We also address charged lepton flavor violation that arises in the model, both at tree-level ($\mu - e$ conversion in nuclei) as well as via loops ($\mu \rightarrow e\gamma$, $\mu \rightarrow 3e$, etc). We present two benchmark scenarios where all flavor violation constraints are satisfied with the Pati-Salam symmetry breaking scale as low as 1.1 TeV.

4.1 Meson decay at tree level

Due to the Z_2 odd nature, X_μ gauge boson couples SM fermions to new vector-like fermions. In the limit of exact Z_2 symmetry, tree-level meson decays are forbidden in our model. However,

once the Z_2 symmetry is softly broken, a mixing between d^c and D^c is induced, as discussed in Sec. 2.4. These processes are helicity suppressed, since the leptoquark gauge boson X_μ does not have a coupling of the type $\bar{d}_L \gamma_\mu e_L X^\mu$ in our setup. The most stringent constraint on the mass

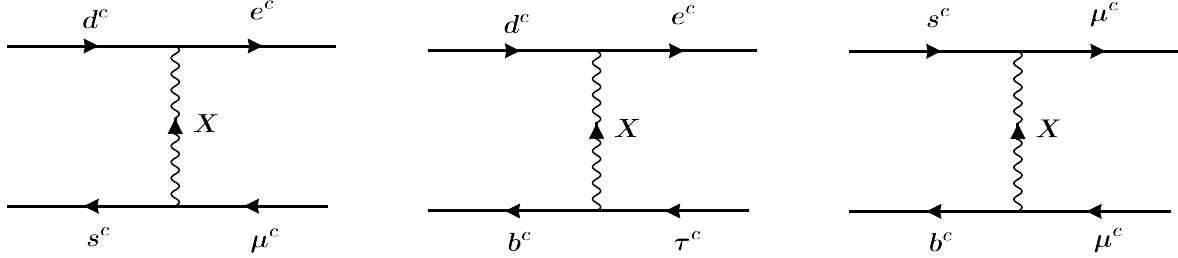


Figure 10: Representative diagrams for meson decay ($K_L \rightarrow \mu e$, $B_d \rightarrow \tau e$, $B_s \rightarrow \mu \mu$)

of X_μ arises from neutral meson decay channels with charged-lepton final states of opposite sign and without neutrinos in the final states, as summarized in Table 2. In our framework, such decays occur only for neutral mesons composed of down-type quarks. The relevant coupling for this process can be found in Eq. (2.127). The 3×3 matrix $K_{d^c e^c}$ appearing in this equation is not a unitary matrix due to the appearance of the x matrix, unlike in the standard Pati–Salam setup. While the matrix elements of x are taken to be small, $|x_{ij}| \sim 0.2$ (see Eq. (2.31)), the matrix x must have rank-three, since the eigenvalues of x times κ_R are the masses of the D' quarks. This is because we wish to satisfy the collider limits on the masses of all three families of D' (see Fig. 9).

To get the mass limit on the X_μ , let's consider the X_μ -induced leptonic decays, $\Phi_{pq} \rightarrow \ell_i^+ \ell_j^-$ (for examples, see Fig. 10) where the pseudoscalar mesons $\Phi_{pq} = (\bar{d}_p d_q)$ are bound states of quark–antiquark pairs. The decay width for helicity-suppressed meson decay is given by [5, 11]

$$\Gamma_{\Phi_{pq} \rightarrow \ell_i^+ \ell_j^-}^{\text{HS}} = \frac{m_{\Phi_{pq}} [g_4(m_X)]^4 f_{\Phi_{pq}}^2}{256\pi m_X^4} \sqrt{\left(1 - (\mu_{\ell_i} + \mu_{\ell_j})^2\right) \left(1 - (\mu_{\ell_i} - \mu_{\ell_j})^2\right)} \times \left(\left(1 - \mu_{\ell_i}^2 - \mu_{\ell_j}^2\right) \left(m_{\ell_i}^2 + m_{\ell_j}^2\right) - 4\mu_{\ell_i}\mu_{\ell_j}m_{\ell_i}m_{\ell_j} \right) \left(\left|K_{d^c e^c}^{pi}\right|^2 \left|K_{d^c e^c}^{qj}\right|^2 \right). \quad (4.1)$$

where $\mu_{\ell_i} = m_{\ell_i}/m_{\Phi_{pq}}$ and $f_{\Phi_{pq}}$ is the decay constant of the pseudoscalar meson.

Benchmark scenario-1: To get a numerical estimation, let's first take the matrix x to be proportional to \mathbb{I} , which means $(\mathbb{I} + x^\dagger x)^{-1/2} x^\dagger \approx 0.2 \mathbb{I}$ (see subsection 2.4 for an explanation for the suppression of 0.2). In that case, $K_{d^c e^c}$ which follows from Eq. (2.129) is

$$K_{d^c e^c} \approx -0.2 V_{d^c e^c}, \quad (4.2)$$

with $V_{d^c e^c} = V_{d^c}^\dagger V_{e^c}$ for which we assume a CKM matrix-like form, with the angle θ_{13} set to $\pi/2$, given by

$$V_{d^c e^c} = \begin{pmatrix} 0 & 0 & 1 \\ -s_{12}c_{23} - c_{12}s_{23}e^{i\delta} & c_{12}c_{23} - e^{i\delta}s_{12}s_{23} & 0 \\ -c_{12}c_{23} + e^{-i\delta}s_{12}s_{23} & -c_{23}s_{12} - e^{-i\delta}c_{12}s_{23} & 0 \end{pmatrix}. \quad (4.3)$$

Process	Measured value/upper limit
$\text{BR}(K_L^0 \rightarrow ee)$	$9.0_{-4.0}^{+6.0} \times 10^{-12}$ [51, 52]
$\text{BR}(K_L^0 \rightarrow \mu\mu)$	$6.84_{-0.11}^{+0.11} \times 10^{-12}$ [53]
$\text{BR}(K_L^0 \rightarrow \mu e)$	$< 4.7 \times 10^{-12}$ [54]
$\text{BR}(B_d^0 \rightarrow ee)$	$< 2.5 \times 10^{-9}$ [55]
$\text{BR}(B_d^0 \rightarrow \mu\mu)$	$< 3.6 \times 10^{-10}$ [56]
$\text{BR}(B_d^0 \rightarrow \tau\tau)$	$< 2.1 \times 10^{-3}$ [57]
$\text{BR}(B_d^0 \rightarrow \mu e)$	$< 1.0 \times 10^{-9}$ [58]
$\text{BR}(B_d^0 \rightarrow \tau e)$	$< 1.6 \times 10^{-5}$ [59]
$\text{BR}(B_d^0 \rightarrow \tau\mu)$	$< 1.5 \times 10^{-5}$ [59]
$\text{BR}(B_s^0 \rightarrow ee)$	$< 9.4 \times 10^{-9}$ [55]
$\text{BR}(B_s^0 \rightarrow \mu\mu)$	$3.0_{-0.4}^{+0.4} \times 10^{-9}$ [56, 60, 61]
$\text{BR}(B_s^0 \rightarrow \tau\tau)$	$< 6.8 \times 10^{-3}$ [57]
$\text{BR}(B_s^0 \rightarrow \mu e)$	$< 5.4 \times 10^{-9}$ [58]
$K^0 - \bar{K}^0 : \Delta M_K$	$(3.484 \pm 0.006) \times 10^{-15}$ GeV [62]
$D^0 - \bar{D}^0 : \Delta M_D$	$(6.25_{-2.90}^{+2.70}) \times 10^{-15}$ GeV [62]
$B_d^0 - \bar{B}_d^0 : \Delta M_d$	$(3.334 \pm 0.013) \times 10^{-13}$ GeV [62]
$B_s^0 - \bar{B}_s^0 : \Delta M_s$	$(1.1683 \pm 0.0013) \times 10^{-11}$ GeV [62]
$\text{BR}(\mu \rightarrow e\gamma)$	$< 4.2 \times 10^{-13}$ [63]
$\text{BR}(\tau \rightarrow e\gamma)$	$< 3.3 \times 10^{-8}$ [64]
$\text{BR}(\tau \rightarrow \mu\gamma)$	$< 4.4 \times 10^{-8}$ [64]
$\text{BR}(\mu \rightarrow eee)$	$< 1.0 \times 10^{-12}$ [65]
$\text{BR}(\tau \rightarrow eee)$	$< 2.7 \times 10^{-8}$ [66]
$\text{BR}(\tau \rightarrow \mu\mu\mu)$	$< 2.1 \times 10^{-8}$ [66]
$\text{BR}(\tau^- \rightarrow e^-\mu\mu)$	$< 2.7 \times 10^{-8}$ [66]
$\text{BR}(\tau^- \rightarrow \mu^-ee)$	$< 1.8 \times 10^{-8}$ [66]
$\text{BR}(\tau^- \rightarrow e^+\mu^-\mu^-)$	$< 1.7 \times 10^{-8}$ [66]
$\text{BR}(\tau^- \rightarrow \mu^+e^-e^-)$	$< 1.5 \times 10^{-8}$ [66]

Table 2: Experimental constraints on rare meson decays, meson-antimeson oscillations, and other cLFV processes.

Here $s_{ij} = \sin \theta_{ij}$ and $c_{ij} = \cos \theta_{ij}$. The motivation for this choice, with a third angle θ_{13} in the unitary matrix set to $\pi/2$, is clear from Table 2 which shows that this choice eliminates the most stringent limit on the mass of X_μ arising from the decay $K_L \rightarrow \mu e$. We can perform a numerical scan of the angle space $(\theta_{12}, \theta_{23})$ for fixed $\theta_{13} = \pi/2$, and fixed CP phase $\delta = 0$, that will compute the minimum M_X required to satisfy all the experimental bounds simultaneously (see Table 2). The resulting pattern is shown in Fig. 11, where the color-bar corresponds to M_X coming from the strongest constraint among the relevant flavor-violating meson decays.

Now, we can optimize all the processes in order to get the lowest allowed limit on M_X for the specific configuration of $\theta_{12}, \theta_{23}, \delta$. We find that the angular configuration $\theta_{12} = 0.16$ rad,

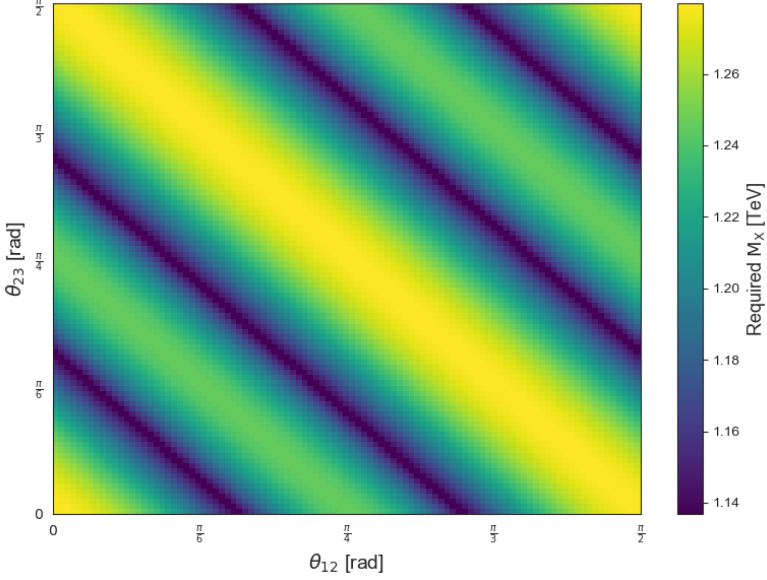


Figure 11: Minimum leptoquark gauge boson mass M_X that is required to satisfy all meson decay constraints, as a function of the mixing angles θ_{12} and θ_{23} , with fixed $\theta_{13} = \pi/2$, $\delta = 0$.

$\theta_{23} = 0.36$ rad, and $\delta = 0.81$ rad provides the lowest value of the leptoquark gauge boson mass M_X consistent with the five decay constraints, which is $M_X \geq 1.1$ TeV. As seen in Table 3, this bound is primarily driven by the rare decay process $B_s \rightarrow \mu\mu$, with $B_s \rightarrow \mu e$ providing a nearly identical lower limit. The constraints from $B_d \rightarrow \tau e$, $B_d \rightarrow \tau \mu$, and $B_s \rightarrow ee$ are significantly weaker and are automatically satisfied.

Decay process	Limit on M_X (GeV)
1. $B_d \rightarrow \tau e$	$\geq 5.7 \times 10^2$
2. $B_d \rightarrow \tau \mu$	$\geq 4.1 \times 10^2$
3. $B_s \rightarrow ee$	≥ 58.4
4. $B_s \rightarrow \mu\mu$	$\geq 1.1 \times 10^3$
5. $B_s \rightarrow \mu e$	$\geq 1.1 \times 10^3$

Table 3: Lower bounds on M_X from various meson decay processes (Benchmark-1)

Benchmark scenario-2: An interesting feature of our model is that, to suppress K -meson decays, imposing a specific structure on the CKM-like matrix is unnecessary. The required flavor suppression can arise from the matrix x instead, which is proportional to the $\textcolor{red}{D}'$ mass matrix. To illustrate this, let's take V_{dc} to be similar to the CKM matrix:

$$V_{dc} = \begin{pmatrix} 0.9745 & 0.2243 & 0.00143 - 0.00367i \\ -0.2241 - 0.00016i & 0.9736 - 0.00004i & 0.04215 \\ 0.00839 - 0.00350i & -0.0410 - 0.00072i & 0.9991 \end{pmatrix}, \quad (4.4)$$

and we take $V_{ec} \simeq \mathbb{I}_3$ for definiteness. We now take x to be a general 3×3 matrix, subject to the condition that it has full rank. This would guarantee that all three of the $\textcolor{red}{D}'$ quarks

have similar masses of order 1.5 TeV. Using the helicity-suppressed decay formula given in Eq. (4.1), we compute the branching ratios for all 13 flavor-violating meson decay channels listed in Table 2, and minimize the X_μ gauge boson mass consistent with all bounds. We summarize the resulting lower bounds on M_X for this benchmark scenario in Table 4. For the

Decay process	Limit on M_X (GeV)
$K_L \rightarrow ee$	≥ 47
$K_L \rightarrow \mu\mu$	$\geq 8.1 \times 10^2$
$K_L \rightarrow \mu e$	$\geq 9.1 \times 10^2$
$B_d \rightarrow ee$	≥ 2.3
$B_d \rightarrow \mu\mu$	≥ 48
$B_d \rightarrow \tau\tau$	≥ 0.10
$B_d \rightarrow \mu e$	≥ 31
$B_d \rightarrow \tau e$	$\geq 5.8 \times 10^2$
$B_d \rightarrow \tau\mu$	$\geq 4.3 \times 10^2$
$B_s \rightarrow ee$	≥ 57.4
$B_s \rightarrow \mu\mu$	$\geq 1.1 \times 10^3$
$B_s \rightarrow \tau\tau$	≥ 0.04
$B_s \rightarrow \mu e$	$\geq 1.1 \times 10^3$

Table 4: Lower bounds on M_X from meson decays (Benchmark-2).

best-fit point, we obtain a representative numerical solution for the matrix x :

$$x \approx \begin{pmatrix} 0.0173 + 0.0108i & 0.0690 + 0.0495i & -0.180 + 0.0062i \\ 0.0401 + 0.0020i & 0.1750 + 0.0059i & 0.0711 - 0.0506i \\ -0.2110 & 0.0487 & -0.00190 - 0.000687i \end{pmatrix}, \quad (4.5)$$

corresponding to physical eigenvalues $\sigma(x) \approx \{0.22, 0.20, 0.20\}$. These eigenvalues, multiplied by $\kappa_R \sim 6$ TeV are the masses of the $\textcolor{red}{D}'$ quarks. The corresponding CKM-like matrix $K_{d^c e^c}$ takes the form

$$K_{d^c e^c} \approx - \begin{pmatrix} 9.48 \times 10^{-5} & -7.08 \times 10^{-5} & 2.12 \times 10^{-1} \\ -7.70 \times 10^{-2} + 4.95 \times 10^{-2}i & -1.73 \times 10^{-1} + 8.05 \times 10^{-3}i & 2.54 \times 10^{-5} + 2.10 \times 10^{-5}i \\ 1.73 \times 10^{-1} + 8.05 \times 10^{-3}i & -7.70 \times 10^{-2} - 4.95 \times 10^{-2}i & 1.12 \times 10^{-4} + 2.18 \times 10^{-5}i \end{pmatrix}. \quad (4.6)$$

The most stringent constraints in this benchmark also come from the $B_s \rightarrow \mu\mu$ and $B_s \rightarrow \mu e$ channels for this benchmark point, which require

$$M_X \gtrsim 1.1 \times 10^3 \text{ GeV}. \quad (4.7)$$

We wish to make an important comment here: In this second benchmark, when the flavor structure is pushed into x , $K_{d^c e^c} = -V_{d^c}^\dagger (\mathbb{I} + x^\dagger x)^{-1/2} x^\dagger V_{e^c}$ is no longer unitary. A priori, dipole amplitudes in charged lepton flavor-violating (cLFV) processes can be in danger because of the absence of a GIM suppression owing to the non-unitarity. For example, the dipole amplitude for

$\mu \rightarrow e\gamma$ will depend on the off-diagonal combination $S \equiv \sum_{q^c} (K)_{q^c e^c} (K)_{q^c \mu^c}^*$ when a light state propagates in the loop. (Loops with an internal exotic fermion carry free X_μ - F couplings and do not involve $K_{d^c e^c}$, so they are unaffected by its non-unitarity.) Accordingly, in optimizing the matrices in Eq. (4.6), we required S to be numerically small, so that the predicted cLFV processes comfortably satisfy existing bounds. Therefore, we will adopt the same $K_{d^c e^c}$ quoted in Eq. (4.6) in all downstream cLFV analyses; the detailed $\mu \rightarrow e\gamma$, $\mu \rightarrow eee$, and μ - e conversion formulas and limits are presented in Sec. 4.4.

4.2 $K_L \rightarrow \mu e$ at one loop level

We should also consider meson decays into lepton pairs at the loop level, because we can have box diagrams containing leptoquark gauge boson and new vector-like quarks, where the suppression coming from the Z_2 soft breaking will be absent. It is not obvious that the one-loop contribution will be subdominant for all of the parameter space of the model. We focus on the $K_L \rightarrow \mu e$ process because it provides the most stringent limit with the CKM-like matrices taken to be identical to the generic CKM matrix (the same structure used in Eq. (4.4) for V_{d^c}). We will perform the calculations in 't Hooft-Feynman gauge, where one should also include contributions from the unphysical Goldstone bosons, which is reflected in Fig. 12. We consider the effective operators under the approximation of vanishing external momenta and negligible light quark masses:

$$\mathcal{L}_{\text{eff}} \supset C_{RR} (\bar{s}^c \gamma_\mu d^c)(\bar{\mu}^c \gamma^\mu e^c) + C_{LR} (\bar{s} \gamma_\mu d)(\bar{\mu}^c \gamma^\mu e^c) + \text{h.c.}, \quad (4.8)$$

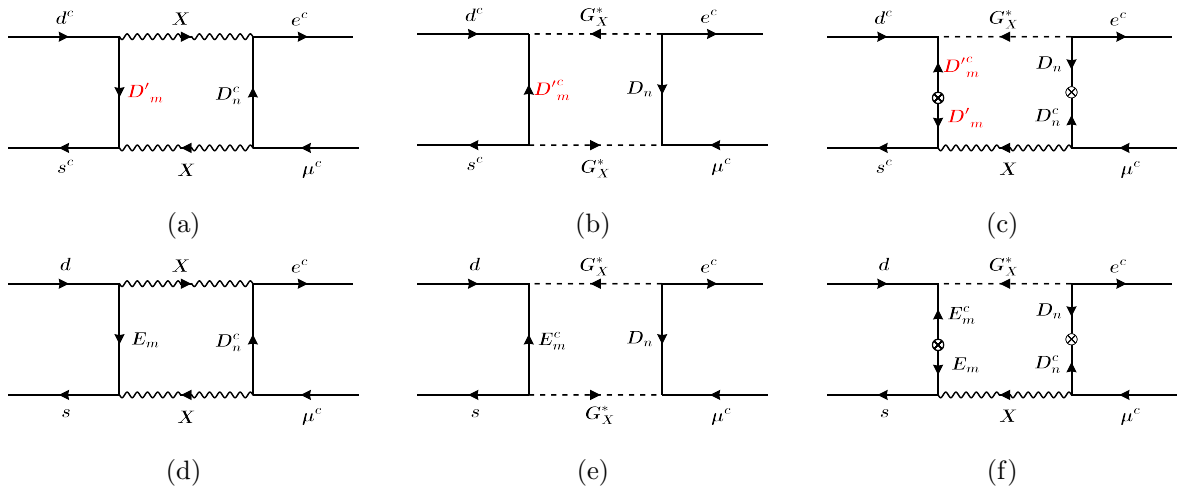


Figure 12: Box diagrams with leptoquark gauge boson and its Goldstone mode contributing to the $K_L \rightarrow \mu e$ decay process. Here, m, n are flavor indices. For topology (c) and (f), there is an additional diagram obtained by interchanging X_μ and G_X on the internal lines. These will give identical contributions to the Wilson coefficients, which has been included in our results.

with the leading-order expressions for the Wilson coefficients:

$$\begin{aligned}
C_{RR}^{(a+b+c)} &= -2 \left(\frac{g_4}{\sqrt{2}} \right)^4 \frac{1}{4\pi^2 M_X^2} \left(\sum_{m,n} \xi_{D'_m} \eta_{D_n^c} A(r_{D'_m}, r_{D_n}) + \frac{1}{32} \sum_{m,n} \xi_{D'_m} \eta_{D_n^c} A(r_{D'_m}, r_{D_n}) r_{D'_m} r_{D_n} \right. \\
&\quad \left. - \sum_{m,n} \xi_{D'_m} \eta_{D_n^c} B(r_{D'_m}, r_{D_n}) r_{D'_m} r_{D_n} \right), \\
C_{LR}^{(d+e+f)} &= -2 \left(\frac{g_4}{\sqrt{2}} \right)^4 \frac{1}{4\pi^2 M_X^2} \left(\sum_{m,n} \xi_{E_m} \eta_{D_n^c} A(r_{E_m}, r_{D_n}) + \frac{1}{32} \sum_{m,n} \xi_{E_m} \eta_{D_n^c} A(r_{E_m}, r_{D_n}) r_{E_m} r_{D_n} \right. \\
&\quad \left. - \sum_{m,n} \xi_{E_m} \eta_{D_n^c} B(r_{E_m}, r_{D_n}) r_{E_m} r_{D_n} \right). \tag{4.9}
\end{aligned}$$

Here we have used the definitions $\xi_{D'_m} = K_{s^c D'_m} K_{d^c D'_m}^*$, $\xi_{E_m} = V_{s E_m} V_{d E_m}^*$, $\eta_{D_n^c} = K_{D_n^c \mu^c} K_{D_n^c e^c}^*$, $r_c = M_c^2/M_X^2$, and

$$\begin{aligned}
A(x_i, x_j) &= \frac{1}{(1-x_i)(1-x_j)} + \frac{1}{(x_i-x_j)} \left[\frac{x_i^2}{(1-x_i)^2} \ln x_i - \frac{x_j^2}{(1-x_j)^2} \ln x_j \right], \\
B(x_i, x_j) &= -\frac{1}{(1-x_i)(1-x_j)} + \frac{1}{(x_i-x_j)} \left[\frac{x_j}{(1-x_j)^2} \ln x_j - \frac{x_i}{(1-x_i)^2} \ln x_i \right]. \tag{4.10}
\end{aligned}$$

The notation $C_{RR}^{(a+b+c)}$ indicates that diagrams (a), (b), and (c) in Fig. 12 contribute to C_{RR} . We use the standard definition of the axial current matrix element [4],

$$\langle 0 | \bar{d} \gamma^\mu \gamma_5 s | K(p_K) \rangle = i f_K p_K^\mu, \tag{4.11}$$

where f_K is the kaon decay constant. The decay width at one-loop in our setup can be written as

$$\Gamma_{K \rightarrow \mu e}^{\text{one-loop}} = \frac{f_K^2 m_K}{64\pi} \lambda^{1/2}(1, r_\mu, r_e) (1 - r_\mu - r_e) (m_\mu - m_e)^2 |C_{LR} - C_{RR}|^2 \tag{4.12}$$

with the definitions of dimensionless ratios $r_\ell \equiv \frac{m_\ell^2}{m_K^2}$ ($\ell = \mu, e$), and the dimensionless Källén function $\lambda(1, x, y) \equiv 1 + x^2 + y^2 - 2(x + y + xy)$. Our four-fermion operators contain only vector/axial quark currents, and because of their non-singlet Ward identities, which enforce $Z_V = Z_A = 1$ (zero anomalous dimensions) for $V^\mu = \bar{q} \gamma^\mu T_a q$ and $A^\mu = \bar{q} \gamma^\mu \gamma_5 T_a q$, all long-distance QCD can be absorbed into f_K . By contrast, scalar/pseudo-scalar densities would require a running factor [67, 68].

Now that we have the setup in place, we can proceed with a benchmark parameter scan to gain an understanding of the variation in the PS scale with vector-like fermion masses involved in the loop. As mentioned before, we will take the benchmark CKM-like matrices (ξ_{E_m}, η_{D_n} etc) to be identical to the CKM matrix. We want to emphasize the point that the entries of the CKM-like matrices entering the amplitude are free input parameters here. In fact, for many choices (such as a diagonal structure), the new physics contributions to meson decay can be minimal. But we are interested in asking the following question: assuming that the mixing is not fine-tuned to minimize the contribution to $K_L \rightarrow \mu e$, how low can M_X be while satisfying the experimental flavor constraints? Fig. 13 presents one benchmark scenario, where we vary the exotic fermion masses for a single generation, under the assumption that $M_{D'} = (1.5, 1.7, 2.1)$ TeV and M_D, M_E exotics lie around a common scale. Specifically, we scan over

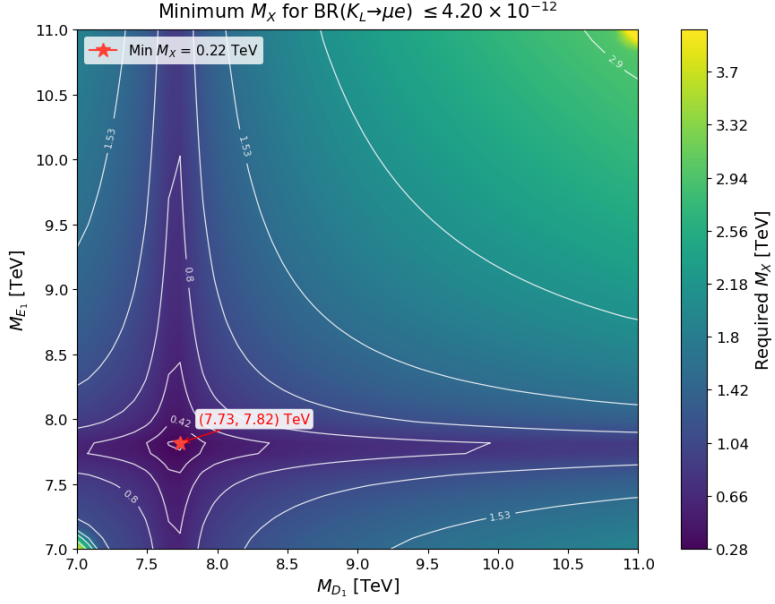


Figure 13: Heatmap showing the contour of M_X (TeV) required to suppress the branching ratio $\text{Br}(K_L \rightarrow \mu^\pm e^\mp) < 4.7 \times 10^{-12}$, as a function of vector-like fermion mass M_{D_1} . For this benchmark, we assume all the heavy fermions have similar masses, and the CKM-like matrices have structures aligned with the standard CKM matrix.

$M_D = (M_{D_1}, 7.7, 8.5)$ TeV and $M_E = (M_{E_1}, 7.9, 8.6)$ TeV. We have shown the contours of M_X up-to 4 TeV satisfying the constraints with different choices of (M_{D_1}, M_{E_1}) .

4.3 Limit on M_X from mass difference of neutral mesons

Neutral meson systems, $\Phi^0 - \bar{\Phi}^0$ with $\Phi^0 \equiv (K^0, D^0, B_s^0, B_d^0)$ are known to exhibit oscillations due to neutral current interactions that change flavor by two units ($\Delta F = 2$). The propagating physical neutral mesons are not CP eigenstates but rather mass eigenstates, M_H and M_L , which are combinations of Φ^0 and $\bar{\Phi}^0$. The small mass difference $\Delta M \equiv M_H - M_L = 2 \text{Re} \langle \bar{\Phi}^0 | \mathcal{H}_{\text{eff}}^{\Delta F=2} | \Phi^0 \rangle$ arises from off-diagonal contributions in the meson mixing matrix. In the SM, this occurs at the one-loop level through the familiar box diagrams involving W and up-type quarks and is loop and CKM suppressed. So, these mass differences can be highly sensitive to new-physics contributions, especially if the scenario introduces new sources of flavor violation or right-handed currents.

In our model, additional contributions to the $\Delta F = 2$ processes are induced through box diagrams involving X_μ, W'_μ , and vector-like fermions. Thus, it is necessary to ΔM for some benchmark scenarios to check whether it sets a more stringent limit on the Patti-Salam scale compared to tree-level meson decay and direct collider bounds.

The effective Hamiltonian for these processes can be written as:

$$\mathcal{H}_{\text{eff}}^{\Delta F=2} = \sum_{i=1}^5 C_i Q_i^{q_i q_j} + \sum_{i=1}^3 \tilde{C}_i \tilde{Q}_i^{q_i q_j}, \quad (4.13)$$

where $q_i q_j = ds, cu, bd, bs$ label the quark flavors involved in the meson mixing. The operator

basis is given by [69–72]:

$$\begin{aligned}
Q_1^{q_i q_j} &= (\bar{q}_{L_i}^\alpha \gamma^\mu q_{L_j}^\alpha)(\bar{q}_{L_i}^\beta \gamma_\mu q_{L_j}^\beta), & \tilde{Q}_1^{q_i q_j} &= (\bar{q}_{R_i}^\alpha \gamma^\mu q_{R_j}^\alpha)(\bar{q}_{R_i}^\beta \gamma_\mu q_{R_j}^\beta), \\
Q_2^{q_i q_j} &= (\bar{q}_{R_i}^\alpha q_{L_j}^\alpha)(\bar{q}_{R_i}^\beta q_{L_j}^\beta), & \tilde{Q}_2^{q_i q_j} &= (\bar{q}_{L_i}^\alpha q_{R_j}^\alpha)(\bar{q}_{L_i}^\beta q_{R_j}^\beta), \\
Q_3^{q_i q_j} &= (\bar{q}_{R_i}^\alpha q_{L_j}^\beta)(\bar{q}_{R_i}^\beta q_{L_j}^\alpha), & \tilde{Q}_3^{q_i q_j} &= (\bar{q}_{L_i}^\alpha q_{R_j}^\beta)(\bar{q}_{L_i}^\beta q_{R_j}^\alpha), \\
Q_4^{q_i q_j} &= (\bar{q}_{R_i}^\alpha q_{L_j}^\alpha)(\bar{q}_{L_i}^\beta q_{R_j}^\beta), \\
Q_5^{q_i q_j} &= (\bar{q}_{R_i}^\alpha q_{L_j}^\beta)(\bar{q}_{L_i}^\beta q_{R_j}^\alpha).
\end{aligned} \tag{4.14}$$

where $q_{L,R} = P_{L,R} q$, with $P_{L,R} = (1 \mp \gamma^5)/2$, and α, β are color indices. As we will see in the next section, the operators Q_1 , \tilde{Q}_1 , Q_4 , and Q_5 are generated at the Pati–Salam scale in our setup. Their hadronic matrix elements can be conveniently expressed in terms of bag parameters B_i . For a neutral meson system $\Phi^0 \equiv \Phi_{q_i q_j}^0$ one has [71]

$$\langle \Phi^0 | Q_1(\mu) | \Phi^0 \rangle = \langle \bar{\Phi}^0 | \tilde{Q}_1(\mu) | \Phi^0 \rangle = \frac{1}{3} M_\Phi f_\Phi^2 B_1(\mu), \tag{4.15}$$

$$\langle \bar{\Phi}^0 | Q_4(\mu) | \Phi^0 \rangle = \frac{1}{4} \left(\frac{M_\Phi}{m_{q_i}(\mu) + m_{q_j}(\mu)} \right)^2 M_\Phi f_\Phi^2 B_4(\mu), \tag{4.16}$$

$$\langle \bar{\Phi}^0 | Q_5(\mu) | \Phi^0 \rangle = \frac{1}{12} \left(\frac{M_\Phi}{m_{q_i}(\mu) + m_{q_j}(\mu)} \right)^2 M_\Phi f_\Phi^2 B_5(\mu). \tag{4.17}$$

where M_Φ is the mass of the Φ^0 meson, f_Φ is its decay constant. Here, the meson states are normalized to $\langle \Phi^0 | \Phi^0 \rangle = \langle \bar{\Phi}^0 | \bar{\Phi}^0 \rangle = 1$. The definitions in Eq. (4.15)–(4.17) are such that in the vacuum-insertion approximation (VIA) one can write,

$$[B_1(\mu)]_{\text{VIA}} = 1, \tag{4.18}$$

$$[B_4(\mu)]_{\text{VIA}} = 1 + \frac{1}{6} \left(\frac{m_{q_i}(\mu) + m_{q_j}(\mu)}{m_\Phi} \right)^2, \tag{4.19}$$

$$[B_5(\mu)]_{\text{VIA}} = 1 + \frac{3}{2} \left(\frac{m_{q_i}(\mu) + m_{q_j}(\mu)}{m_\Phi} \right)^2. \tag{4.20}$$

The central values for the $B_i(\mu)$ and the other relevant parameters to calculate ΔM for $\Phi^0 \equiv (K^0, D^0, B_s^0, B_d^0)$ have been provided in Appendix B.1.

Now, to connect new contributions at high scales to low-energy observables such as neutral meson mass differences, it is necessary to evolve the Wilson coefficients C_i from Eq. (4.13), which is defined at the Pati–Salam scale ($\Lambda \sim M_X$), down to the appropriate hadronic scale μ where the matrix elements are evaluated. This renormalization group running will account for QCD effects, which can mix operators and change the values of the coefficients. The hadronic scale depends on the meson that we are considering: for examples, for kaons we should use $\mu_K = 2 \text{ GeV}$, for charm mesons $\mu_D = 2.8 \text{ GeV}$, and for bottom mesons $\mu_B = 4.6 \text{ GeV}$, which align with the lattice QCD computations [70]. The analytical formula for the running of the coefficients can be represented as [73]:

$$C_r(\mu) = \sum_i \sum_s \left(b_i^{(r,s)} + \eta c_i^{(r,s)} \right) \eta^{a_i} C_s(\Lambda), \tag{4.21}$$

where $\eta = \alpha_s(\Lambda)/\alpha_s(m_t)$, and the parameters $a_j, b_j^{(r,i)}, c_j^{(r,i)}$ are called the magic numbers. With $\Lambda = 4.3$ TeV, $\alpha_s(m_Z) = 0.118$, and $m_t^{\overline{\text{MS}}}(m_t) = 162.7$ GeV, we get $\eta = \alpha_s(\Lambda)/\alpha_s(m_t) = 0.078/0.108 = 0.716$. The magic numbers for Φ^0 meson systems have been provided in Appendix B.1. The magic numbers that are used to evolve the coefficients \tilde{C}_{1-3} are identical to those for C_{1-3} , since QCD running is independent of chirality structure in these cases. Neglecting this running may introduce larger theoretical uncertainties, and there will be possibilities that we may end up with incorrect estimations of ΔM due to the strong operator mixing under QCD. So, we will consider all possible induced four-fermion operators Q_i at the Pati-Salam scale, compute the corresponding Wilson coefficients $C_i(\Lambda)$ at that scale, and evolve them to the hadronic scale using Eq. (4.21). This will enable us to consistently evaluate their contribution to the meson mass splittings at low energies. At the hadronic scale, for K^0 system, we find,

$$\begin{aligned} C_2(\mu_K) &= 2.82 C_2(\Lambda), & C_3(\mu_K) &= -5.01 \times 10^{-3} C_2(\Lambda), \\ C_4(\mu_K) &= 5.66 C_4(\Lambda) + 1.64 C_5(\Lambda), & C_5(\mu_K) &= 0.22 C_4(\Lambda) + 0.87 C_5(\Lambda). \end{aligned} \quad (4.22)$$

For the D^0 meson, we find the coefficients to be

$$\begin{aligned} C_2(\mu_D) &= 2.54 C_2(\Lambda), & C_3(\mu_D) &= -2.5 \times 10^{-2} C_2(\Lambda), \\ C_4(\mu_D) &= 4.70 C_4(\Lambda) + 1.27 C_5(\Lambda), & C_5(\mu_D) &= 0.17 C_4(\Lambda) + 0.87 C_5(\Lambda). \end{aligned} \quad (4.23)$$

And for the $B_{d,s}^0$ systems, we get

$$\begin{aligned} C_2(\mu_B) &= 2.20 C_2(\Lambda), & C_3(\mu_B) &= -4 \times 10^{-2} C_2(\Lambda), \\ C_4(\mu_B) &= 3.67 C_4(\Lambda) + 0.92 C_5(\Lambda), & C_5(\mu_B) &= 0.11 C_4(\Lambda) + 0.87 C_5(\Lambda). \end{aligned} \quad (4.24)$$

4.3.1 $K^0 - \bar{K}^0$ oscillation

We first compute the leptoquark gauge-boson (X_μ) contributions to the $\Delta S = 2$ effective Hamiltonian. We can read the Feynman rules for the relevant box diagrams from Eqs. (2.127)–(2.136).

Fig. 14 shows the box diagrams involving the leptoquark gauge boson and its Goldstone mode, as well as the mixed gauge–Goldstone diagrams that will induce the relevant Wilson coefficients at the Pati-Salam scale. Each topology in Fig. 14 should be understood as the sum of two diagrams with the crossing of the internal lines. For example, the box in Fig. 14 (a) corresponds to the sum of the “annihilation” and “scattering” diagrams shown in Fig. 15 (a-1) and Fig. 15 (a-2). For the mixed gauge–Goldstone diagrams in Fig. 14 (g)–(i), there is, in addition, a second diagram that we obtain by interchanging X_μ and G_X on the internal lines. This diagram makes the same contribution to the Wilson coefficients, and we account for it through an overall multiplicity factor, even though we show only one representative diagram. The same comments hold for $D^0 - \bar{D}^0$ mixing topologies as well.

As mentioned earlier, we see that the operators Q_1, \tilde{Q}_1, Q_4 , and Q_5 contribute to K -meson mixing in our setup. The leading-order expressions for the corresponding Wilson coefficients are computed under the approximation of vanishing external momenta and negligible light quark masses:

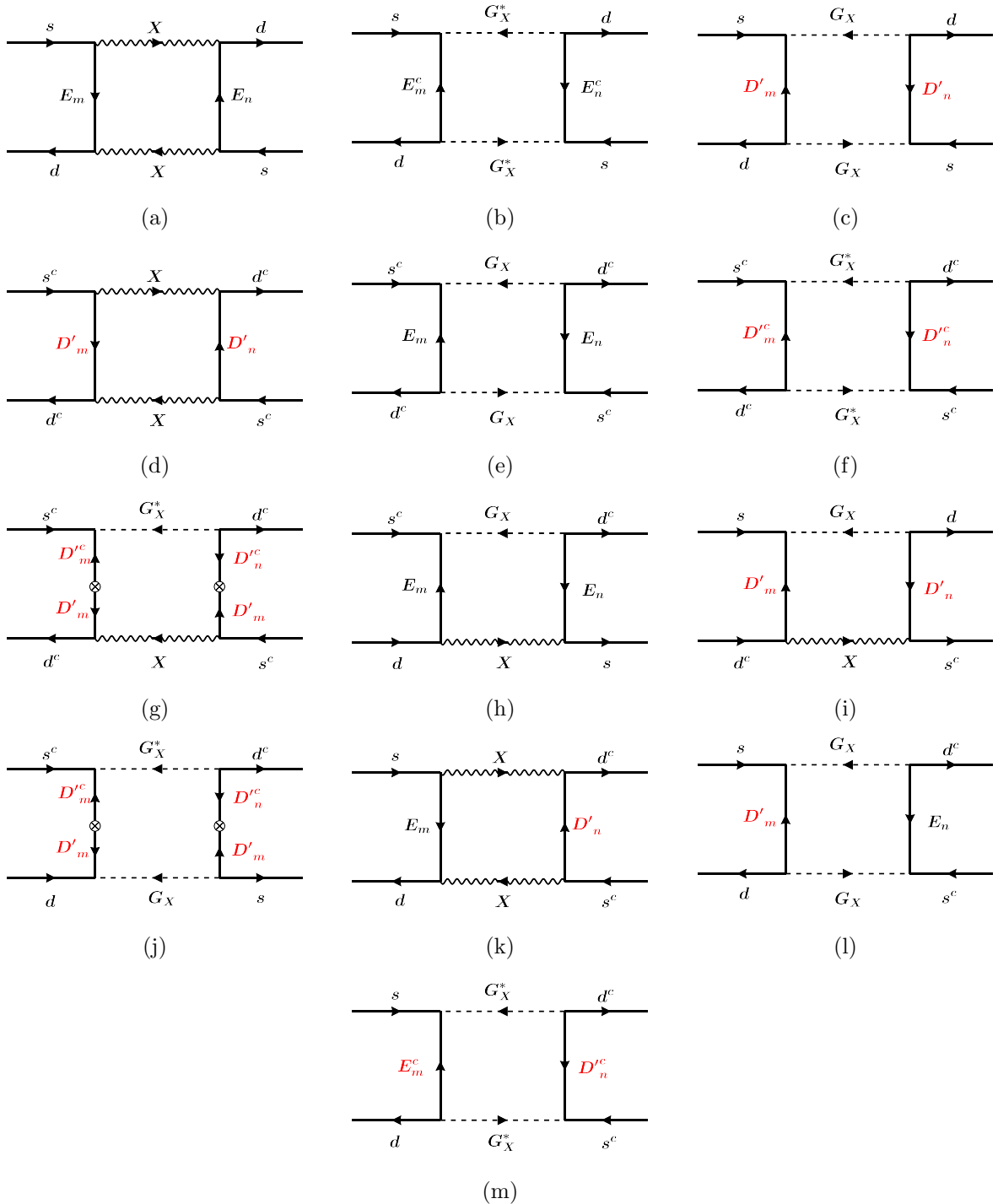


Figure 14: Representative Feynman diagrams contributing to the K -meson oscillation. Here, m, n are the flavor indices for the vector-like fermions, and the color indices are implicit.



Figure 15: Decomposition of the box topology in Fig. 14(a). The “annihilation” term of diagram (a-1) is equal to the “scattering” term of diagram (a-2).

$$C_1^{(a+b+c)} = - \left(\frac{g_4}{\sqrt{2}} \right)^4 \frac{1}{4\pi^2 M_X^2} \left[\sum_{m,n} \xi_{E_m} \xi_{E_n} A(t_{E_m}, t_{E_n}) + \frac{1}{16} \sum_{m,n} \xi_{E_m} \xi_{E_n} A(t_{E_m}, t_{E_n}) t_{E_m} t_{E_n} \right], \quad (4.25)$$

$$\tilde{C}_1^{(d+e+f+g)} = -2 \left(\frac{g_4}{\sqrt{2}} \right)^4 \frac{1}{4\pi^2 M_X^2} \left[\sum_{m,n} \xi_{D'_m} \xi_{D'_n} A(t_{D'_m}, t_{D'_n}) + \frac{1}{16} \sum_{m,n} \xi_{D'_m} \xi_{D'_n} A(t_{D'_m}, t_{D'_n}) t_{D'_m} t_{D'_n} \right. \\ \left. + \frac{1}{4} \sum_{m,n} \xi_{D'_m} \xi_{D'_n} B(t_{D'_m}, t_{D'_n}) t_{D'_m} t_{D'_n} \right], \quad (4.26)$$

$$C_4^{(h+i+j)} = + \left(\frac{g_4}{\sqrt{2}} \right)^4 \frac{1}{8\pi^2 M_X^2} \frac{m_d m_s}{M_X^2} \left[\sum_{m,n} \xi_{D'_m} \xi_{D'_n} A(t_{D'_m}, t_{D'_n}) + \sum_{m,n} \xi_{E_m} \xi_{E_n} A(t_{E_m}, t_{E_n}) \right. \\ \left. + \sum_{m,n} \xi_{D'_m} \xi_{D'_n} B(t_{D'_m}, t_{D'_n}) t_{D'_m} t_{D'_n} \right], \quad (4.27)$$

$$C_5^{(k+l+m)} = -2 \left(\frac{g_4}{\sqrt{2}} \right)^4 \frac{1}{16\pi^2 M_X^2} \left[\sum_{m,n} \xi_{E_m} \xi_{D'_n} A(t_{E_m}, t_{D'_n}) + \frac{1}{4} \sum_{m,n} \xi_{E_m} \xi_{D'_n} A(t_{E_m}, t_{D'_n}) t_{E_m} t_{D'_n} \right]. \quad (4.28)$$

Here we have defined $\xi_{D'_m} = K_{d^c D'_m} K_{s^c D'_m}^*$, $\xi_{E_m} = V_{dE_m} V_{sE_n}^*$, $t_\alpha = M_\alpha^2/M_X^2$, and, $A(x_i, x_j)$, $B(x_i, x_j)$ is already defined in Eq. (4.10). As before, the notation $C_1^{(a+b+c)}$ indicates that diagrams (a), (b), and (c) in Fig. 14 generate $Q_1 = (\bar{q}_{Li}^\alpha \gamma^\mu q_{Lj}^\alpha)(\bar{q}_{Li}^\beta \gamma_\mu q_{Lj}^\beta)$ operator. We should make several comments here:

(i) The extra factor of 2 in the contribution from \tilde{C}_1 compared to C_1 comes after considering the color flow. Specifically, after decomposing diagrams d, f, and g, we see that 8 diagrams contribute to the right-chirality structure, compared to only 4 diagrams for the left-chirality diagram (a).

(ii) Even though the Wilson coefficient $C_4^{(h+i+j)}$ is proportional to light quark masses as $m_d m_s / M_X^2$, Eq. (4.22) shows that it can induce C_5 at the hadronic scale through QCD running, which will contribute to the mixing.

(iii) The factor of 2 in $C_5^{(k+l+m)}$ appears from matching the induced operator $(\bar{q}_{L_i}^\alpha \gamma^\mu q_{L_j}^\alpha)(\bar{q}_{R_i}^\beta \gamma_\mu q_{R_j}^\beta)$ to the operator Q_5 using a Fierz transformation:

$$(\bar{q}_{Li}^\alpha \gamma^\mu q_{Lj}^\alpha)(\bar{q}_{Ri}^\beta \gamma_\mu q_{Rj}^\beta) = 2(\bar{q}_{Li}^\alpha q_{Rj}^\beta)(\bar{q}_{Ri}^\beta q_{Lj}^\alpha).$$

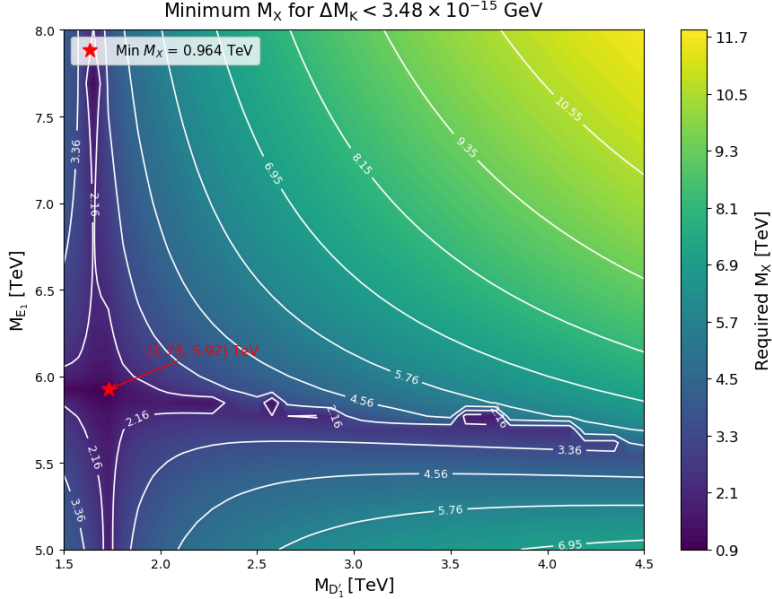


Figure 16: Minimum leptoquark mass M_X (in TeV) required by the $K^0 - \bar{K}^0$ mixing bound $\Delta M_K < 3.48 \times 10^{-15}$ GeV, shown as a function of the exotic-fermion masses $M_{D'_1}$ and M_{E_1} . The CKM-like mixing matrices are fixed according to Benchmark 2, Eq. (4.4), and the star denotes the global minimum in the scan.

With all the ingredients in our hands, we can go ahead and check a numerical example by considering the CKM-like matrices $(\xi_{E_m}, \xi_{D'_m})$ to have the structure like in Eq. (4.4) (Benchmark-2). Fig. 16 presents this benchmark, where we vary the vector-like fermion masses for a single generation, assuming that the exotics have a similar scale. Specifically, we scan over $M_{D'} = (M_{D'_1}, 1.7, 1.5)$ TeV and $M_E = (M_{E_1}, 5.9, 6.5)$ TeV. We find that in this setup, M_X can be as low as ~ 964 GeV, for the choice $(M_{D'_1}, M_{E_1}) = (1.73, 5.92)$ TeV.

4.3.2 $D^0 - \bar{D}^0$ oscillation

The recipe to obtain a lower limit on leptoquark gauge boson mass, M_X , from $D^0 - \bar{D}^0$ oscillation is the same as $K^0 - \bar{K}^0$ oscillation. First, we read the Feynman rules from Eq. (2.136)–(2.137) that identify the diagrams that contribute to $D^0 - \bar{D}^0$ mixing in Fig. 17. Now, the W' gauge boson will have new contributions to $D^0 - \bar{D}^0$ mixing, which were absent in the $K^0 - \bar{K}^0$ case. The contribution from the $W - W'$ box diagrams is negligible in our setup, as it will be suppressed by the small soft Z_2 breaking VEV w .

We now present the individual new physics contributions from the gauge boson, the Goldstone boson, and the mixed gauge-Goldstone boson. As shown in Fig. 17, the operators Q_1 , \tilde{Q}_1 , Q_4 , and Q_5 are induced similar to the $K^0 - \bar{K}^0$ oscillation. We can write down the leading-order expressions for Wilson coefficients following the conventions mentioned in Sec. 2.8:

$$C_1^{(a+b+c)} = - \left(\frac{g_4}{\sqrt{2}} \right)^4 \frac{1}{4\pi^2 M_X^2} \left[\sum_{m,n} \zeta_{E_m} \zeta_{E_n} A(t_{E_m}, t_{E_n}) + \frac{1}{16} \sum_{m,n} \zeta_{E_m} \zeta_{E_n} A(t_{E_m}, t_{E_n}) t_{E_m} t_{E_n} \right], \quad (4.29)$$

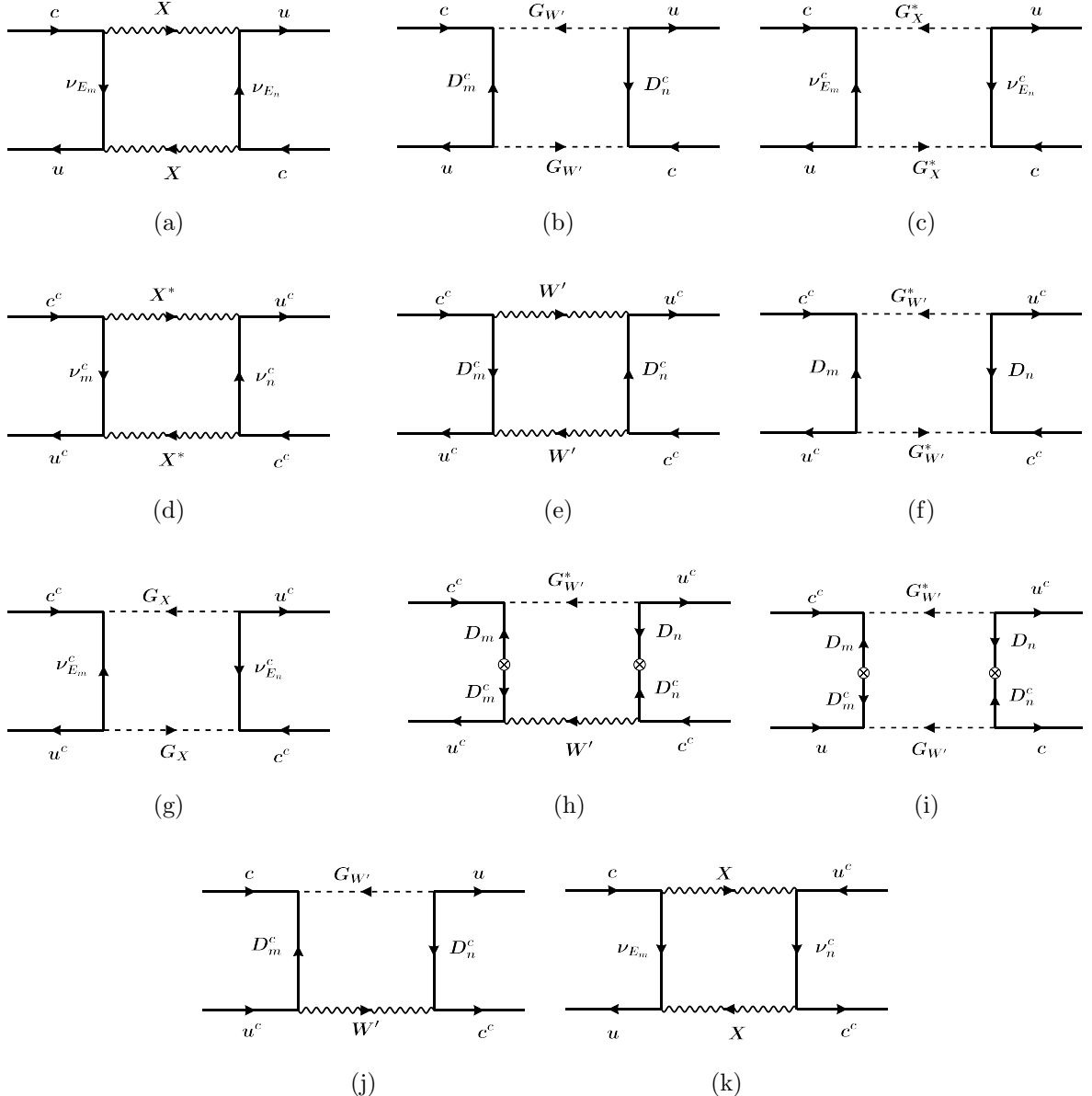


Figure 17: Representative Feynman diagrams contributing to the D -meson oscillation with heavy fermions running in the loop. Here, m, n are the flavor indices for the exotic fermions, and color indices are implicit.

$$\begin{aligned}
\tilde{C}_1^{(d+e+f+g+h)} = & - \left(\frac{g_4}{\sqrt{2}} \right)^4 \frac{1}{4\pi^2 M_X^2} \sum_{m,n} \zeta_{\nu_m^c} \zeta_{\nu_n^c} A(t_{\nu_m^c}, t_{\nu_n^c}) \\
& - \left(\frac{g_R}{\sqrt{2}} \right)^4 \frac{1}{4\pi^2 M_{W'}^2} \left[\sum_{m,n} \zeta_{D_m^c} \zeta_{D_n^c} A(r_{D_m^c}, r_{D_n^c}) \right. \\
& + \frac{1}{16} \sum_{m,n} \zeta_{D_m^c} \zeta_{D_n^c} A(r_{D_m}, r_{D_n}) r_{D_m} r_{D_n} \\
& \left. + \frac{1}{2} \sum_{m,n} \zeta_{D_m^c} \zeta_{D_n^c} B(r_{D_m}, r_{D_n}) r_{D_m} r_{D_n} \right], \tag{4.30}
\end{aligned}$$

$$C_4^{(i+j)} = \left(\frac{g_R}{\sqrt{2}}\right)^4 \frac{1}{16\pi^2 M_{W'}^2} \frac{m_u m_c}{M_{W'}^2} \left[\sum_{m,n} \zeta_{D_m^c} \zeta_{D_n^c} B(r_{D_m}, r_{D_n}) r_{D_m} r_{D_n} + 2 \sum_{m,n} \zeta_{D_m^c} \zeta_{D_n^c} A(r_{D_m}, r_{D_n}) \right], \quad (4.31)$$

$$C_5^{(k)} = -2 \left(\frac{g_4}{\sqrt{2}}\right)^4 \frac{1}{16\pi^2 M_X^2} \sum_{m,n} \zeta_{\nu_{E_m}} \zeta_{\nu_{E_n}} A(t_{\nu_{E_m}}, t_{\nu_{E_n}}). \quad (4.32)$$

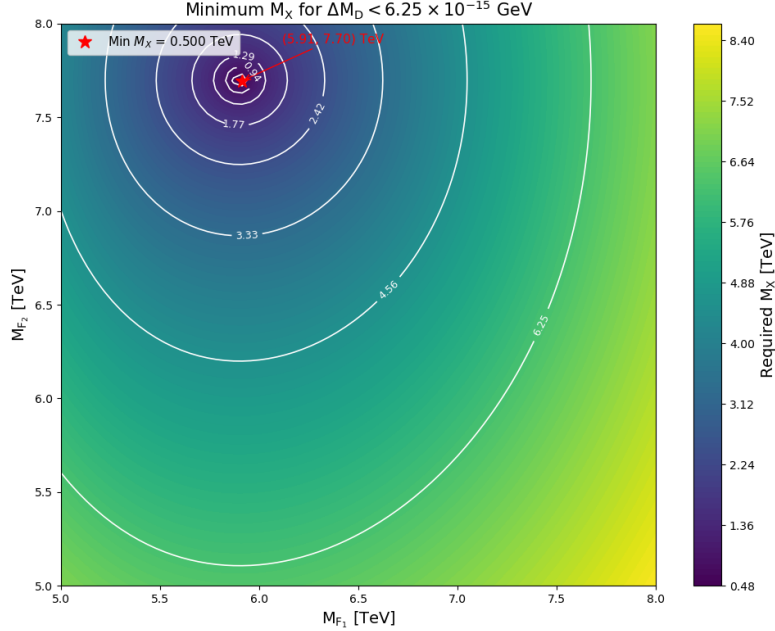


Figure 18: Heatmap showing the minimum value of M_X (in TeV) required to satisfy the constraint $\Delta M_D < 6.25 \times 10^{-15}$ GeV, as a function of the exotic fermion masses. For benchmark scenarios where the heavy fermions ν_E, ν^c, D are of similar mass scale and the CKM-like mixing matrices are followed by benchmark-2, the required value of M_X can be as low as ~ 500 GeV.

Here we use the definition $\zeta_{E_m} = V_{uE_m} V_{cE_m}^*$, $\zeta_{\nu_m^c} = V_{u\nu_m^c} V_{c\nu_m^c}^*$, $\zeta_{D_m^c} = K_{D_m^c u}^* K_{D_m^c c}$, $t_\alpha = M_\alpha^2/M_X^2$, $r_\alpha = M_\alpha^2/M_{W'}^2$, and, $A(x_i, x_j)$, $B(x_i, x_j)$ are already defined in Eq. (4.10). Now, to get a rough numerical estimation, we take the same CKM-like structure as in Eq. (4.4), and perform a parameter scan over $M_{\nu_E, \nu^c} \sim M_1 = (M_{F_1}, 5.9, 6.2)$ TeV and $M_D \sim M_2 = (M_{F_2}, 7.7, 6.5)$ TeV. We find that M_X can be as low as 500 GeV for the choice $(M_{F_1}, M_{F_2}) = (5.91, 7.70)$ TeV, while satisfying the experimental constraint $\Delta M_D < 6.25 \times 10^{-15}$ GeV, as illustrated in Fig. 18.

4.3.3 $B_q^0 - \bar{B}_q^0$ oscillation

The calculation of new contributions to $B_q^0 - \bar{B}_q^0$ oscillation ($q = d, s$) closely follows that of the $K^0 - \bar{K}^0$ system. The only difference is that it involves different generations of the down-type quarks. As a result, the hadronic matrix elements and the magic numbers would differ, as given in Appendix B.3.

For the benchmark scenario, we adopt the CKM-like matrices structured as defined in Eq. (4.4) and perform a scan over exotic fermion masses: $M_{\textcolor{red}{D}'} = (M_{\textcolor{red}{D}'_1}, 1.7, 1.5)$ TeV and

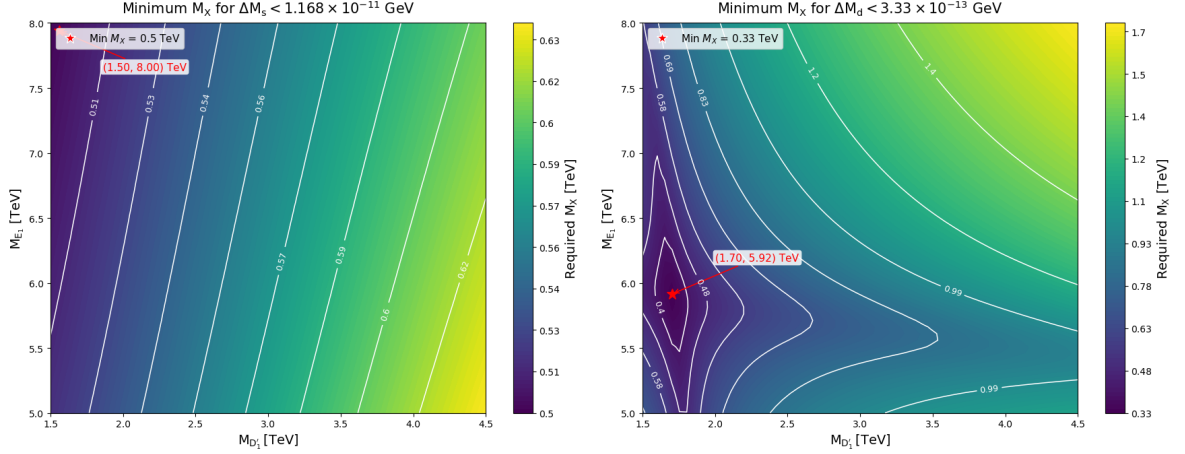


Figure 19: With a comparable benchmark scenario as $K^0 - \bar{K}^0$ oscillation, we show the required value of M_X with the variation of the vector-like fermion masses for $B_s^0 - \bar{B}_s^0$ oscillation (left), and for $B_d^0 - \bar{B}_d^0$ oscillation (right).

$M_E = (M_{E_1}, 5.9, 6.5)$ TeV. We observe from Fig. 19 that the required value of M_X can be as low as ~ 500 GeV from $B_s^0 - \bar{B}_s^0$ oscillation and as ~ 330 GeV from $B_d^0 - \bar{B}_d^0$ oscillation.

4.3.4 Tree-level meson mixing processes

Here we present the tree-level meson mixing processes mediated by heavy neutral gauge boson and neutral Higgs boson interactions that change flavor. They will contribute to $\bar{K}^0 - K^0$ and $\bar{B}^0 - B^0$ mass differences.

Neutral Higgs boson effects: Since we are interested in the stringent limits that can be placed on κ_R through meson oscillation, let us consider $\tilde{\chi}(2, 2, 1)$, and ignore the possible mixings of $\tilde{\chi}$ with other fields which has been discussed in Sec. 2.7 extensively. It is obvious from Eq. (2.14)

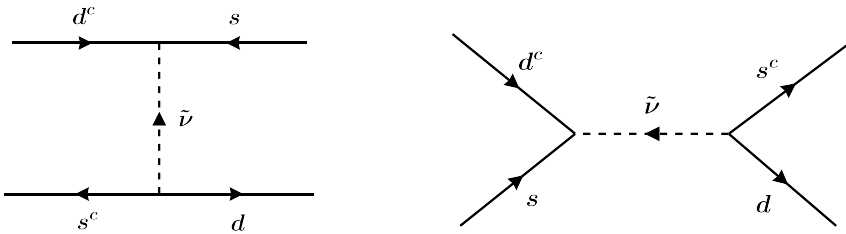


Figure 20: For example, $\bar{K}^0 - K^0$ mixing diagrams induced by neutral Higgs bosons.

that $\tilde{\nu}_E^c$ interactions are flavor diagonal and the absence of scalar-pseudo-scalar mixing allows us to write $\tilde{\nu} = \text{Re}[\tilde{\nu}] + i \text{Im}[\tilde{\nu}]$. In the limit of soft Z_2 breaking VEV $w = 0$, the physical states become $H_I = \text{Im}[\tilde{\nu}]$ and $H_R = \text{Re}[\tilde{\nu}]$ with mass $m_{H_I}^2 \approx m_{H_R}^2 \approx \alpha \kappa_R^2$ where α parameter can be determined from the Higgs-boson self interactions [74]. Therefore, the relevant interaction becomes (for example, for $\Delta S = 1$ processes)

$$\mathcal{L}_Y^0 = \frac{-ig_L}{\sqrt{2}M_{W_L}} \left(\sum_{i=u,c,t} \lambda_i m_i \right) (H_I \bar{s} \gamma_5 d - H_R \bar{s} d), \quad (4.33)$$

with $\lambda_i = V_{si}^* K_{icdc}$ where $V_{si} = (V_d^\dagger V_u)_{si}$ and $K_{icdc} = K_{dcic}^\dagger = (-V_{u^c}^\dagger x (\mathbb{I} + x^\dagger x)^{-1/2} V_{dc})_{icdc}$ as defined in Eq. (2.140). Now we can write the effective Hamiltonian leading to meson mixing using the conventional effective operators defined in Eq. (4.14) as :

$$\mathcal{H}_{\text{eff}}^{\tilde{\nu}} = \left(\frac{C^2(\Lambda)}{2m_{H_I}^2} + \frac{C^2(\Lambda)}{2m_{H_R}^2} \right) \left(Q_2^{ds} + \tilde{Q}_2^{ds} \right) + \left(\frac{C^2(\Lambda)}{m_{H_R}^2} - \frac{C^2(\Lambda)}{m_{H_L}^2} \right) Q_4^{ds}, \quad (4.34)$$

where $\Lambda \sim \kappa_R$ and $C = \frac{g_L}{M_{W_L}} \left(\sum_{i=u,c,t} \lambda_i m_i \right)$ and we evolve the Wilson coefficients from the high scale κ_R down to the hadronic scale using renormalization group running. To estimate this effect, let us take $m_{H_I} \simeq m_{H_R} \simeq 2$ TeV, V_{si} given by the CKM matrix, V_{u^c} , V_{dc} as identity, and the benchmark matrix x from Eq. (4.5). For this choice, we obtain

$$\Delta M_K^{(\tilde{\nu})} \simeq 2.8 \times 10^{-15} \text{ GeV}, \quad (4.35)$$

which is satisfied by the K -meson mixing bound (see Table 2). An interesting point to note here is that the flavor-changing matrix x allows us to realize neutral Higgs bosons at a lower scale than the conventional limits from meson mixing in left-right symmetric models, where the limit is about 20 TeV [75, 76].

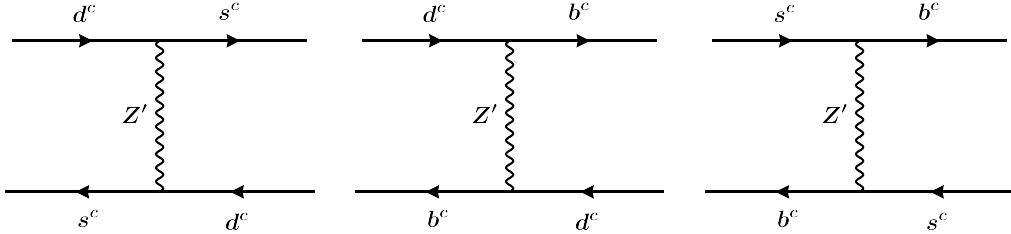


Figure 21: K - and B -meson mixing diagrams induced by Z' .

Neutral heavy gauge boson Z' effects: As we have seen already, because of the soft breaking of Z_2 symmetry, the fields d^c and D^c mix, and as a consequence, the neutral gauge boson Z' has flavor changing effect (d^c and D^c do not have the same T_{3R} charge) and contributes to K - and B -meson mixing at tree level through its coupling with d^c shown in Eq. (2.157). However, this contribution is highly suppressed in our setup. The tree-level exchange will induce the operator \tilde{Q}_1 , so that

$$\mathcal{H}_{\text{eff}}^{Z'} = \tilde{C}_1 \tilde{Q}_1, \quad \tilde{C}_1 \sim \frac{g_R^2}{2M_{Z'}^2} (P^{dc})^\dagger P^{dc}, \quad (4.36)$$

where P^{dc} is defined in Eq. (2.157). For a numerical estimation we take $M_{Z'} = 5.6$ TeV, V_{dc} to be the same structure as in Eq. (4.4), and let's use the benchmark matrix x shown in Eq. (4.5). Including the appropriate hadronic matrix elements, we find,

$$\Delta M_K^{(Z')} \sim 1.3 \times 10^{-21} \text{ GeV}, \quad \Delta M_{B_d}^{(Z')} \sim 1.2 \times 10^{-17} \text{ GeV}, \quad \Delta M_{B_s}^{(Z')} \sim 5.8 \times 10^{-18} \text{ GeV}, \quad (4.37)$$

and all of them are well within the experimental limits.

There are also flavor-changing processes induced by the Z -boson at tree-level in the model. The relevant couplings are given in Eq. (2.146). However, these processes are highly suppressed, as the off-diagonal couplings of the Z , such as $\bar{d}_L \gamma_\mu s Z^\mu$ have coefficients of order $Y_d^2 v^2 / \kappa_R^2 \lesssim$

10^{-8} (with the largest Y_d identified as $Y_b \simeq 16 \times 10^{-2}$). The resulting contributions to $K^0 - \overline{K^0}$ mixing, for example, are several orders of magnitude below the experimental limit.

4.4 Limit on M_X from cLFV through leptoquark gauge boson X_μ

Charged lepton-flavor violation (cLFV) processes such as $\mu \rightarrow e\gamma$ decay are highly suppressed in the SM, with a branching ratio in the unobservable range of order $\sim 10^{-54}$, induced by non-zero neutrino masses and mixing angles [77, 78]. Thus, any positive signal in the experimental searches for such processes will be clear evidence for a new dynamics. In this section, we present the detailed calculations for lepton-flavor violation (LFV) processes through leptoquark gauge boson X_μ exchange in the muonic sector, focusing on $\mu \rightarrow e\gamma$ radiative decay, $\mu \rightarrow eee$ decay, and μ - e conversion in a muonic atom in our setup.

4.4.1 $\mu \rightarrow e\gamma$ decay

One of the most studied processes of LFV is $\mu \rightarrow e\gamma$ decay. This decay probes the dipole operator with a chirality flip on the external muon and can provide dominant constraints on flavor structure in scenarios with quark-lepton correlation at the TeV scale. The amplitude

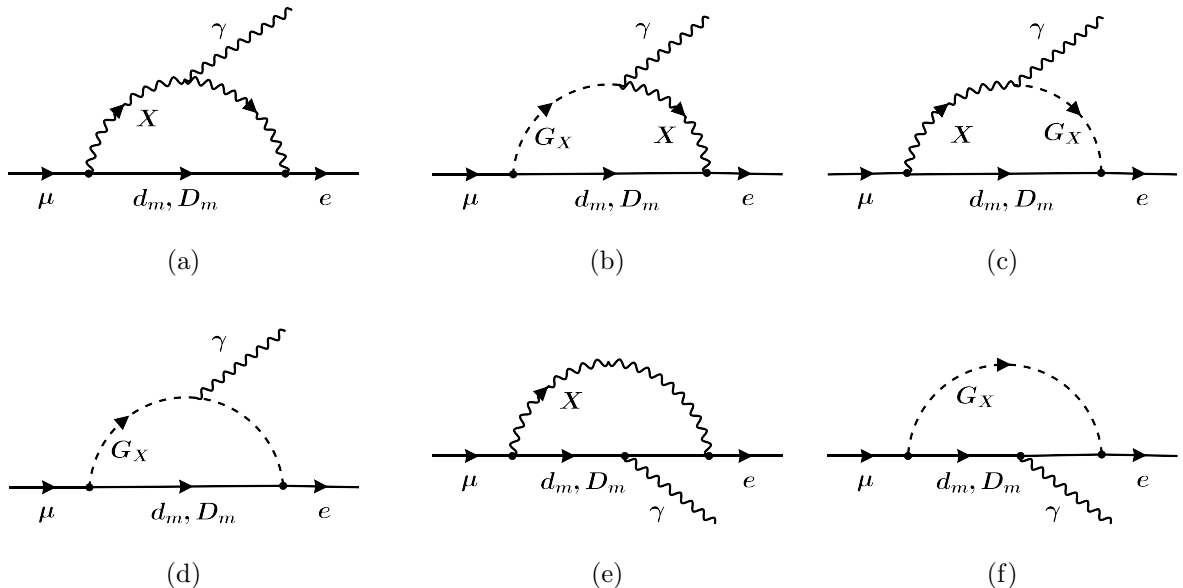


Figure 22: One loop contributions from leptoquark gauge boson to $\mu^c \rightarrow e^c \gamma$ amplitude in Feynman–t Hooft gauge. The chirality of the fermions and couplings can be understood from Eqs. (2.127) and (2.128).

for the physical decay process $\mu(p_1) \rightarrow e(p_2) + \gamma(q)$ can be written purely in terms of the gauge-invariant dipole form,

$$T(\mu \rightarrow e\gamma) = \epsilon_\lambda^*(q) \bar{u}_e(p_2) \left[i\sigma^{\lambda\nu} q_\nu (\sigma_L P_L + \sigma_R P_R) \right] u_\mu(p_1), \quad (4.38)$$

where $\epsilon_\lambda^*(q)$ is the polarization vector of the outgoing photon, $\sigma^{\lambda\nu} = (i/2)[\gamma^\lambda, \gamma^\nu]$ is the anti-symmetric tensor, and $P_{R,L} = (1 \pm \gamma_5)/2$ are the chirality projectors. The form factors $\sigma_{L,R}$ are obtained by computing the diagrams shown in Fig. 22.

In the limit $m_e \rightarrow 0$, the decay width can be written as [79, 80]

$$\Gamma(\mu \rightarrow e\gamma) = \frac{m_\mu^3}{16\pi} (|\sigma_L|^2 + |\sigma_R|^2). \quad (4.39)$$

In our setup, X_μ couples only to right-handed leptons (their left-handed partners are not charged under $SU(4)_C$), as can be seen from the relevant Lagrangian terms in Eqs. (2.127) and (2.128). Thus, the chirality flip must occur on the external lepton legs in these diagrams. From Eq. (4.38), this implies $\sigma_L \propto m_\mu$ and $\sigma_R \propto m_e$. Taking $m_e \simeq 0$, it is justified to neglect σ_R and to work in the limit $|\sigma_L|^2 \gg |\sigma_R|^2$.

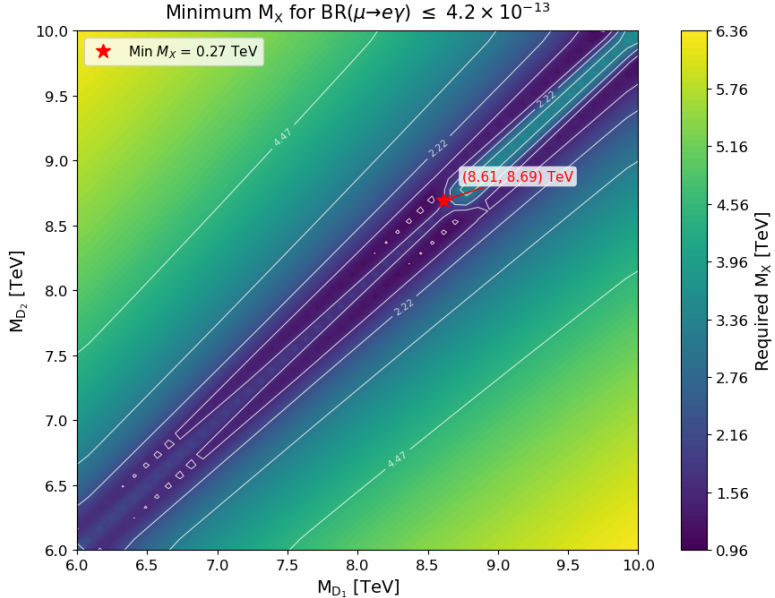


Figure 23: Minimum M_X required by the $\text{BR}(\mu \rightarrow e\gamma) \leq 4.2 \times 10^{-13}$ across the (M_{D_1}, M_{D_2}) plane (with $M_{D_3} = 6.7$ TeV fixed). The colorbar indicates the required M_X in TeV, with the white lines representing iso- M_X contours. The red star marks the global minimum on the scan.

We perform the calculations in 't Hooft-Feynman gauge instead of unitary gauge following Ref. [80]. Summing the vector and would-be Goldstone boson exchanges provides a finite, gauge-invariant result, which can be expressed as follows:

$$\sigma_L = \frac{N_c e g_4^2}{2} \sum_m \left[\rho_m^d \left(Q_d \mathcal{I}_1(t_m) + Q_X \mathcal{I}_2(t_m) \right) + \rho_m^D \left(Q_D \mathcal{I}_1(t_m) + Q_X \mathcal{I}_2(t_m) \right) \right]. \quad (4.40)$$

Here m is the flavor index, $t_m = \frac{M_m^2}{M_X^2}$, $Q_d = Q_D = -1/3$, $Q_X = 2/3$ are the electric charges of the internal down-type fermion and the gauge boson X_μ respectively, in the units of e , and $N_c = 3$ is the number of color flow in the loop. The loop kernels can be expressed as:

$$\mathcal{I}_1(t) = \frac{m_\mu}{(-i) 16\pi^2 M_X^2} \left(\frac{-5t^3 + 9t^2 - 30t + 8}{12(t-1)^3} + \frac{3t^2 \ln t}{2(t-1)^4} \right), \quad (4.41)$$

$$\mathcal{I}_2(t) = \frac{m_\mu}{(-i) 16\pi^2 M_X^2} \left(\frac{-4t^3 + 45t^2 - 33t + 10}{12(t-1)^3} - \frac{3t^3 \ln t}{2(t-1)^4} \right). \quad (4.42)$$

where the three-gauge-boson vertex (see Fig. 22 (a)) of the outgoing photon γ_α with momentum q , incoming X_μ and X_ν^* with momentum p and \bar{p} has the Feynman rule: $ie Q_X \left(g^{\mu\nu} (p - \bar{p})^\alpha - \right.$

$g^{\alpha\mu}(q+p)^\nu + g^{\alpha\nu}(q+\bar{p})^\mu\right)$. And the coupling of the vertex of γ_μ with incoming X_α^* and G_X has the form $ieQ_XM_Xg^{\mu\alpha}$.

As for the coefficient ρ_m in Eq. (4.40), we decompose it into two physically distinct pieces, depending on whether a light quark (ρ_m^d) or a heavy quark (ρ_m^D) runs in the loop. When light quarks, $d_m^c = (d^c, s^c, b^c)$, are flowing internally, Eq. (2.127) gives us the form of ρ_m :

$$\rho_m^d = K_{d_m^c e^c}^\dagger K_{d_m^c \mu^c} \quad (4.43)$$

where the definition of $K_{d^c e^c}$ can be read from Eq. (2.129) which is not necessarily unitary (see the discussion in section 4.1). A sizable deviation of $K_{d^c e^c}$ from unitarity will not guarantee GIM cancellation in Eq. (4.40) anymore, and it can have a large impact on cLFV, since the loop kernels in Eqs. (4.41)-(4.42) will pick up contributions which are not suppressed by the small quark masses. This type of enhanced cLFV rates at observable levels has been studied for low-scale right-handed neutrinos [81, 82]. As discussed earlier in Sec. 4.1, while optimizing the for meson decays, we already took this situation into account, and made sure that the optimized K (see Eq. (4.6)) simultaneously takes care of the meson decays and the cLFV processes while lowering the scale of the PS gauge boson. And the matrix x carries the information of the overall suppression coming from the softly broken Z_2 symmetry, which further limits direct couplings of X to purely SM states.

When heavy vector-like quarks $D_m^c = (D_1^c, D_2^c, D_3^c)$ run in the loops, we get the form of ρ_m from Eq. (2.128):

$$\rho_m^D = K_{D_m^c e^c}^\dagger K_{D_m^c \mu^c}, \quad (4.44)$$

where $K_{D^c e^c}^\dagger$ can be read from Eq. (2.132). When evaluating ρ_m^D , we use the benchmark-2 structure as in Eq. (4.4) for $K_{D^c e^c}$ in the scans and we present the results in Fig. 23. Now, to have a quantitative estimation, we scan over (M_{D_1}, M_{D_2}) while fixing $M_{D_3} = 6.7$ TeV. At each point, we compute the $\mu \rightarrow e\gamma$ branching ratio using the expression

$$\text{BR}(\mu \rightarrow e\gamma) = \frac{m_\mu^3}{16\pi \Gamma_\mu} |\sigma_L|^2, \quad (4.45)$$

with $\Gamma_\mu = G_F^2 m_\mu^5 / (192\pi^3)$ and determine the minimum M_X required at that point by solving the constraint $\text{BR} \leq 4.2 \times 10^{-13}$ (see Table 2). Fig. 23 shows the resulting contours of the required M_X throughout the (M_{D_1}, M_{D_2}) plane.

One comment about the diagonal valley that we see in this plot: it is not any special requirement of lowering the PS scale; rather, it is an artifact of the choice for CKM-like matrices. In detail, with the benchmark choice for our case, the dominant contribution comes when heavy quarks D_m^c run in the loop. The CKM-weighted dipole sum from Eq. (4.40) in that case reads as,

$$\sigma_L \approx \sum_{m=1}^3 \rho_m^D F_m, \quad F_m \equiv Q_D \mathcal{I}_1(t_m) + Q_X \mathcal{I}_2(t_m).$$

Unitarity requires $\sum_m \rho_m^D = 0$. Along the degenerate line $M_{D_1} = M_{D_2}$ (so $F_1 = F_2 \equiv F$), we have

$$\sigma_L = (\rho_1^D + \rho_2^D)F + \rho_3^D F_3 = \rho_3^D (F_3 - F),$$

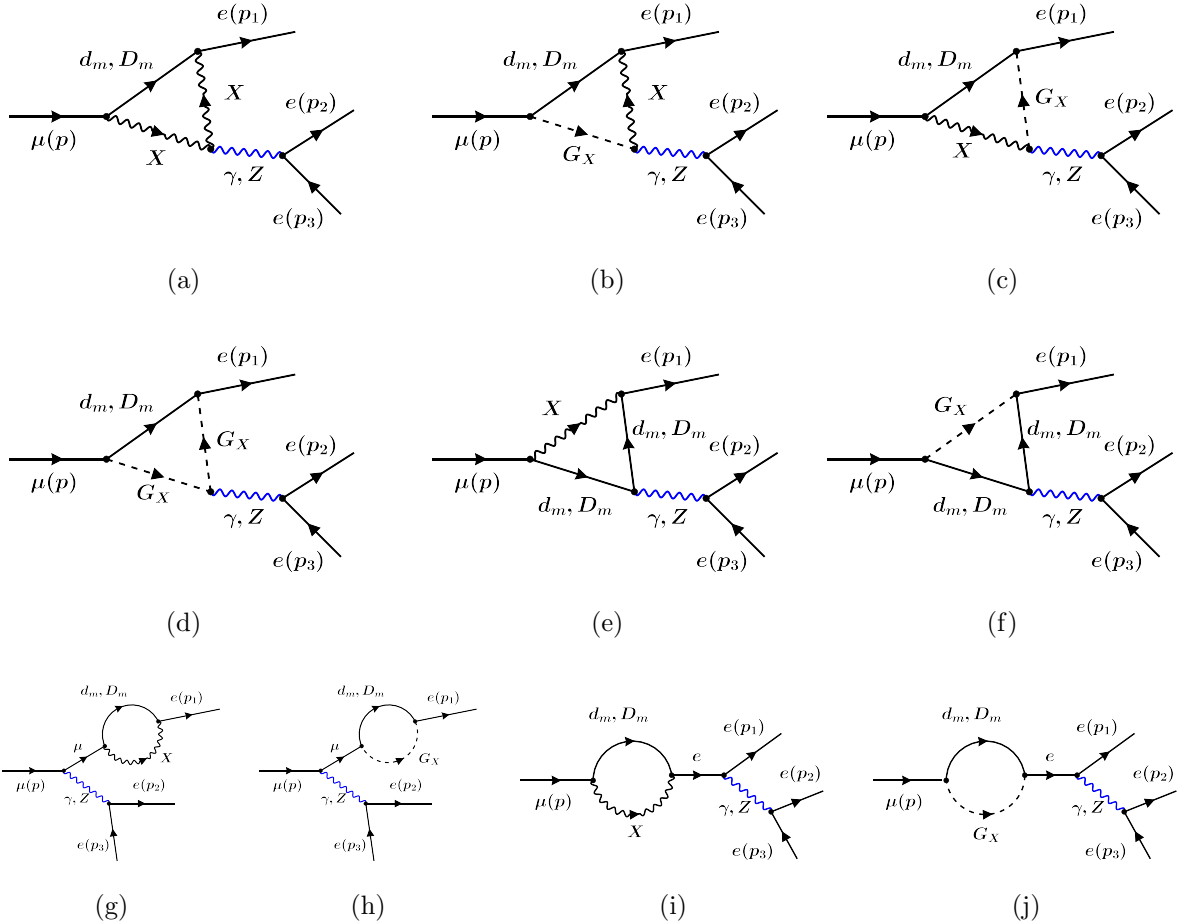


Figure 24: Penguin topologies contributing to the $\mu \rightarrow eee$ decay through monopole and dipole transitions. m indicates the flavor index of the internal fermion field. The chirality and the coupling for the external fermion lines can be understood from Eqs. (2.127) and (2.128). The set of diagrams related by $p_1 \leftrightarrow p_2$ is implied.

leaving only the small weight $\rho_3^D \approx V_{D_3^c e^c}^* V_{D_3^c \mu^c}$ times a loop difference, that is the reason we see the valley. Moving away from the degeneracy with $F_{1,2} = F \pm \delta F$, will lift $|\sigma_L|$,

$$\sigma_L \simeq \rho_3^D (F_3 - F) + (\rho_1^D - \rho_2^D) \delta F.$$

Since we will be using the same benchmark throughout, this pattern will also appear in the subsequent sections.

4.4.2 $\mu \rightarrow eee$

This flavor-violating decay arises at one-loop in our setup (see Fig. 24–25). Unlike $\mu \rightarrow e\gamma$, this mode receives contributions from the off-shell photon. In addition, Z penguins and box diagrams also contribute to this process, which involve leptoquark gauge bosons in the loop. As a result, even when the dipole form factor σ_L is suppressed and $\mu \rightarrow e\gamma$ is effectively absent, these contributions can make $\mu \rightarrow eee$ competitive and more constraining.

We start with the effective Lagrangian (at the scale m_μ) which contributes to the $\mu \rightarrow eee$

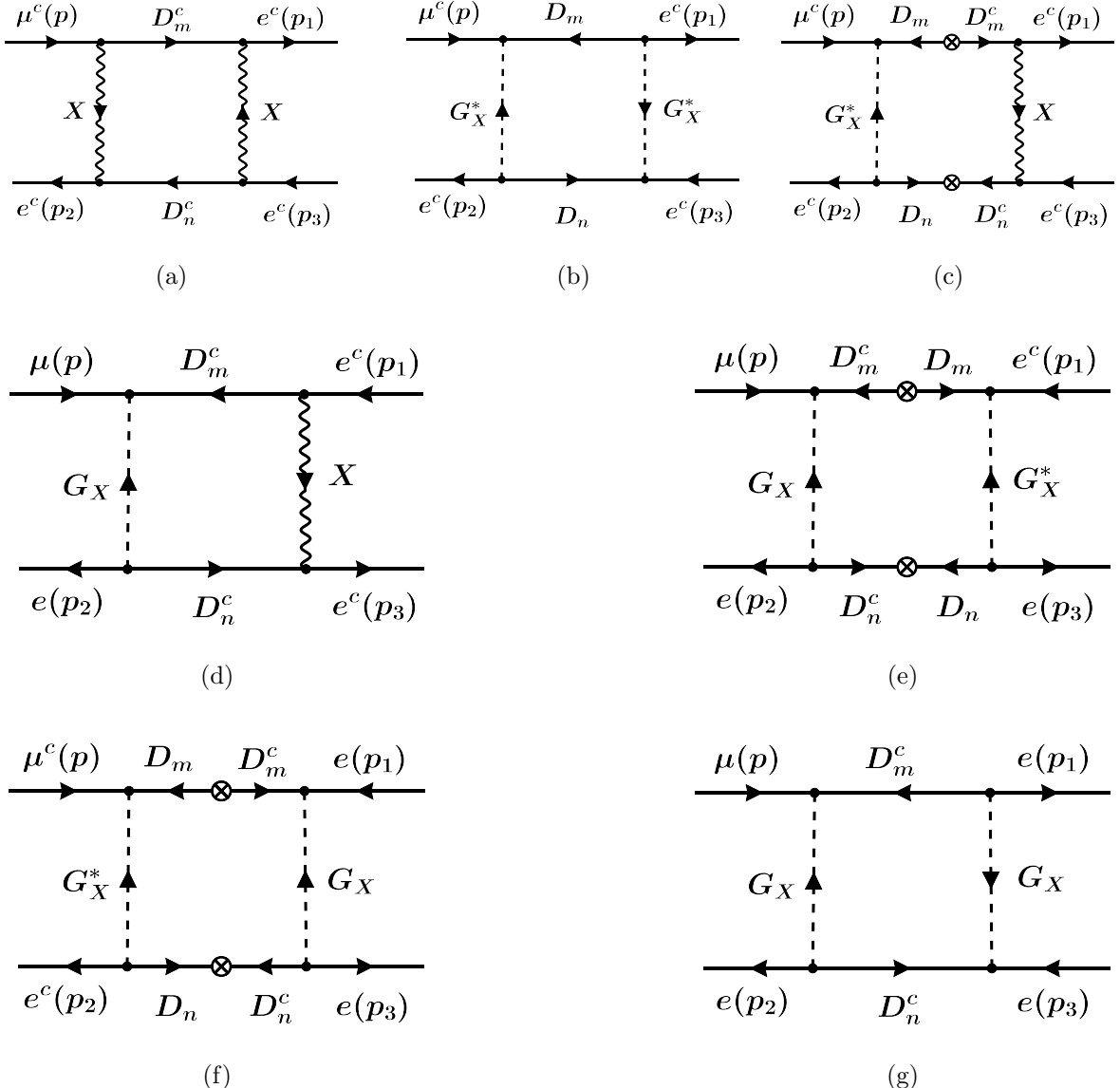


Figure 25: Box topologies contributing to the $\mu \rightarrow eee$ decay. m, n denotes the flavor indices of the internal heavy field. The set of diagrams related by $p_1 \leftrightarrow p_2$ is implied as well.

process [83]:

$$\begin{aligned}
 \mathcal{L}_{\mu \rightarrow eee} = & -\frac{4G_F}{\sqrt{2}} \left[m_\mu A_R \bar{\mu}_L \sigma^{\mu\nu} e_R F_{\mu\nu} + m_\mu A_L \bar{\mu}_R \sigma^{\mu\nu} e_L F_{\mu\nu} \right. \\
 & + h_1 (\bar{\mu}_R e_L) (\bar{e}_R e_L) + h_2 (\bar{\mu}_L e_R) (\bar{e}_L e_R) + h_3 (\bar{\mu}_R \gamma^\mu e_R) (\bar{e}_R \gamma_\mu e_R) + h_4 (\bar{\mu}_L \gamma^\mu e_L) (\bar{e}_L \gamma_\mu e_L) \\
 & \left. + h_5 (\bar{\mu}_R \gamma^\mu e_R) (\bar{e}_L \gamma_\mu e_L) + h_6 (\bar{\mu}_L \gamma^\mu e_L) (\bar{e}_R \gamma_\mu e_R) \right] + \text{h.c.}
 \end{aligned} \tag{4.46}$$

where the Fierz rearrangement has been used in the four-fermion operators. Here, G_F is the Fermi constant, and $A_{L,R}$ and h_i are dimensionless coupling constants for the corresponding operators with the assumption that the momentum dependencies of the form factors are negligible. Several comments on the Lagrangian are warranted:

The first comment is about the photonic contribution to this decay process. There are two types of amplitudes for photonic transition $\mu \rightarrow e\gamma^*$, the monopole and dipole transitions. In

the Lagrangian, we have converted the monopole contribution to the vector-vector interaction. The smallness of A_R in our model has already been discussed previously in Sec. 4.4.1, and the matching between Eqs. (4.38) and (4.46) gives us $A_L = \sigma_L/(4\sqrt{2} G_F m_\mu)$. The extra factor of 1/2 comes from the basis change between $\epsilon_\mu q_\nu$ and $F_{\mu\nu} = i(q_\mu \epsilon_\nu - q_\nu \epsilon_\mu)$.

The second comment is on the vector-vector interactions (terms with h_3 , h_4 , h_5 , and h_6 coefficients). We are considering lepton flavor violation mediated by the leptoquark gauge boson, X_μ . As we know, in our setup, X_μ would couple right-handed leptons to the down isospin dominantly. So, only h_3 and h_5 will contribute through penguins and boxes. The other two coefficients, h_4 and h_6 , will be induced only through self-energy corrections or Goldstone contributions in boxes which are strongly suppressed. For example, in the topology of Fig. 25 (g), h_4 is induced with a suppression of $m_\mu m_e^3/M_X^4$ with external momentum set to zero, which gives essentially zero contribution.

The third comment is about the scalar four-fermion operators, h_1 and h_2 . From Fig. 25 (d, e, f), we see that they also suffer suppression from light lepton mass $\sim m_\mu m_e/M_X^2$. As a result, they are also subleading in the parameter space of our model.

Since we presented the detailed expression for the dipole form factor σ_L in the previous section, we now concentrate on the neutral-current Wilson coefficients h_3 and h_5 . These coefficients capture the short-distance neutral-current effects arising from γ/Z penguins and box diagrams mediated by the vector leptoquark X_μ (see Figs. 24–25). They are finite, gauge-independent, and satisfy the Slavnov–Taylor identities when the self-energy subtractions are included, following the procedure of Refs. [84, 85]. These coefficients have the general form:

$$h_3 = \frac{3}{16\pi^2} \left(\frac{g_4}{g_L} \right)^2 \left(\frac{M_W}{M_X} \right)^2 \left[e^2 \left(\mathcal{F}_1^{(\gamma Z)} + \mathcal{F}_2^{(\gamma Z)} \right) + g_4^2 \mathcal{F}^{(B)} \right], \quad (4.47)$$

$$h_5 = \frac{3e^2}{16\pi^2} \left(\frac{g_4}{g_L} \right)^2 \left(\frac{M_W}{M_X} \right)^2 \left(\mathcal{F}_1^{(\gamma Z)} + \mathcal{F}_2^{(\gamma Z)} \right). \quad (4.48)$$

The functions $\mathcal{F}_{1,2}^{(\gamma Z)}$ and $\mathcal{F}^{(B)}$ are the gauge-independent combinations of the photon penguin with the Z penguin and the photon penguin with the box diagrams. For $\mathcal{F}_{1,2}^{(\gamma Z)}$, we implement the same method used in $\mu \rightarrow e\gamma$ of separating the light $d_m = (d, s, b)$ and heavy $D_m = (D_1, D_2, D_3)$ internal fermions flowing in the loop. We define

$$\mathcal{F}_1^{(\gamma Z)} = \sum_{m=1}^3 \rho_m^d [Q_F F_{\gamma Z}^F(t_m) + Q_V F_{\gamma Z}^V(t_m)], \quad (4.49)$$

$$\mathcal{F}_2^{(\gamma Z)} = \sum_{m=1}^3 \rho_m^D [Q_F F_{\gamma Z}^F(T_m) + Q_V F_{\gamma Z}^V(T_m)], \quad (4.50)$$

with $Q_F = -\frac{1}{3}$, $Q_V = +\frac{2}{3}$, $t_i = m_{d_i}^2/m_X^2$, and $T_i = m_{D_i}^2/m_X^2$, and the flavor structure $\rho_m^{d,D}$ follows the same definition as in Eqs. (4.43)–(4.44). The penguin form factors are given as:

$$F_{\gamma Z}^F(t) = \frac{14t^2 - 21t + 1}{12(t-1)^3} + \frac{-9t^2 + 16t - 4}{6(t-1)^4} \ln t, \quad (4.51)$$

$$F_{\gamma Z}^V(t) = \frac{6t^4 - 18t^3 - 32t^2 + 87t - 37}{12(t-1)^3} + \frac{t(8t^3 - 2t^2 - 15t + 6)}{6(t-1)^4} \ln t. \quad (4.52)$$

We see that the function $F_{\gamma Z}(t)$ develops an infrared log-singularity in the limit $t = m_f^2/m_X^2 \rightarrow 0$, corresponding to a light-fermion loop in the effective theory. In the Standard Model, this

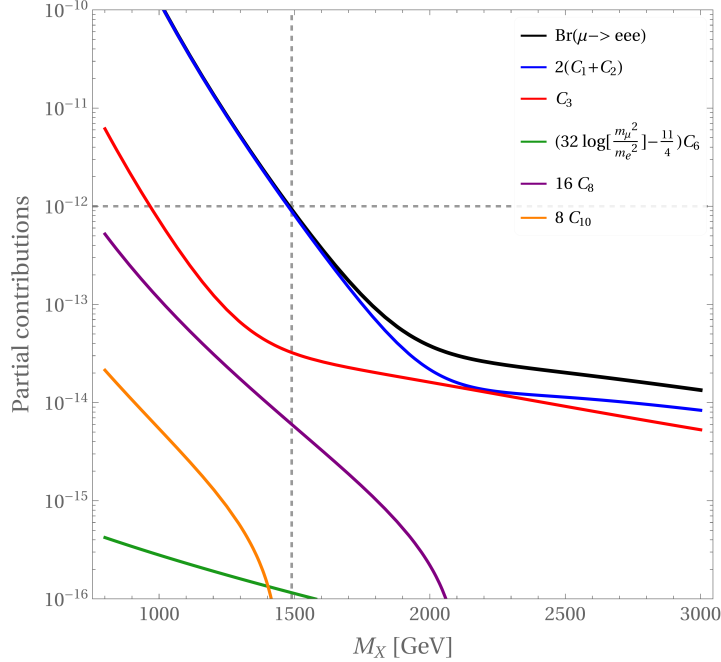


Figure 26: Decomposition of $\text{Br}(\mu \rightarrow eee)$ as a function of M_X at fixed mixings and heavy down-quark masses $M_D = (7640, 7600, 6700)$ GeV. The black curve represents the total rate, while the colored curves show the relevant individual terms in Eq. (4.56). When the dipole piece C_6 is suppressed, the contact contributions $C_{1,2,3}$ can dominate.

logarithm reproduces the leading term associated with the operator mixing $Q_{7\gamma} \rightarrow Q_9$ [86]. In our framework, the same light fermion contribution cancels against the Standard Model part, and we end up having a finite, gauge-independent short-distance contribution in the Wilson coefficients h_3 .

As for the box diagram form factor, we can express it as follows:

$$\mathcal{F}^{(B)} = \sum_{m,n=1}^3 \rho_m^D \rho_n^D [f_V^{R,BZ}(T_m, T_n) + f_V^{R,B'Z}(T_m, T_n)] \quad (4.53)$$

where the symmetric two-mass kernels are given by

$$f_V^{R,BZ}(x, y) = \frac{xy}{4} \left[\frac{3x(xy(xy + x - 6) + 4) - (x - 1)(xy(xy - 2) + 4)}{(x - 1)^2(xy - 1)^2} \ln x + \frac{3y(-4xy + x + y + 2)}{(y - 1)^2(xy - 1)^2} \ln y + \frac{12 - 3y}{(x - 1)(y - 1)} + \frac{2xy - 5}{xy - 1} \right], \quad (4.54)$$

$$f_V^{R,B'Z}(x, y) = \frac{xy}{4} \left[\frac{3x^2y(xy + x - 2) - (x - 1)(xy(xy - 2) + 4)}{(x - 1)^2(xy - 1)^2} \ln x + \frac{3y(x + y - 2)}{(y - 1)^2(xy - 1)^2} \ln y - \frac{3y^2}{(x - 1)(y - 1)} + \frac{2xy - 5}{xy - 1} \right], \quad (4.55)$$

which are UV-finite and symmetric under $x \leftrightarrow y$ exchange.

Now that we have finite, gauge-independent contributions to $\mu \rightarrow eee$ in hand, we can

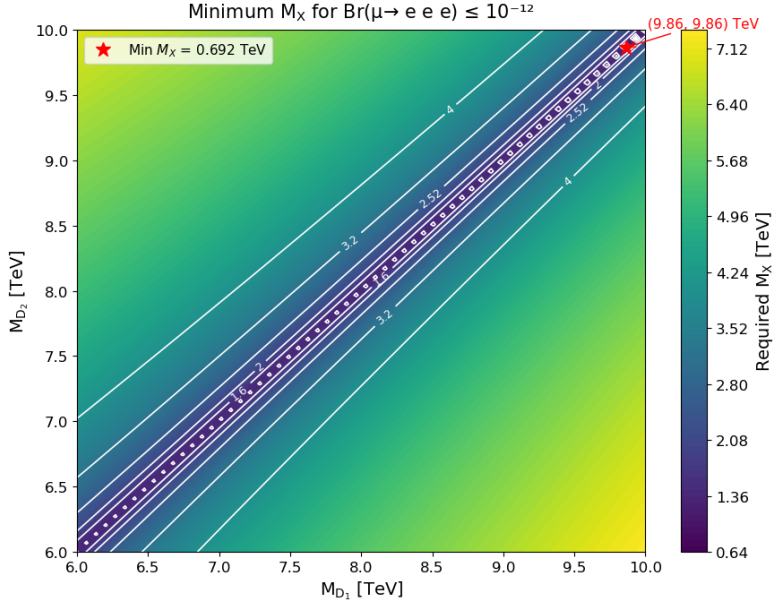


Figure 27: Minimum M_X required by the $\text{Br}(\mu \rightarrow eee) \leq 1.0 \times 10^{-12}$ in the (M_{D_1}, M_{D_2}) plane (with $M_{D_3} = 6.7$ TeV fixed). The color bar indicates the required M_X in TeV, with the white lines representing iso- M_X contours. We show the global minimum on the scan with a red star.

write down the kinematically integrated branching ratio, following Ref. [83]:

$$\text{Br}(\mu \rightarrow eee) = 2(C_1 + C_2) + (C_3 + C_4) + 32 \left[\ln \left(\frac{m_\mu^2}{m_e^2} \right) - \frac{11}{4} \right] (C_5 + C_6) + 16(C_7 + C_8) + 8(C_9 + C_{10}). \quad (4.56)$$

Here the coefficients are given by

$$\begin{aligned} C_1 &= \frac{|h_1|^2}{16} + |h_3|^2, & C_2 &= \frac{|h_2|^2}{16} + |h_4|^2, & C_3 &= |h_5|^2, & C_4 &= |h_6|^2, \\ C_5 &= |eA_R|^2, & C_6 &= |eA_L|^2, & C_7 &= \Re(eA_R h_4^*), & C_8 &= \Re(eA_L h_3^*), \\ C_9 &= \Re(eA_R h_6^*), & C_{10} &= \Re(eA_L h_5^*). \end{aligned} \quad (4.57)$$

For completeness, we have included all the contributions here, but as we discussed, not all will have significant contributions to this decay in our setup. To have a clear picture, we plot in Fig. 26 the major contributors. As expected, A_L , h_3 , and h_5 play important roles. The contribution coming from the pure dipole term C_6 will always show up in $\mu \rightarrow e\gamma$ process first, because here they will always have a kinematic suppression given by

$$\frac{B(\mu \rightarrow eee)}{B(\mu \rightarrow e\gamma)} \simeq \frac{\alpha}{3\pi} \left[\ln \left(\frac{m_\mu^2}{m_e^2} \right) - \frac{11}{4} \right] = 0.006, \quad (4.58)$$

which we can check with any benchmark case in our setup. For example, with $M_D = (7.64, 7.60, 6.70)$ TeV, independent of M_X , the ratio is ~ 0.006 . For the scan in Fig. 27, we use the same benchmark scenario as in $\mu \rightarrow e\gamma$, since the same mixing and couplings enter into the calculation. The plot shows the minimum M_X that is required to satisfy $\text{Br}(\mu \rightarrow eee) \leq 10^{-12}$ (see Table 2) in the (M_{D_1}, M_{D_2}) plane, keeping $M_{D_3} = 6.7$ TeV fixed. The diagonal valley is also visible in the plot, as we were expecting from the discussions of the previous section.

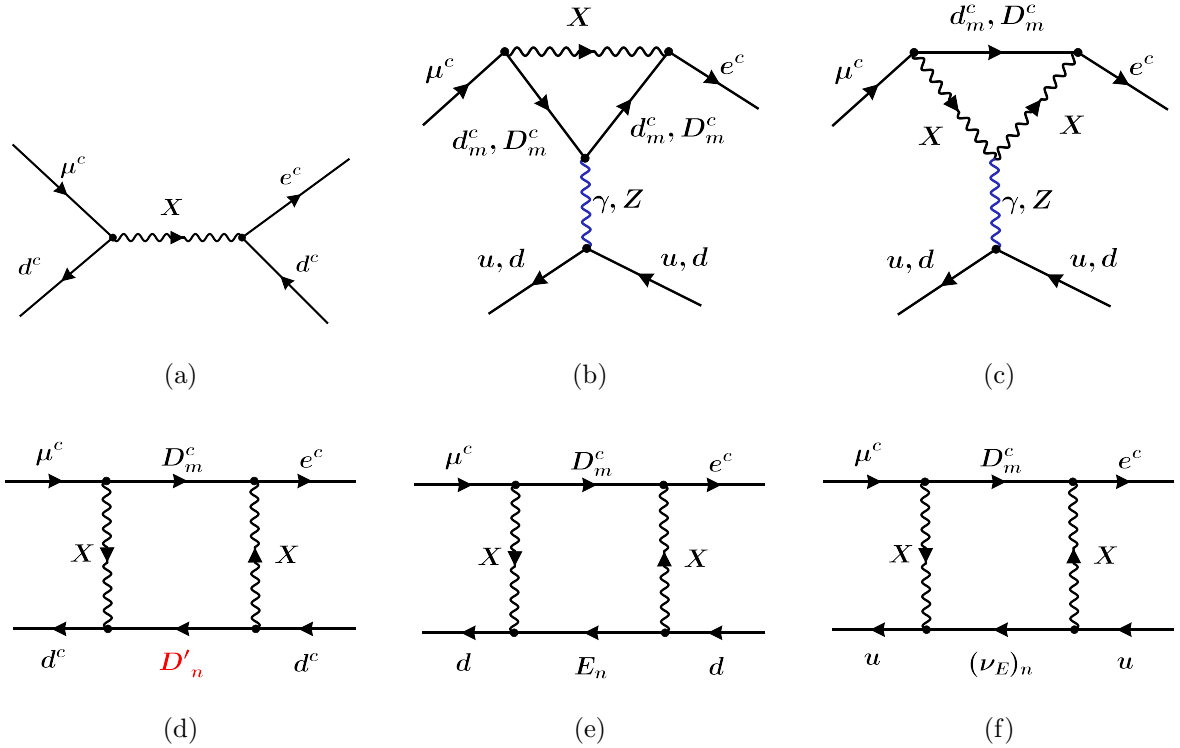


Figure 28: Some representative diagrams that contribute to the $\mu - e$ conversion. (a) shows the tree-level contribution mediated by the leptoquark gauge boson X_μ . (b) and (c) represent γ/Z penguin diagrams, other diagrams with the unphysical modes can be inferred by replacing the external lepton legs in $\mu \rightarrow eee$ process (see Fig. 24) with valence quarks. (d)-(f) are the box diagrams involving two different classes of VLQ where $\mu \rightarrow e$ conversion can happen while interacting with both chiralities of quarks.

4.4.3 $\mu - e$ conversion in nuclei

Among the well-studied cLFV processes, coherent $\mu - e$ conversion in nuclei has a special place. When an atom captures a negative muon, it can fall to the $1s$ orbital and form a muonic atom. Instead of the usual decay or nuclear capture, this muon can convert into an electron through a flavor-violating transition, leaving the nucleus intact [87]. This neutrino-less process will conserve lepton number but violate flavor by one unit. We are interested in the coherent conversion where all nucleons contribute constructively. As a result, its rate can be significantly enhanced, especially when flavor-violating gauge boson interactions are present in the theory. This process can be more constraining in some parts of the parameter space where $\mu \rightarrow e\gamma$ and/or $\mu \rightarrow eee$ rates remain small. Unlike these two processes, tree-level diagrams contribute to $\mu - e$ conversion. It is also induced at the one-loop level as shown in Fig. 28.

We can write down the most general LFV interaction Lagrangian that contributes to the

$\mu \rightarrow e$ conversion in nuclei following Ref. [88]:

$$\begin{aligned} \mathcal{L}_{\text{int}} = & -\frac{4G_F}{\sqrt{2}} (m_\mu A_R \bar{\mu} \sigma^{\mu\nu} P_L e F_{\mu\nu} + m_\mu A_L \bar{\mu} \sigma^{\mu\nu} P_R e F_{\mu\nu}) \\ & - \frac{G_F}{\sqrt{2}} \sum_q \left[(g_{LS(q)} \bar{e} P_R \mu + g_{RS(q)} \bar{e} P_L \mu) \bar{q} q + (g_{LP(q)} \bar{e} P_R \mu + g_{RP(q)} \bar{e} P_L \mu) \bar{q} \gamma_5 q \right. \\ & \left. + (g_{LV(q)} \bar{e} \gamma^\mu P_L \mu + g_{RV(q)} \bar{e} \gamma^\mu P_R \mu) \bar{q} \gamma_\mu q + (g_{LA(q)} \bar{e} \gamma^\mu P_L \mu + g_{RA(q)} \bar{e} \gamma^\mu P_R \mu) \bar{q} \gamma_\mu \gamma_5 q \right. \\ & \left. + \frac{1}{2} (g_{LT(q)} \bar{e} \sigma^{\mu\nu} P_R \mu + g_{RT(q)} \bar{e} \sigma^{\mu\nu} P_L \mu) \bar{q} \sigma_{\mu\nu} q \right] + \text{h.c.} \end{aligned} \quad (4.59)$$

where all the g 's are all dimensionless coupling constants for the corresponding operators, where the momentum dependencies have been neglected. The magnitude of each coupling depends on the type of new physics under consideration that contributes to LFV. Actually, many of the terms won't play a significant role in our setup. First, since we are interested in the coherent processes in which the final state of the nucleus is the same as the initial one, the matrix elements $\langle N | \bar{q} \gamma_5 q | N \rangle$, $\langle N | \bar{q} \gamma_\mu \gamma_5 q | N \rangle$, and $\langle N | \bar{q} \sigma_{\mu\nu} q | N \rangle$ vanish. And specific to our setup, as discussed in the previous section, A_R and the scalar current $\bar{q} q$ are negligible. Only the dipole term with A_L , vector current $\bar{q} \gamma_\mu q$ with lepton flavor violation in the right-handed chirality, $\bar{e}^c \gamma^\mu \mu^c$ and their interference will contribute.

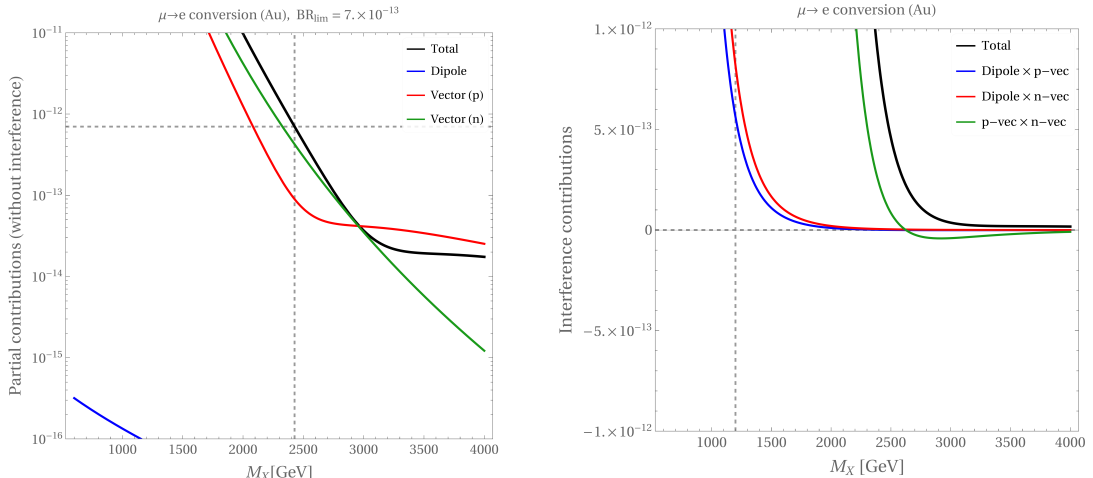


Figure 29: Individual and interference contributions to the $\mu \rightarrow e$ conversion rate in gold [89]. The left panel shows the partial branching fractions from dipole and vector (proton and neutron) terms without interference, and the right panel presents their interference terms. The vector contributions dominate over the dipole part, and the total rate surpasses the current experimental limit $\text{BR}_{\text{lim}}(\mu \rightarrow e) = 7.0 \times 10^{-13}$ for $M_X \leq 2.5$ TeV. For this plot, we take the exotic mass benchmark $(M_{D_1}, M_{D_2}, M_{D_3}) = (7640, 7600, 6700)$ GeV, the same combination that was taken to plot Fig. 26.

Now there are a few new features in this conversion that are absent in the $\mu \rightarrow eee$ process. First, here we have a tree-level contribution mediated by the leptoquark gauge boson X_μ . Second, in the box diagrams, different classes of vector-like fermions can run in the loop, and $\bar{\mu}^c \gamma_\mu e^c$ current can couple to both chiral currents $\bar{q}^c \gamma_\mu q^c$ and $\bar{q} \gamma_\mu q$ (see Fig. 28). This

simplifies the interaction Lagrangian specific to our setup:

$$\mathcal{L}_{\mu \rightarrow e \text{ conv}} = -\frac{4G_F}{\sqrt{2}} \left[m_\mu A_L \mu \sigma^{\mu\nu} e^c F_{\mu\nu} + \frac{1}{4} \sum g_{RV(q)} (\bar{e}^c \gamma^\mu \mu^c) (\bar{q} \gamma_\mu q + \bar{q}^c \gamma_\mu q^c) \right] + \text{h.c.} \quad (4.60)$$

As a result, the final formula will be simplified as well and take this simple form:

$$\Gamma_{\text{conv}} = 2G_F^2 \left| A_L^* D + \tilde{g}_{RV}^{(p)} V^{(p)} + \tilde{g}_{RV}^{(n)} V^{(n)} \right|^2. \quad (4.61)$$

Here $A_L = \sigma_L / (4\sqrt{2} G_F m_\mu)$ has already been discussed elaborately in the previous sections and can be used directly from Eqs. (4.40)–(4.42). The effective couplings $\tilde{g}_{RV}^{(p/n)}$ in Eq. (4.61) are given by

$$\tilde{g}_{RV}^{(p)} = 2g_{RV(u)} + g_{RV(d)}, \quad (4.62)$$

$$\tilde{g}_{RV}^{(n)} = g_{RV(u)} + 2g_{RV(d)}. \quad (4.63)$$

and the overlap integrals $D, V^{(p)}, V^{(n)}$ are listed in the appendix C for convenience. We follow closely the discussions of the previous section on $\mu \rightarrow eee$ from Ref. [84, 85] for the calculation of $g_{RV(q)}$. Here, we should make one comment on the tree-level contribution to the vector current (see Fig. 28 (a)). It is extremely suppressed in our setup due to the structure of the optimized CKM-like matrix (see Eq. (4.6)), which was needed to eliminate the K -meson decays. Thus, the same flavor alignment that ensures vanishing $\text{Br}(K \rightarrow \mu e)$ also guarantees that the tree-level $\mu \rightarrow e$ conversion is highly suppressed. For an order of magnitude estimate, we use

$$\text{Br}_{\mu \rightarrow e \text{ con(Ti)}}^{\text{tree}} \sim \frac{2G_F^2}{\Gamma_{\text{capt}}^{\text{Ti}}} \left| 2 \left(\frac{g_4}{g_L} \right)^2 \left(\frac{M_W}{M_X} \right)^2 \left(V^{(p)} + 2V^{(n)} \right) (K_{d^c e^c})_{11} (K_{d^c e^c})_{12}^* \right|^2 \quad (4.64)$$

with the overlap integrals, $V^{(p)}, V^{(n)}$, in units of $m_\mu^{5/2}$ and the total capture rate, $\Gamma_{\text{capt}}^{\text{Ti}}$ in units of 10^6 s^{-1} listed in Table 9, the choice for K_{ij} from Eq. (4.6) and $M_X \sim 1 \text{ TeV}$, we find the $\text{Br}_{\mu \rightarrow e \text{ con(Ti)}}^{\text{tree}} \sim 2 \times 10^{-18}$. The gauge invariant and finite combinations from penguins and box diagrams yields the expression

$$g_{RV(q)} = \frac{3}{16\pi^2} \left(\frac{g_4}{g_L} \right)^2 \left(\frac{M_W}{M_X} \right)^2 \left[e^2 \left(\mathcal{F}_1^{(\gamma Z)} + \mathcal{F}_2^{(\gamma Z)} \right) + g_4^2 \mathcal{G}^B \right], \quad (4.65)$$

where the form for $\mathcal{F}_1^{(\gamma Z)}, \mathcal{F}_2^{(\gamma Z)}$ has been discussed in Eqs. (4.49)–(4.52). For the box contribution \mathcal{G}^B , we have taken the different classes of vector-like fermions D', E, ν_E at the same mass scale and the CKM-like mixing exactly as ρ^H (see Eq. (4.4) in benchmark-2), so that $\mathcal{G}^B \sim \mathcal{F}^B$ and we use the mass kernels defined in Eqs. (4.54)–(4.55) for the parameter scan. To emphasize the point that $\mu \rightarrow e$ conversion in itself can be more constraining when $\mu \rightarrow e\gamma$ and $\mu \rightarrow eee$ processes are absent, we present Fig. 29. The left panel shows the individual contributions, and the right panel includes the interference terms to keep track of possible cancellations. In our setup, the vector contribution (p - or n -type, depending on the relevant mass scale) clearly surpasses the dipole part. Because of the attractiveness from the experimental point of view (the emitted electron has a mono-energetic spectrum at $E_e \simeq 105 \text{ MeV}$, well above the Michel endpoint (52.8 MeV), so no need for coincidence measurement), several experiments have already searched for it [89, 90, 93], and future experiments [91, 92] are aiming to push the

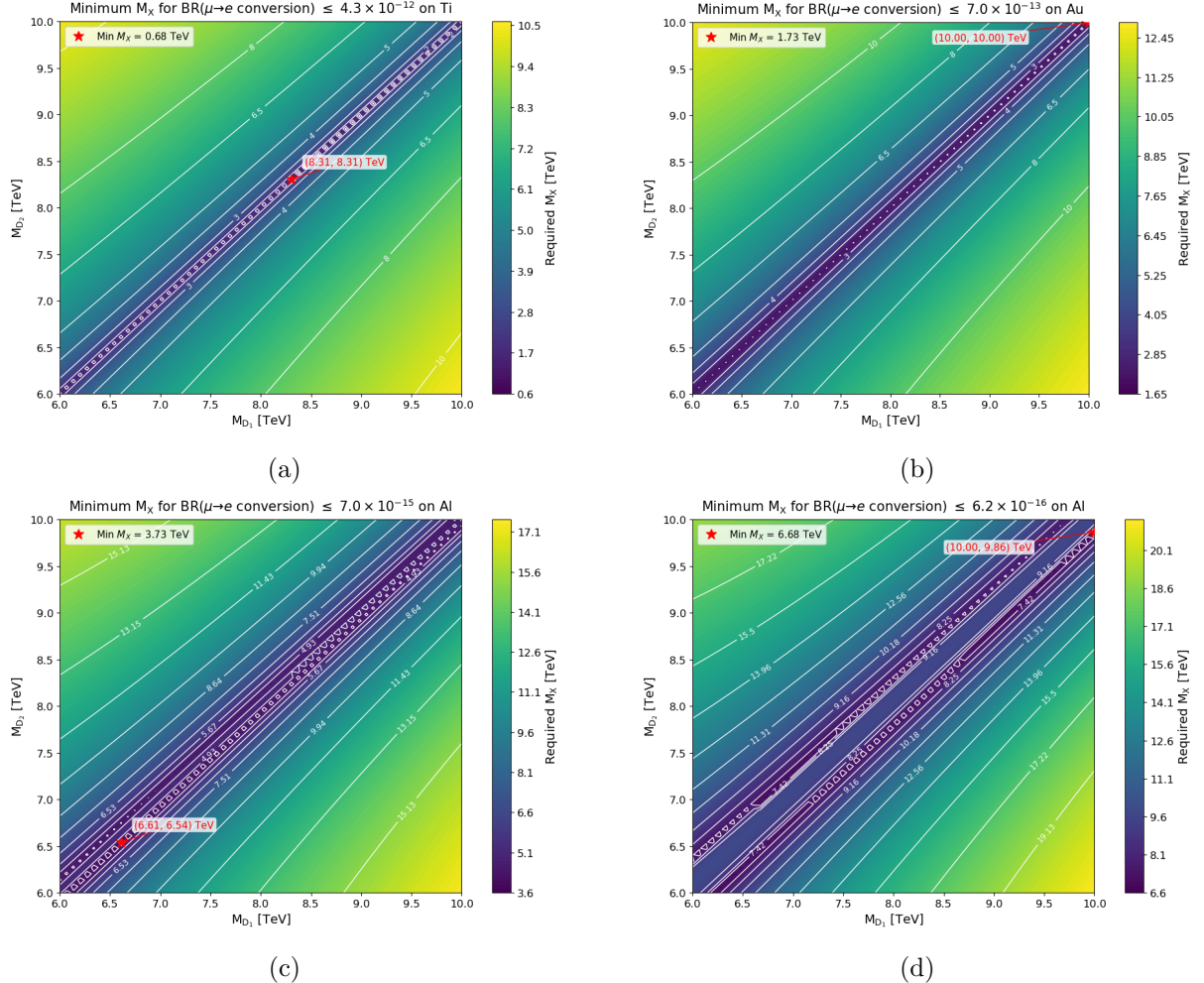


Figure 30: Minimum M_X required to satisfy the experimental and projected bounds on $\text{Br}(\mu \rightarrow e \text{ conv})$ from various targets: Plots in (a) and (b) correspond to the current SINDRUM II limits on Ti [90] and Au [89], respectively. Plots (c) and (d) represent the expected sensitivities of future experiments, COMET Phase I [91] and Mu2e [92] respectively, both using aluminum targets. Each plot shows contours of the minimum M_X required in the (M_{D_1}, M_{D_2}) plane (with $M_{D_3} = 6.7$ TeV fixed).

sensitivity much further. Specially, the upcoming Mu2e experiment at Fermilab will improve the sensitivity by nearly four orders of magnitude [92], which will enable us to probe our low-scale leptoquark gauge boson X_μ up to about 20 TeV in the benchmark scenarios considered here (see Fig. 30 (d)). For all plots in Fig. 30, we have made our usual choice for CKM-like mixings from Eq. (4.4) and plotted the contours of minimum M_X required to satisfy the experimental bounds on $\text{Br}(\mu \rightarrow e \text{ conv})$ in the (M_{D_1}, M_{D_2}) plane, with $M_{D_3} = 6.7$ TeV fixed.

4.4.4 Global fit with the three cLFV processes

Now we proceed to combine the three cLFV channels in a single fit, since they depend on the same parameters in the flavor sector. For loops involving light down-type quarks, we use the CKM matrix with soft-breaking suppression (see Eq. (4.6)). For loops involving vector-like

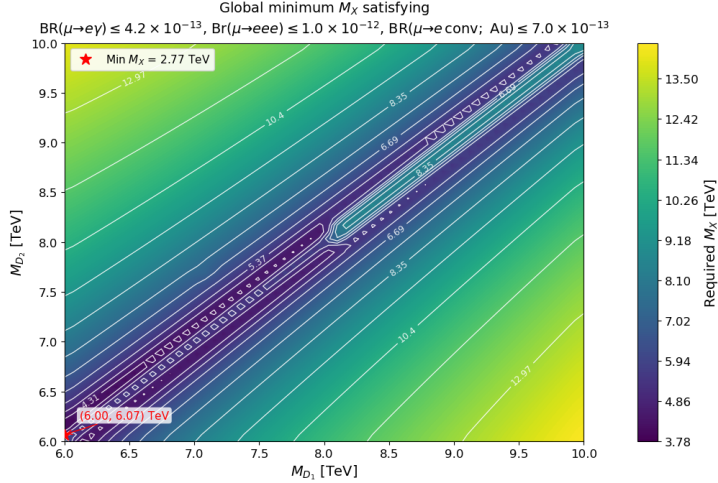


Figure 31: Global requirement on M_X from the combined constraints $\text{BR}(\mu \rightarrow e\gamma) \leq 4.2 \times 10^{-13}$, $\text{Br}(\mu \rightarrow eee) \leq 1.0 \times 10^{-12}$, and $\text{BR}(\mu \rightarrow e \text{ conv.; Au}) \leq 7.0 \times 10^{-13}$. The color at each point in the (M_{D_1}, M_{D_2}) plane with $M_{D_3} = 6.7$ TeV fixed gives the information of the smallest mediator mass M_X that satisfies all three limits simultaneously. White curves are contours of constant M_X . Throughout the scenario, we have made sure that all three processes share the same CKM-like structure and exotic-fermion content.

quarks, we use the same CKM-like matrix (see Eq. (4.4)), ensuring that all processes share a common flavor ansatz. At each point in the (M_{D_1}, M_{D_2}) plane (where $M_{D_3} = 6.7$ TeV is fixed), we scan over the mediator mass M_X and determine the minimum value that satisfies all current bounds simultaneously:

$$M_X^{\text{req}}(M_{D_1}, M_{D_2}) = \max \left\{ M_X^{(\mu \rightarrow e\gamma)}, M_X^{(\mu \rightarrow eee)}, M_X^{(\mu \rightarrow e \text{ conv.; Au})} \right\},$$

with $\text{BR}(\mu \rightarrow e\gamma) \leq 4.2 \times 10^{-13}$, $\text{Br}(\mu \rightarrow eee) \leq 1.0 \times 10^{-12}$, and $\text{BR}(\mu \rightarrow e \text{ conv.; Au}) \leq 7.0 \times 10^{-13}$ (see Table 2). The resulting heat map in Fig. 31 shows the required M_X^{req} with iso-lines indicating constant values of M_X . We have also shown the global minimum ($M_X \sim 2.8$ TeV with $(M_{D_1}, M_{D_2}) \sim (6.00, 6.07)$ TeV) within the scan for this benchmark. Now, it is possible that for some combination of this benchmark parameter, destructive interference among dipole, $\gamma - Z$, and box diagrams is locally relaxing one channel, but the global fit would automatically select the most constraining process at each point, which is the reason for showing this fit. Fig. 31 represents the resulting M_X^{req} surface and its iso-contours.

5 Conclusions

In this work, we have presented a concrete model of low-scale quark-lepton unification based on the Pati-Salam gauge symmetry $SU(2)_L \times SU(2)_R \times SU(4)_C$ with an E_6 -inspired particle spectrum. In addition to the SM fermions, our model features multi-TeV vector-like down-type quarks and leptons, together with a minimal Higgs sector that achieves two-step breaking of the Pati-Salam gauge group. One of the crucial components of this construction is a softly broken Z_2 symmetry, under which the SM fermions are even, while the exotic states (except D'^c), including X_μ , W'_μ are odd, which allows for realizing the low-scale unification. The soft

breaking in the right-handed down-quark sector induces small mixings that permit tree-level meson decays mediated by X_μ , but the branching ratios are helicity and mixing suppressed, with unsuppressed contributions arising only at one loop.

We have analyzed the collider signatures, meson decays, neutral meson oscillations, as well as charged lepton flavor violation mediated by X_μ , and we have shown that this framework can realize quark-lepton unification at accessible energies in a phenomenologically rich way, while remaining compatible with current collider and flavor constraints. While flavor observables by themselves are consistent with M_X being as low as 1.1 TeV, the LHC limit on the Z'_μ boson translates into an indirect bound on $M_X \gtrsim 4.3$ TeV. We have also discussed the distinctive collider signatures of the TeV-scale vector-like down-type quark with baryon number $-2/3$, whose existence is a natural consequence of a consistent baryon-number assignment in the model.

Within this setup, neutrino masses arise from two sources. One is through an effective dimension-7 operator, which is generated after integrating out the heavy neutral leptons of the model. The second source is a radiative contribution of the scotogenic type. Depending on the region of the parameter space, either mechanism can dominate, or both can participate comparably to explain the observed neutrino masses with TeV-scale new physics.

Looking ahead, our results show that this low-scale realization is a well-defined target for both the energy and intensity frontiers. The same leptoquark gauge boson X_μ and vector-like fermions that are essential for low-scale unification also control the rates for $\mu \rightarrow e\gamma$, $\mu \rightarrow eee$, and $\mu \rightarrow e$ conversion, which makes flavor experiments such as MEG II, Mu3e, Mu2e, and COMET directly sensitive to the relevant parameter space. Parallel searches for leptoquark gauge bosons and vector-like quarks at the LHC and future colliders can probe the same structure from the high-energy side, providing complementary tests of quark-lepton unification at accessible scales.

In summary, the heart of our work is to show that quarks and leptons can be made indistinguishable by a gauge symmetry realized at experimentally accessible energy scales.

Acknowledgments

The works of KSB and SB are supported in part by US Department of Energy Grant Number DE-SC 0016013. SS acknowledges the financial support from the Slovenian Research Agency (research core funding No. P1-0035 and N1-0321). The authors acknowledge the Center for Theoretical Underground Physics and Related Areas (CETUP* 2024) and the Institute for Underground Science at Sanford Underground Research Facility (SURF) for hospitality and for providing a conducive environment during the finalization of this work. The authors thank Jogesh Pati for useful comments and for his enthusiastic support.

A Coefficients in renormalization group equations

The beta function coefficients used for the running of the SM gauge couplings of Eq. (2.74)-(2.75) are given below: [94],

$$b_i = \left(\frac{41}{10}, -\frac{19}{6}, -7 \right), \quad B_{ij} = \begin{pmatrix} \frac{199}{50} & \frac{27}{10} & \frac{44}{5} \\ \frac{9}{10} & \frac{35}{6} & 12 \\ \frac{11}{10} & \frac{9}{2} & -26 \end{pmatrix}, \quad C_{if} = \begin{pmatrix} \frac{17}{10} & \frac{1}{2} & \frac{3}{2} \\ \frac{3}{2} & \frac{3}{2} & \frac{1}{2} \\ 2 & 2 & 0 \end{pmatrix}, \quad (\text{A.1})$$

with $f = u, d, e$. For completeness, we also note the Yukawa sector beta functions that enter into the coupled equations with gauge coupling running,

$$16\pi^2 \frac{dY_{u,d,e}}{dt} = Y_{u,d,e} \left(\beta_{u,d,e}^{(1)} + \beta_{u,d,e}^{(2)} \right), \quad (\text{A.2})$$

where we considered only the one-loop contributions in our numerical analysis. At one-loop, they can be written as,

$$\beta_u^{(1)} = \frac{3}{2} \left(Y_u^\dagger Y_u - Y_d^\dagger Y_d \right) + Y_2(S) - \left(\frac{17}{20} g_1^2 + \frac{9}{4} g_2^2 + 8g_3^2 \right), \quad (\text{A.3})$$

$$\beta_d^{(1)} = \frac{3}{2} \left(Y_d^\dagger Y_d - Y_u^\dagger Y_u \right) + Y_2(S) - \left(\frac{1}{4} g_1^2 + \frac{9}{4} g_2^2 + 8g_3^2 \right), \quad (\text{A.4})$$

$$\beta_e^{(1)} = \frac{3}{2} Y_e^\dagger Y_e + Y_2(S) - \frac{9}{4} (g_1^2 + g_2^2), \quad (\text{A.5})$$

with

$$Y_2(S) = \text{Tr} \left(3Y_u^\dagger Y_u + 3Y_d^\dagger Y_d + Y_e^\dagger Y_e \right). \quad (\text{A.6})$$

B Input parameters for meson mixing

B.1 $K^0 - \bar{K}^0$ oscillation

The non-vanishing magic numbers used in Eq. (4.21) for the kaon system are given below [73]:

$$\begin{aligned} a_i &= (0.29, -0.69, 0.79, -1.1, 0.14) \\ b_i^{(11)} &= (0.82, 0, 0, 0, 0), & c_i^{(11)} &= (-0.016, 0, 0, 0, 0), \\ b_i^{(22)} &= (0, 2.4, 0.011, 0, 0), & c_i^{(22)} &= (0, -0.23, -0.002, 0, 0), \\ b_i^{(23)} &= (0, -0.63, 0.17, 0, 0), & c_i^{(23)} &= (0, -0.018, 0.0049, 0, 0), \\ b_i^{(32)} &= (0, -0.019, 0.028, 0, 0), & c_i^{(32)} &= (0, 0.0028, -0.0093, 0, 0), \\ b_i^{(33)} &= (0, 0.0049, 0.43, 0, 0), & c_i^{(33)} &= (0, 0.00021, 0.023, 0, 0), \\ b_i^{(44)} &= (0, 0, 0, 4.4, 0), & c_i^{(44)} &= (0, 0, 0, -0.68, 0.0055), \\ b_i^{(45)} &= (0, 0, 0, 1.5, -0.17), & c_i^{(45)} &= (0, 0, 0, -0.35, -0.0062), \\ b_i^{(54)} &= (0, 0, 0, 0.18, 0), & c_i^{(54)} &= (0, 0, 0, -0.026, -0.016), \\ b_i^{(55)} &= (0, 0, 0, 0.061, 0.82), & c_i^{(55)} &= (0, 0, 0, -0.013, 0.018). \end{aligned}$$

Table 5 gives the relevant constants for the $K^0 - \bar{K}^0$ phenomenological analysis [71]:

μ	M_K	f_K	$(m_d + m_s)$	B_1^{sd}	B_4^{sd}	B_5^{sd}
2 GeV	497.67 MeV	156.1 MeV	135 ± 18 MeV	0.527 ± 0.022	0.9 ± 0.2	0.6 ± 0.1

Table 5: Input parameters used for ΔM_K estimation.

B.2 $D^0 - \bar{D}^0$ oscillation

The non-vanishing magic numbers are given below [70]:

$$\begin{aligned}
a_i &= (0.286, -0.692, 0.787, -1.143, 0.143) \\
b_i^{(11)} &= (0.837, 0, 0, 0, 0), & c_i^{(11)} &= (-0.016, 0, 0, 0, 0), \\
b_i^{(22)} &= (0, 2.163, 0.012, 0, 0), & c_i^{(22)} &= (0, -0.20, -0.002, 0, 0), \\
b_i^{(23)} &= (0, -0.567, 0.176, 0, 0), & c_i^{(23)} &= (0, -0.016, 0.006, 0, 0), \\
b_i^{(32)} &= (0, -0.032, 0.031, 0, 0), & c_i^{(32)} &= (0, -0.004, -0.010, 0, 0), \\
b_i^{(33)} &= (0, 0.008, 0.474, 0, 0), & c_i^{(33)} &= (0, 0, 0.025, 0, 0), \\
b_i^{(44)} &= (0, 0, 0, 3.63, 0), & c_i^{(44)} &= (0, 0, 0, -0.56, 0.006), \\
b_i^{(45)} &= (0, 0, 0, 1.21, -0.19), & c_i^{(45)} &= (0, 0, 0, -0.29, -0.006), \\
b_i^{(54)} &= (0, 0, 0, 0.14, 0), & c_i^{(54)} &= (0, 0, 0, -0.019, -0.016), \\
b_i^{(55)} &= (0, 0, 0, 0.045, 0.839), & c_i^{(55)} &= (0, 0, 0, -0.009, 0.018).
\end{aligned}$$

Table 6 gives the constants in the $D^0 - \bar{D}^0$ phenomenological analysis [71]:

μ	M_D	f_D	$(m_u + m_c)$	B_1^{cu}	B_4^{cu}	B_5^{cu}
2.8 GeV	1.86 GeV	212 ± 14 MeV	1.17 ± 0.12 GeV	0.85 ± 0.09	1.10 ± 0.11	1.37 ± 0.14

Table 6: Input parameters used for ΔM_D estimation.

B.3 $B_q^0 - \bar{B}_q^0$ oscillation

The non-vanishing magic numbers are given below [95]:

$$\begin{aligned}
a_i &= (0.286, -0.692, 0.787, -1.143, 0.143) \\
b_i^{(11)} &= (0.865, 0, 0, 0, 0), & c_i^{(11)} &= (-0.017, 0, 0, 0, 0), \\
b_i^{(22)} &= (0, 1.879, 0.012, 0, 0), & c_i^{(22)} &= (0, -0.18, -0.003, 0, 0), \\
b_i^{(23)} &= (0, -0.493, 0.18, 0, 0), & c_i^{(23)} &= (0, -0.014, 0.008, 0, 0), \\
b_i^{(32)} &= (0, -0.044, 0.035, 0, 0), & c_i^{(32)} &= (0, -0.005, -0.012, 0, 0), \\
b_i^{(33)} &= (0, 0.011, 0.54, 0, 0), & c_i^{(33)} &= (0, 0, 0.028, 0, 0), \\
b_i^{(44)} &= (0, 0, 0, 2.87, 0), & c_i^{(44)} &= (0, 0, 0, -0.48, -0.005), \\
b_i^{(45)} &= (0, 0, 0, 0.961, -0.22), & c_i^{(45)} &= (0, 0, 0, -0.25, -0.006), \\
b_i^{(54)} &= (0, 0, 0, 0.09, 0), & c_i^{(54)} &= (0, 0, 0, -0.013, -0.016), \\
b_i^{(55)} &= (0, 0, 0, 0.029, 0.863), & c_i^{(55)} &= (0, 0, 0, -0.007, 0.019).
\end{aligned}$$

Table 7 and 8 gives the relevant constants for the $B_{d,s}^0 - \bar{B}_{d,s}^0$ phenomenological analysis respectively [71]:

μ	M_{B_d}	f_{B_d}	$(m_b + m_d)$	B_1^{bd}	B_4^{bd}	B_5^{bd}
4.2 GeV	5.2795 GeV	(200 ± 20) MeV	4.22 ± 0.08 GeV	0.81 ± 0.08	1.14 ± 0.13	1.72 ± 0.19

Table 7: Input parameters used for ΔM_{B_d} estimation.

μ	M_{B_s}	f_{B_s}	$(m_b + m_s)$	B_1^{bs}	B_4^{bs}	B_5^{bs}
4.2 GeV	497.67 GeV	245 ± 25 MeV	4.30 ± 0.08 GeV	0.527 ± 0.022	0.9 ± 0.2	0.6 ± 0.1

Table 8: Input parameters used for ΔM_{B_s} estimation.

C Input parameters for $\mu \rightarrow e$ conversion in nuclei

Nucleus	D	$V^{(p)}$	$V^{(n)}$	Γ_{capt}
Al	0.0362	0.0161	0.0173	0.69
Ti	0.0864	0.0396	0.0468	2.59
Au	0.1890	0.0974	0.1460	13.07

Table 9: Values of the input parameters for different nuclei used in the calculation.

The overlap integrals, D , $V^{(p)}$, and $V^{(n)}$, in units of $m_\mu^{5/2}$ are listed in the Table from Ref. [88]. The total capture rates, Γ_{capt} in units of 10^6 s^{-1} are used from Ref. [96].

References

- [1] J. C. Pati and A. Salam, “Is Baryon Number Conserved?,” *Phys. Rev. Lett.* **31** (1973) 661–664.
- [2] J. C. Pati and A. Salam, “Lepton Number as the Fourth Color,” *Phys. Rev. D* **10** (1974) 275–289. [Erratum: *Phys. Rev. D* 11, 703–703 (1975)].
- [3] A. V. Kuznetsov and N. V. Mikheev, “Vector leptoquarks could be rather light?,” *Phys. Lett. B* **329** (1994) 295–299, [arXiv:hep-ph/9406347](https://arxiv.org/abs/hep-ph/9406347).
- [4] G. Valencia and S. Willenbrock, “Quark - lepton unification and rare meson decays,” *Phys. Rev. D* **50** (1994) 6843–6848, [arXiv:hep-ph/9409201](https://arxiv.org/abs/hep-ph/9409201).
- [5] A. D. Smirnov, “Mass limits for scalar and gauge leptoquarks from $K(L)0 \rightarrow e^- + \mu^- + \nu$, $B0 \rightarrow e^- + \tau^- + \nu$ decays,” *Mod. Phys. Lett. A* **22** (2007) 2353–2363, [arXiv:0705.0308 \[hep-ph\]](https://arxiv.org/abs/0705.0308).
- [6] F. Gursey, P. Ramond, and P. Sikivie, “A Universal Gauge Theory Model Based on E6,” *Phys. Lett. B* **60** (1976) 177–180.
- [7] A. V. Kuznetsov and N. V. Mikheev, “Could vector leptoquarks be rather light?,” in *8th International Seminar on High-energy Physics.* 5, 1994. [arXiv:hep-ph/9409321](https://arxiv.org/abs/hep-ph/9409321).

[8] R. R. Volkas, “Prospects for mass unification at low-energy scales,” *Phys. Rev. D* **53** (1996) 2681–2698, [arXiv:hep-ph/9507215](https://arxiv.org/abs/hep-ph/9507215).

[9] R. Foot, “An Alternative $SU(4) \times SU(2)L \times SU(2)R$ model,” *Phys. Lett. B* **420** (1998) 333–339, [arXiv:hep-ph/9708205](https://arxiv.org/abs/hep-ph/9708205).

[10] R. Foot and G. Filewood, “Implications of TeV scale $SU(4) \times SU(2)L \times SU(2)R$ quark-lepton-lepton unification,” *Phys. Rev. D* **60** (1999) 115002, [arXiv:hep-ph/9903374](https://arxiv.org/abs/hep-ph/9903374).

[11] M. J. Dolan, T. P. Dutka, and R. R. Volkas, “Lowering the scale of Pati-Salam breaking through seesaw mixing,” *JHEP* **05** (2021) 199, [arXiv:2012.05976](https://arxiv.org/abs/2012.05976) [hep-ph].

[12] C. Helsens and M. Selvaggi, “Search for high-mass resonances at FCC-hh,” tech. rep., CERN, Geneva, 2018. <https://cds.cern.ch/record/2642473>.

[13] K. S. Babu, S. Nandi, and Z. Tavartkiladze, “New Mechanism for Neutrino Mass Generation and Triply Charged Higgs Bosons at the LHC,” *Phys. Rev. D* **80** (2009) 071702, [arXiv:0905.2710](https://arxiv.org/abs/0905.2710) [hep-ph].

[14] G. Bambhaniya, J. Chakrabortty, S. Goswami, and P. Konar, “Generation of neutrino mass from new physics at TeV scale and multilepton signatures at the LHC,” *Phys. Rev. D* **88** no. 7, (2013) 075006, [arXiv:1305.2795](https://arxiv.org/abs/1305.2795) [hep-ph].

[15] E. Ma, “Verifiable radiative seesaw mechanism of neutrino mass and dark matter,” *Phys. Rev. D* **73** (2006) 077301, [arXiv:hep-ph/0601225](https://arxiv.org/abs/hep-ph/0601225).

[16] Z.-j. Tao, “Radiative seesaw mechanism at weak scale,” *Phys. Rev. D* **54** (1996) 5693–5697, [arXiv:hep-ph/9603309](https://arxiv.org/abs/hep-ph/9603309).

[17] J. Preskill, “Cosmological Production of Superheavy Magnetic Monopoles,” *Phys. Rev. Lett.* **43** (1979) 1365.

[18] R. Jeannerot, S. Khalil, G. Lazarides, and Q. Shafi, “Inflation and monopoles in supersymmetric $SU(4)C \times SU(2)(L) \times SU(2)(R)$,” *JHEP* **10** (2000) 012, [arXiv:hep-ph/0002151](https://arxiv.org/abs/hep-ph/0002151).

[19] R. Barbieri and A. Tesi, “ B -decay anomalies in Pati-Salam $SU(4)$,” *Eur. Phys. J. C* **78** no. 3, (2018) 193, [arXiv:1712.06844](https://arxiv.org/abs/1712.06844) [hep-ph].

[20] M. Blanke and A. Crivellin, “ B Meson Anomalies in a Pati-Salam Model within the Randall-Sundrum Background,” *Phys. Rev. Lett.* **121** no. 1, (2018) 011801, [arXiv:1801.07256](https://arxiv.org/abs/1801.07256) [hep-ph].

[21] J. Heeck and D. Teresi, “Pati-Salam explanations of the B -meson anomalies,” *JHEP* **12** (2018) 103, [arXiv:1808.07492](https://arxiv.org/abs/1808.07492) [hep-ph].

[22] J. Fuentes-Martin, G. Isidori, J. Pagès, and B. A. Stefanek, “Flavor non-universal Pati-Salam unification and neutrino masses,” *Phys. Lett. B* **820** (2021) 136484, [arXiv:2012.10492](https://arxiv.org/abs/2012.10492) [hep-ph].

[23] T. Kobayashi, S. Raby, and R.-J. Zhang, “Searching for realistic 4d string models with a Pati-Salam symmetry: Orbifold grand unified theories from heterotic string compactification on a $Z(6)$ orbifold,” *Nucl. Phys. B* **704** (2005) 3–55, [arXiv:hep-ph/0409098](https://arxiv.org/abs/hep-ph/0409098).

[24] M. Cvetic, T. Li, and T. Liu, “Supersymmetric Pati-Salam models from intersecting D6-branes: A Road to the standard model,” *Nucl. Phys. B* **698** (2004) 163–201, [arXiv:hep-th/0403061](https://arxiv.org/abs/hep-th/0403061).

[25] B. Assel, K. Christodoulides, A. E. Faraggi, C. Kounnas, and J. Rizos, “Classification of Heterotic Pati-Salam Models,” *Nucl. Phys. B* **844** (2011) 365–396, [arXiv:1007.2268](https://arxiv.org/abs/1007.2268) [hep-th].

[26] A. H. Chamseddine, A. Connes, and W. D. van Suijlekom, “Beyond the Spectral Standard Model: Emergence of Pati-Salam Unification,” *JHEP* **11** (2013) 132, [arXiv:1304.8050](https://arxiv.org/abs/1304.8050) [hep-th].

[27] J. L. Hewett and T. G. Rizzo, “Low-Energy Phenomenology of Superstring Inspired E(6) Models,” *Phys. Rept.* **183** (1989) 193.

[28] R. N. Mohapatra and R. Marshak, “Local B-L Symmetry of Electroweak Interactions, Majorana Neutrinos and Neutron Oscillations,” *Phys. Rev. Lett.* **44** (1980) 1316–1319. [Erratum: Phys. Rev. Lett. 44, 1643 (1980)].

[29] C. S. Aulakh and A. Girdhar, “SO(10) a la Pati-Salam,” *Int. J. Mod. Phys. A* **20** (2005) 865–894, [arXiv:hep-ph/0204097](https://arxiv.org/abs/hep-ph/0204097).

[30] N. Arkani-Hamed, S. Dimopoulos, and G. R. Dvali, “The Hierarchy problem and new dimensions at a millimeter,” *Phys. Lett. B* **429** (1998) 263–272, [arXiv:hep-ph/9803315](https://arxiv.org/abs/hep-ph/9803315).

[31] R. de Adelhart Toorop, F. Bazzocchi, and L. Merlo, “The Interplay Between GUT and Flavour Symmetries in a Pati-Salam x S4 Model,” *JHEP* **08** (2010) 001, [arXiv:1003.4502 \[hep-ph\]](https://arxiv.org/abs/1003.4502).

[32] S. F. King, “A to Z of Flavour with Pati-Salam,” *JHEP* **08** (2014) 130, [arXiv:1406.7005 \[hep-ph\]](https://arxiv.org/abs/1406.7005).

[33] S. Saad, “Fermion Masses and Mixings, Leptogenesis and Baryon Number Violation in Pati-Salam Model,” *Nucl. Phys. B* **943** (2019) 114630, [arXiv:1712.04880 \[hep-ph\]](https://arxiv.org/abs/1712.04880).

[34] E. Ma, “Particle Dichotomy and Left-Right Decomposition of E(6) Superstring Models,” *Phys. Rev. D* **36** (1987) 274.

[35] K. S. Babu, X.-G. He, and E. Ma, “New Supersymmetric Left-Right Gauge Model: Higgs Boson Structure and Neutral Current Analysis,” *Phys. Rev. D* **36** (1987) 878.

[36] L. Allwicher, P. Arnan, D. Barducci, and M. Nardecchia, “Perturbative unitarity constraints on generic Yukawa interactions,” *JHEP* **10** (2021) 129, [arXiv:2108.00013 \[hep-ph\]](https://arxiv.org/abs/2108.00013).

[37] R. N. Mohapatra and G. Senjanovic, “Neutrino Mass and Spontaneous Parity Nonconservation,” *Phys. Rev. Lett.* **44** (1980) 912.

[38] W. Grimus and L. Lavoura, “The Seesaw mechanism at arbitrary order: Disentangling the small scale from the large scale,” *JHEP* **11** (2000) 042, [arXiv:hep-ph/0008179](https://arxiv.org/abs/hep-ph/0008179).

[39] T.-T. Lu and S.-H. Shiou, “Inverses of 2×2 block matrices,” *Computers & Mathematics with Applications* **43** no. 1-2, (2002) 119–129.

[40] K. S. Babu, J. C. Pati, and F. Wilczek, “Suggested new modes in supersymmetric proton decay,” *Phys. Lett. B* **423** (1998) 337–347, [arXiv:hep-ph/9712307](https://arxiv.org/abs/hep-ph/9712307).

[41] A. Alloul, N. D. Christensen, C. Degrande, C. Duhr, and B. Fuks, “FeynRules 2.0 - A complete toolbox for tree-level phenomenology,” *Comput. Phys. Commun.* **185** (2014) 2250–2300, [arXiv:1310.1921 \[hep-ph\]](https://arxiv.org/abs/1310.1921).

[42] C. Degrande, C. Duhr, B. Fuks, D. Grellscheid, O. Mattelaer, and T. Reiter, “UFO - The Universal FeynRules Output,” *Comput. Phys. Commun.* **183** (2012) 1201–1214, [arXiv:1108.2040 \[hep-ph\]](https://arxiv.org/abs/1108.2040).

[43] J. Alwall, R. Frederix, S. Frixione, V. Hirschi, F. Maltoni, O. Mattelaer, H. S. Shao, T. Stelzer, P. Torrielli, and M. Zaro, “The automated computation of tree-level and next-to-leading order differential cross sections, and their matching to parton shower simulations,” *JHEP* **07** (2014) 079, [arXiv:1405.0301 \[hep-ph\]](https://arxiv.org/abs/1405.0301).

[44] **ATLAS** Collaboration, G. Aad *et al.*, “Search for high-mass dilepton resonances using 139 fb^{-1} of pp collision data collected at $\sqrt{s} = 13 \text{ TeV}$ with the ATLAS detector,” *Phys. Lett. B* **796** (2019) 68–87, [arXiv:1903.06248 \[hep-ex\]](https://arxiv.org/abs/1903.06248).

[45] G. Altarelli, B. Mele, and M. Ruiz-Altaba, “Searching for New Heavy Vector Bosons in $p\bar{p}$ Colliders,” *Z. Phys. C* **45** (1989) 109. [Erratum: Z.Phys.C 47, 676 (1990)].

[46] **ATLAS** Collaboration, “Prospects for searches for heavy Z' and W' bosons in fermionic final states with the ATLAS experiment at the HL-LHC,” .

[47] **ATLAS** Collaboration, G. Aad *et al.*, “Search for vector-boson resonances decaying into a top quark and a bottom quark using pp collisions at $\sqrt{s} = 13$ TeV with the ATLAS detector,” *JHEP* **12** (2023) 073, [arXiv:2308.08521 \[hep-ex\]](https://arxiv.org/abs/2308.08521).

[48] **ATLAS** Collaboration, M. Aaboud *et al.*, “Search for R-parity-violating supersymmetric particles in multi-jet final states produced in $p\bar{p}$ collisions at $\sqrt{s} = 13$ TeV using the ATLAS detector at the LHC,” *Phys. Lett. B* **785** (2018) 136–158, [arXiv:1804.03568 \[hep-ex\]](https://arxiv.org/abs/1804.03568).

[49] **ATLAS** Collaboration, M. Aaboud *et al.*, “Search for new phenomena in a lepton plus high jet multiplicity final state with the ATLAS experiment using $\sqrt{s} = 13$ TeV proton-proton collision data,” *JHEP* **09** (2017) 088, [arXiv:1704.08493 \[hep-ex\]](https://arxiv.org/abs/1704.08493).

[50] **CMS** Collaboration, A. M. Sirunyan *et al.*, “Searches for physics beyond the standard model with the M_{T2} variable in hadronic final states with and without disappearing tracks in proton-proton collisions at $\sqrt{s} = 13$ TeV,” *Eur. Phys. J. C* **80** no. 1, (2020) 3, [arXiv:1909.03460 \[hep-ex\]](https://arxiv.org/abs/1909.03460).

[51] G. Valencia, “Long distance contribution to $K(L) \rightarrow \text{lepton+ lepton-}$,” *Nucl. Phys. B* **517** (1998) 339–352, [arXiv:hep-ph/9711377](https://arxiv.org/abs/hep-ph/9711377).

[52] D. Gomez Dumm and A. Pich, “Long distance contributions to the $K(L) \rightarrow \mu+\mu-$ decay width,” *Phys. Rev. Lett.* **80** (1998) 4633–4636, [arXiv:hep-ph/9801298](https://arxiv.org/abs/hep-ph/9801298).

[53] **E871** Collaboration, D. Ambrose *et al.*, “Improved branching ratio measurement for the decay $K0(L) \rightarrow \mu+\mu-$,” *Phys. Rev. Lett.* **84** (2000) 1389–1392.

[54] **BNL** Collaboration, D. Ambrose *et al.*, “New limit on muon and electron lepton number violation from $K0(L) \rightarrow \mu+- e+$ decay,” *Phys. Rev. Lett.* **81** (1998) 5734–5737, [arXiv:hep-ex/9811038](https://arxiv.org/abs/hep-ex/9811038).

[55] **LHCb** Collaboration, R. Aaij *et al.*, “Search for the Rare Decays $B_s^0 \rightarrow e^+e^-$ and $B^0 \rightarrow e^+e^-$,” *Phys. Rev. Lett.* **124** no. 21, (2020) 211802, [arXiv:2003.03999 \[hep-ex\]](https://arxiv.org/abs/2003.03999).

[56] **CMS** Collaboration, A. M. Sirunyan *et al.*, “Measurement of properties of $B_s^0 \rightarrow \mu^+\mu^-$ decays and search for $B^0 \rightarrow \mu^+\mu^-$ with the CMS experiment,” *JHEP* **04** (2020) 188, [arXiv:1910.12127 \[hep-ex\]](https://arxiv.org/abs/1910.12127).

[57] **LHCb** Collaboration, R. Aaij *et al.*, “Search for the decays $B_s^0 \rightarrow \tau^+\tau^-$ and $B^0 \rightarrow \tau^+\tau^-$,” *Phys. Rev. Lett.* **118** no. 25, (2017) 251802, [arXiv:1703.02508 \[hep-ex\]](https://arxiv.org/abs/1703.02508).

[58] **LHCb** Collaboration, R. Aaij *et al.*, “Search for the lepton-flavour violating decays $B_{(s)}^0 \rightarrow e^\pm\mu^\mp$,” *JHEP* **03** (2018) 078, [arXiv:1710.04111 \[hep-ex\]](https://arxiv.org/abs/1710.04111).

[59] **Belle** Collaboration, H. Atmacan *et al.*, “Search for $B^0 \rightarrow \tau^\pm\ell^\mp$ ($\ell = e, \mu$) with a hadronic tagging method at Belle,” *Phys. Rev. D* **104** no. 9, (2021) L091105, [arXiv:2108.11649 \[hep-ex\]](https://arxiv.org/abs/2108.11649).

[60] **ATLAS** Collaboration, M. Aaboud *et al.*, “Study of the rare decays of B_s^0 and B^0 mesons into muon pairs using data collected during 2015 and 2016 with the ATLAS detector,” *JHEP* **04** (2019) 098, [arXiv:1812.03017 \[hep-ex\]](https://arxiv.org/abs/1812.03017).

[61] **LHCb** Collaboration, R. Aaij *et al.*, “Measurement of the $B_s^0 \rightarrow \mu^+\mu^-$ branching fraction and effective lifetime and search for $B^0 \rightarrow \mu^+\mu^-$ decays,” *Phys. Rev. Lett.* **118** no. 19, (2017) 191801, [arXiv:1703.05747 \[hep-ex\]](https://arxiv.org/abs/1703.05747).

[62] **Particle Data Group** Collaboration, S. Navas *et al.*, “Review of particle physics,” *Phys. Rev. D* **110** no. 3, (2024) 030001.

[63] **MEG** Collaboration, A. M. Baldini *et al.*, “Search for the lepton flavour violating decay $\mu^+ \rightarrow e^+ \gamma$ with the full dataset of the MEG experiment,” *Eur. Phys. J. C* **76** no. 8, (2016) 434, [arXiv:1605.05081 \[hep-ex\]](https://arxiv.org/abs/1605.05081).

[64] **BaBar** Collaboration, B. Aubert *et al.*, “Searches for Lepton Flavor Violation in the Decays $\tau^+ \rightarrow e^+ \gamma$ and $\tau^+ \rightarrow \mu^+ \gamma$,” *Phys. Rev. Lett.* **104** (2010) 021802, [arXiv:0908.2381 \[hep-ex\]](https://arxiv.org/abs/0908.2381).

[65] **SINDRUM** Collaboration, U. Bellgardt *et al.*, “Search for the Decay $\mu^+ \rightarrow e^+ e^+ e^-$,” *Nucl. Phys. B* **299** (1988) 1–6.

[66] K. Hayasaka *et al.*, “Search for Lepton Flavor Violating Tau Decays into Three Leptons with 719 Million Produced Tau+Tau- Pairs,” *Phys. Lett. B* **687** (2010) 139–143, [arXiv:1001.3221 \[hep-ex\]](https://arxiv.org/abs/1001.3221).

[67] A. J. Buras, “Weak Hamiltonian, CP violation and rare decays,” in *Les Houches Summer School in Theoretical Physics, Session 68: Probing the Standard Model of Particle Interactions*, pp. 281–539. 6, 1998. [arXiv:hep-ph/9806471](https://arxiv.org/abs/hep-ph/9806471).

[68] M. E. Peskin and D. V. Schroeder, *An Introduction to quantum field theory*. Addison-Wesley, Reading, USA, 1995.

[69] L. Di Luzio, M. Kirk, A. Lenz, and T. Rauh, “ ΔM_s theory precision confronts flavour anomalies,” *JHEP* **12** (2019) 009, [arXiv:1909.11087 \[hep-ph\]](https://arxiv.org/abs/1909.11087).

[70] **UTfit** Collaboration, M. Bona *et al.*, “Model-independent constraints on $\Delta F = 2$ operators and the scale of new physics,” *JHEP* **03** (2008) 049, [arXiv:0707.0636 \[hep-ph\]](https://arxiv.org/abs/0707.0636).

[71] M. Bauer, S. Casagrande, U. Haisch, and M. Neubert, “Flavor Physics in the Randall-Sundrum Model: II. Tree-Level Weak-Interaction Processes,” *JHEP* **09** (2010) 017, [arXiv:0912.1625 \[hep-ph\]](https://arxiv.org/abs/0912.1625).

[72] R. Dcruz, “Flavor physics constraints on left-right symmetric models with universal seesaw,” *Nucl. Phys. B* **1001** (2024) 116519, [arXiv:2301.10786 \[hep-ph\]](https://arxiv.org/abs/2301.10786).

[73] M. Ciuchini *et al.*, “Delta M(K) and epsilon(K) in SUSY at the next-to-leading order,” *JHEP* **10** (1998) 008, [arXiv:hep-ph/9808328](https://arxiv.org/abs/hep-ph/9808328).

[74] G. Senjanovic and P. Senjanovic, “Suppression of Higgs Strangeness Changing Neutral Currents in a Class of Gauge Theories,” *Phys. Rev. D* **21** (1980) 3253.

[75] R. N. Mohapatra, G. Senjanovic, and M. D. Tran, “Strangeness Changing Processes and the Limit on the Right-handed Gauge Boson Mass,” *Phys. Rev. D* **28** (1983) 546.

[76] Y. Zhang, H. An, X. Ji, and R. N. Mohapatra, “General CP Violation in Minimal Left-Right Symmetric Model and Constraints on the Right-Handed Scale,” *Nucl. Phys. B* **802** (2008) 247–279, [arXiv:0712.4218 \[hep-ph\]](https://arxiv.org/abs/0712.4218).

[77] S. T. Petcov, “The Processes $\mu \rightarrow e + \gamma$, $\mu \rightarrow e + \bar{e}$, $\nu' \rightarrow \nu + \gamma$ in the Weinberg-Salam Model with Neutrino Mixing,” *Sov. J. Nucl. Phys.* **25** (1977) 340. [Erratum: Sov.J.Nucl.Phys. 25, 698 (1977), Erratum: Yad.Fiz. 25, 1336 (1977)].

[78] MEG II Collaboration, “New limit on the $\mu^+ \rightarrow e^+ \gamma$ decay with the meg ii experiment,” *Eur. Phys. J. C* **85** no. 10, (2025) 1177, [arXiv:2504.15711 \[hep-ex\]](https://arxiv.org/abs/2504.15711).

[79] T. P. Cheng and L. F. Li, *Gauge theory of elementary particle physics: Problems and solutions*. 2000.

[80] L. Lavoura, “General formulae for $f(1) \rightarrow f(2)$ gamma,” *Eur. Phys. J. C* **29** (2003) 191–195, [arXiv:hep-ph/0302221](https://arxiv.org/abs/hep-ph/0302221).

[81] S. Antusch, C. Biggio, E. Fernandez-Martinez, M. B. Gavela, and J. Lopez-Pavon, “Unitarity of the Leptonic Mixing Matrix,” *JHEP* **10** (2006) 084, [arXiv:hep-ph/0607020](https://arxiv.org/abs/hep-ph/0607020).

[82] A. Abada, C. Biggio, F. Bonnet, M. B. Gavela, and T. Hambye, “Low energy effects of neutrino masses,” *JHEP* **12** (2007) 061, [arXiv:0707.4058 \[hep-ph\]](https://arxiv.org/abs/0707.4058).

[83] Y. Kuno and Y. Okada, “Muon decay and physics beyond the standard model,” *Rev. Mod. Phys.* **73** (2001) 151–202, [arXiv:hep-ph/9909265](https://arxiv.org/abs/hep-ph/9909265).

[84] F. Bishara, J. Brod, M. Gorbahn, and U. Moldanazarova, “Generic one-loop matching conditions for rare meson decays,” *JHEP* **07** (2021) 230, [arXiv:2104.10930 \[hep-ph\]](https://arxiv.org/abs/2104.10930).

[85] J. Brod and M. Gorbahn, “The Z Penguin in Generic Extensions of the Standard Model,” *JHEP* **09** (2019) 027, [arXiv:1903.05116 \[hep-ph\]](https://arxiv.org/abs/1903.05116).

[86] G. Buchalla, A. J. Buras, and M. E. Lautenbacher, “Weak Decays beyond Leading Logarithms,” *Rev. Mod. Phys.* **68** (1996) 1125–1144, [arXiv:hep-ph/9512380](https://arxiv.org/abs/hep-ph/9512380).

[87] A. Czarnecki, W. J. Marciano, and K. Melnikov, “Coherent muon electron conversion in muonic atoms,” *AIP Conf. Proc.* **435** no. 1, (1998) 409–418, [arXiv:hep-ph/9801218](https://arxiv.org/abs/hep-ph/9801218).

[88] R. Kitano, M. Koike, and Y. Okada, “Detailed calculation of lepton flavor violating muon electron conversion rate for various nuclei,” *Phys. Rev. D* **66** (2002) 096002, [arXiv:hep-ph/0203110](https://arxiv.org/abs/hep-ph/0203110). [Erratum: *Phys. Rev. D* 76, 059902 (2007)].

[89] **SINDRUM II** Collaboration, W. H. Bertl *et al.*, “A Search for muon to electron conversion in muonic gold,” *Eur. Phys. J. C* **47** (2006) 337–346.

[90] **SINDRUM II** Collaboration, C. Dohmen *et al.*, “Test of lepton flavor conservation in $\mu \rightarrow e$ conversion on titanium,” *Phys. Lett. B* **317** (1993) 631–636.

[91] **COMET** Collaboration, R. Abramishvili *et al.*, “COMET Phase-I Technical Design Report,” *PTEP* **2020** no. 3, (2020) 033C01, [arXiv:1812.09018 \[physics.ins-det\]](https://arxiv.org/abs/1812.09018).

[92] **Mu2e** Collaboration, F. Abdi *et al.*, “Mu2e Run I Sensitivity Projections for the Neutrinoless Conversion Search in Aluminum,” *Universe* **9** no. 1, (2023) 54, [arXiv:2210.11380 \[hep-ex\]](https://arxiv.org/abs/2210.11380).

[93] S. Ahmad *et al.*, “Search for Muon - Electron and Muon - Positron Conversion,” *Phys. Rev. D* **38** (1988) 2102.

[94] H. Arason, D. J. Castano, B. Keszthelyi, S. Mikaelian, E. J. Piard, P. Ramond, and B. D. Wright, “Renormalization group study of the standard model and its extensions. 1. The Standard model,” *Phys. Rev. D* **46** (1992) 3945–3965.

[95] D. Becirevic, M. Ciuchini, E. Franco, V. Gimenez, G. Martinelli, A. Masiero, M. Papinutto, J. Reyes, and L. Silvestrini, “ $B_d - \bar{B}_d$ mixing and the $B_d \rightarrow J/\psi K_s$ asymmetry in general SUSY models,” *Nucl. Phys. B* **634** (2002) 105–119, [arXiv:hep-ph/0112303](https://arxiv.org/abs/hep-ph/0112303).

[96] T. Suzuki, D. F. Measday, and J. P. Roalsvig, “Total Nuclear Capture Rates for Negative Muons,” *Phys. Rev. C* **35** (1987) 2212.